Master Thesis

Integration of Activated Carbon and Membrane Technology for Decolourisation of Glucose Syrup

carried out for the purpose of obtaining the degree of Diplom-Ingenieur (Dipl.-Ing. or DI)

submitted at TU Wien

Faculty of Mechanical and Industrial Engineering

by

Alexander Trischack, BSc

Mat. No.: 11778871

under the supervision of

Univ.Prof. Dipl.-Ing. Dr.techn Michael, Harasek

Dr. Amal, El Gohary Ahmed

Camila, Cabeza BSc MSc

Institute of Chemical, Environmental and Bioscience Engineering

Vienna, December 2024

_____

Signature

This work has been supported by COMET Center CHASE and the Institute of Chemical, Environmental & Bioscience Engineering at the Technische Universität Wien funded within the COMET – Competence Centers for Excellence Technologies programme by BMK, the BMDW and the Federal Provinces of Upper Austria and Vienna. The COMET programme is managed by the Austrian Research Promotion Agency

I confirm, that the printing of this thesis requires the approval of the examination board.

Affidavit

I declare in lieu of oath, that I wrote this thesis and carried out the associated research myself, using only the literature cited in this volume. If text passages from sources are used literally, they are marked as such.

I confirm that this work is original and has not been submitted for examination elsewhere, nor is it currently under consideration for a thesis elsewhere.

I acknowledge that the submitted work will be checked electronically-technically using suitable and state-of-the-art means (plagiarism detection software). On the one hand, this ensures that the submitted work was prepared according to the high-quality standards within the applicable rules to ensure good scientific practice "Code of Conduct" at the TU Wien. On the other hand, a comparison with other student theses avoids violations of my personal copyright.

Place and Date *Signature*

Acknowledgements

First of all, I want to thank Prof. Michael Harasek for giving me the opportunity to work on this project and his constant support. My appreciation extends to all the members of this research group for always helping me as well as their friendly company.

Especially, I want to thank Dr. Amal El Gohary Ahmed and Camila Cabeza for their guidance, help and relentless support during the whole research work.

I thank Dr. Christian Jordan for his great advises and support at my experiments and Dr. Neda Asasian Kolur for her special knowledge in adsorption.

Additionally, I want to thank Mario Minauf and his colleagues from AGRANA, who provided the glucose syrup as well as expertise.

Thanks goes also to my friends and study colleagues for the great time, the strong teamwork for the hardest exams and of course the cheering of each other.

Last but not least I want to thank my family for all the emotional support and patience during my whole studies.

Table of Contents

Abstract

Glucose syrup, mainly used as a sweetener but also utilised for many other applications, is produced by acidic and/or enzymatic hydrolysis of starch. This process leads to the formation of a brownish colour, primarily due to the Maillard reaction and caramelisation, which can result in an undesired appearance and flavour. Usually, the colour compounds are removed by activated carbon (AC) and ion exchange resin. The latter is already restricted in organic food industries due to new EU standards. Modern membrane technology in combination with AC adsorption could lead to a more energy-efficient and environmentally friendly decolourisation process. This research studied the improvements in glucose syrup decolourisation of a complementary process including membrane separation followed by AC adsorption. A fundamental study on AC adsorption without membrane-based pre-treatment is carried out with different syrup dilutions and AC dosages. Furthermore, ultrafiltration (UF) and nanofiltration (NF) membranes are tested as a pre-treatment by seven different multistage membrane configurations. The results showed that the adsorption process follows multilayer adsorption without initial monolayer coverage and is dominated by intraparticle diffusion. The AC separation by filtration with 2 to 3 µm filter paper was the leading cause of sugar loss of approximately 5 % at the adsorption process. By membrane multistage based pre-treatment AC dosage reduction of more than 60 % was achieveable, especially with tight UF (5 kDa) followed by tight NF (150 – 300 Da). This proves the potential of membrane technology in combination with AC adsorption in creating a less resource consuming and more energy efficient process. However, sugar losses due to sugar-rich side streams in the retentate must be addressed in future studies.

Kurzfassung

Glukosesirup, ein weit verbreitetes Süßungsmittel mit vielen weiteren Anwendungen, wird durch saure und/oder enzymatische Hydrolyse aus Stärke hergestellt. Dieser Prozess führt, aufgrund von Maillard-Reaktionen und Karamellisierung, zur Bildung einer bräunlichen Farbe, was zu einem unerwünschten Aussehen und Geschmack führen kann. Üblicherweise werden die Farbstoffe durch Aktivkohle und Ionenaustauscherharz entfernt, wobei letzteres bereits durch einige Regularien in der Lebensmittelindustrie nur beschränk anwendbar ist. Mittels moderner Membrantechnologie kombiniert mit Aktivkohleadsorption könnte ein energieeffizienterer und umweltfreundlicherer Entfärbungsprozess erreicht werden. In dieser Forschungsarbeit wurden die Verbesserungen bei der Entfärbung von Glukosesirup durch ein komplementäres Verfahren mit Membrantechnik und anschließender Aktivkohleadsorption untersucht. Aktivkohleadsorption wurde zuerst ohne Membrantrennverfahren mit verschiedenen Sirupverdünnungen und Aktivkohledosierungen untersucht. Darüber hinaus wurden Ultrafiltrations- (UF) und Nanofiltrations- (NF) Membranen als eine Vorbehandlung des Sirups mit sieben verschiedenen mehrstufigen Membrankonfigurationen getestet. Die Ergebnisse zeigen, dass der Adsorptionsprozess einer mehrschichtigen Adsorption ohne anfängliche einschichtiger-Bedeckung folgt, welcher durch Intrapartikeldiffusion dominiert wird. Die Aktivkohleabscheidung durch Filtration mit 2 bis 3 µm Filterpapier war mit ca. 5 % die Hauptursache für den Zuckerverlust beim Adsorptionsprozess. Eine mehrstufige Membranvorbehandlung führte zu einer Reduktion der Aktivkohledosierung um mehr als 60 %, insbesondere aufgrund einer Konfiguration mit tight UF (5 kDa) gefolgt von tight NF (150 - 300 Da). Damit wurde gezeigt, dass die Membrantechnologie in Kombination mit Aktivkohleadsorption großes Potenzial zeigt, einen weniger ressourcenintensiven und energieeffizienten Prozess zu schaffen. Allerdings müssen die Zuckerverluste durch die zuckerreiche Nebenströme des Retentats in zukünftigen Studien weiter untersucht werden.

1 Introduction and Motivation

Glucose syrups are “A purified and concentrated aqueous solution of nutritive saccharides derived from starch”, mainly used as a sweetener in food and beverages but also have other applications, e.g., in fermentation processes and building industry [1]. In the EU and UK saccharification products such as glucose syrups are one of the main products derived from starch, accounting for 49 % of 8.6 million tons of starch produced annually [2]. Glucose syrup is produced by hydrolysis of starch, which can be carried out using acids, enzymes or a combination of both, resulting in different glucose syrups [3]. These syrups typically have brown to yellow colouration, likely due to Maillard Reaction or caramelisation during the processing [1].

To meet quality standards for further applications, removing the colour compounds from glucose syrup is necessary. This is typically achieved using activated carbon (AC) and/or ion exchange resin. AC primarily removes organic impurities, such as proteins and other colour precursors. On the other hand, ion exchange resins are used to improve the quality of the syrup by removing further impurities to ensure a clear, stable and consistent product. While both methods are effective at colour removal, ion exchange resins can remove also ionic impurities. However, due to the high costs associated with resin regeneration, the resin itself, the use of expensive chemicals and disposal of the chemical effluent, a combination of an AC and ion exchange resin treatment is common. [1]

Ion exchange resins are restricted for use in organic products [4], a strongly growing market [5]. As a result, AC is currently the only treatment available to obtain a starch hydrolysate with high quality in colour. This necessitates the use of large amounts of AC. Therefore, research into optimal process conditions and alternative technologies to complement AC decolourisation is required to obtain a syrup with high colour quality, taste and long shelf life. Membrane separation is one promising technology for decolourisation as investigated by Cabeza et al. [6] achieving more than 27 % colour removal of starch hydrolysates by ultrafiltration. Atiyeh et al. [7] reported that less AC is required after membrane separation on a comparable solution. Furthermore, Cabeza et al. [8] demonstrated that a multistage membrane process could reduce colour by more than 50 %. Thus, a combination of AC with multistage membrane technology is a promising resource efficient process for quality improving of glucose syrups.

The objective of this thesis is to investigate decolourisation using AC in combination with membrane technology, aiming to develop a more sustainable method capable of producing colourless glucose syrup. Additionally, the study explores the mechanism and kinetics of the adsorption process as well as the effect of different conditions of the parameters AC dosage, adsorption time and sugar concentration.

2 Literature Review

2.1 Starch

Most plant tissues are containing starch in granular and amorphous form in defined cells. It is found in a wide range of plants, such as seeds (maise, wheat, sorghum, rice), tubers (potato), roots (tapioca, sweet potato, arrowroot), pith (sago palm) and fruits (banana). While theoretically all these plants could be utilised for starch production, the most important are maise, wheat, potato and tapioca (cassava, manioc). The choice of plant depends on factors such as the geographical location, climate, sophistication of plant, whether production is seasonal or continuous, raw material storage and transport, political considerations (financial incentives) and other factors. [3]

Starch is a polysaccharide composed of monosaccharides and is one of the three main polysaccharides found in nature alongside cellulose and glycogen [9]. It serves as the primary energy storage polysaccharide in plants [10]. The starch polymer is formed by α-D-glucopyranose monosaccharides [9] and includes the two main components: amylose and amylopectin, with the amylopectin accounting for around 75 % of the starch [10].

Starch production is a well-established sector with a wide range of applications ranging from food and beverage sector, glucose and fructose syrups, ethanol production, application in the paper industry as well as for production of acids and bioplastics. In general starch biorefinery starts with the milling of the starch containing crop, followed by a physical separation process and, dependent on the application, enzymatic conversion. The milling process can be carried out by the so called wet or dry milling dependent on the following use. An overview of the applications can be found in Figure 2.1. [11]

Despite its broad applicability the main use of starch remains in food, where it is the most important nutrient of humans [10]. The largest volumes of starch are used to produce glucose, maltose and high fructose corn syrup (HFCS), alongside fuel ethanol [11]. In 2013 glucose syrup marked was valued $24 billion and was estimated to reach $33 billion in 2018 [12]. In the EU and UK, saccharification products such as glucose syrups account for 49 % of the consumption of the 8.6 million tons starch produced annually [2]. These facts underscore the importance of the glucose syrup industry and highlight the potential for improvements in terms of sustainability and economy through innovative technologies.

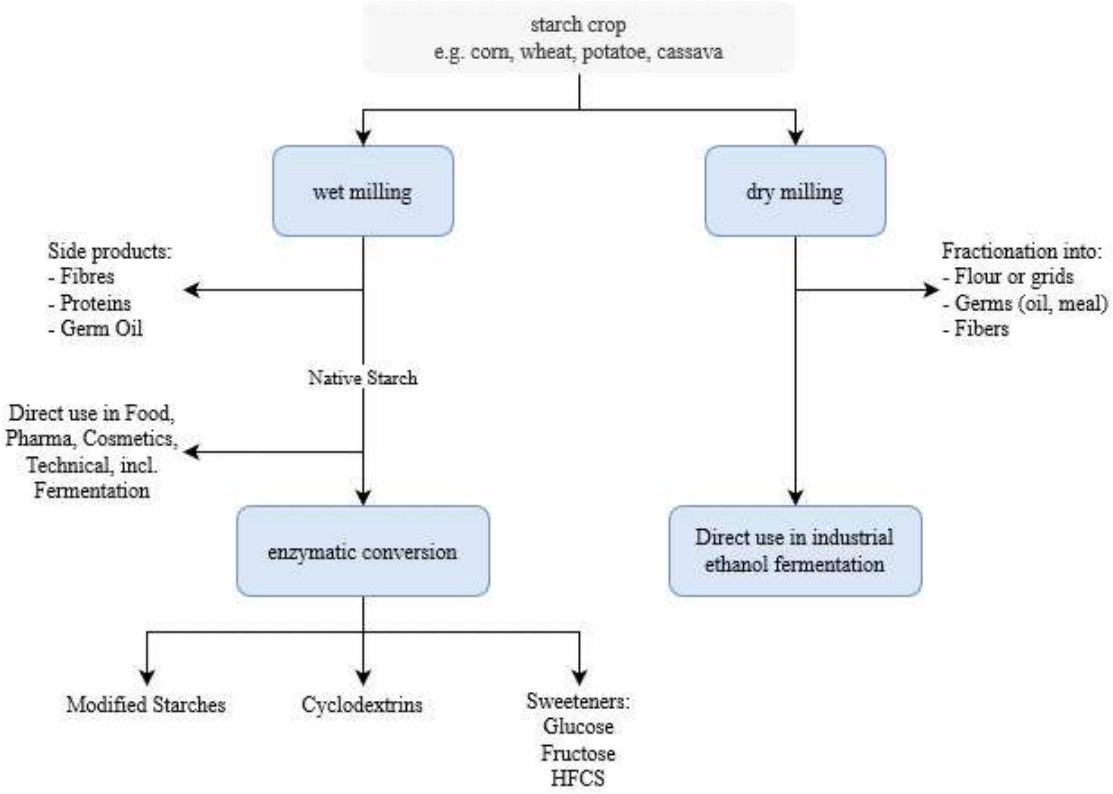

Figure 2.1: Starch biorefinery [11]

2.2 Glucose Syrup

Glucose syrup is defined as "a purified concentrated aqueous solution of nutritive saccharides obtained from starch and/or inulin. Glucose syrup has a dextrose equivalent (DE) content of not less than 20.0% m/m (expressed as D-glucose on a dry basis), and a total solids content of not less than 70.0% m/m." according to the Codex Alimentarius of the WHO [13] and the European Council of EU [14].

It can also be referred to as "glucose" or "corn syrup", a term commonly used in the USA. These terms can be bit misleading since many commercial products labelled as such may contain very little glucose, sometimes less than 1%, and may not necessarily be made from corn. In glucose syrup industry, "glucose" actually refers to glucose syrup and the monomer α-D-glucose is referred to as dextrose, which can exist as dextrose monohydrate or anhydrous dextrose. [3]

Glucose syrups are the hydrolysis products of starch consisting of some glucose monomer, varying quantities of dimer, oligosaccharides, and polysaccharides, depending on the specific glucose syrup and its manufacturing process. Other sugars may be present as byproducts from the manufacturing process, known as reversion products. Although they are present in small quantities, these sugars can lead to undesirable off-flavours, especially in processes involving acid hydrolysis. The main compounds are presented in Figure 2.2. [3]

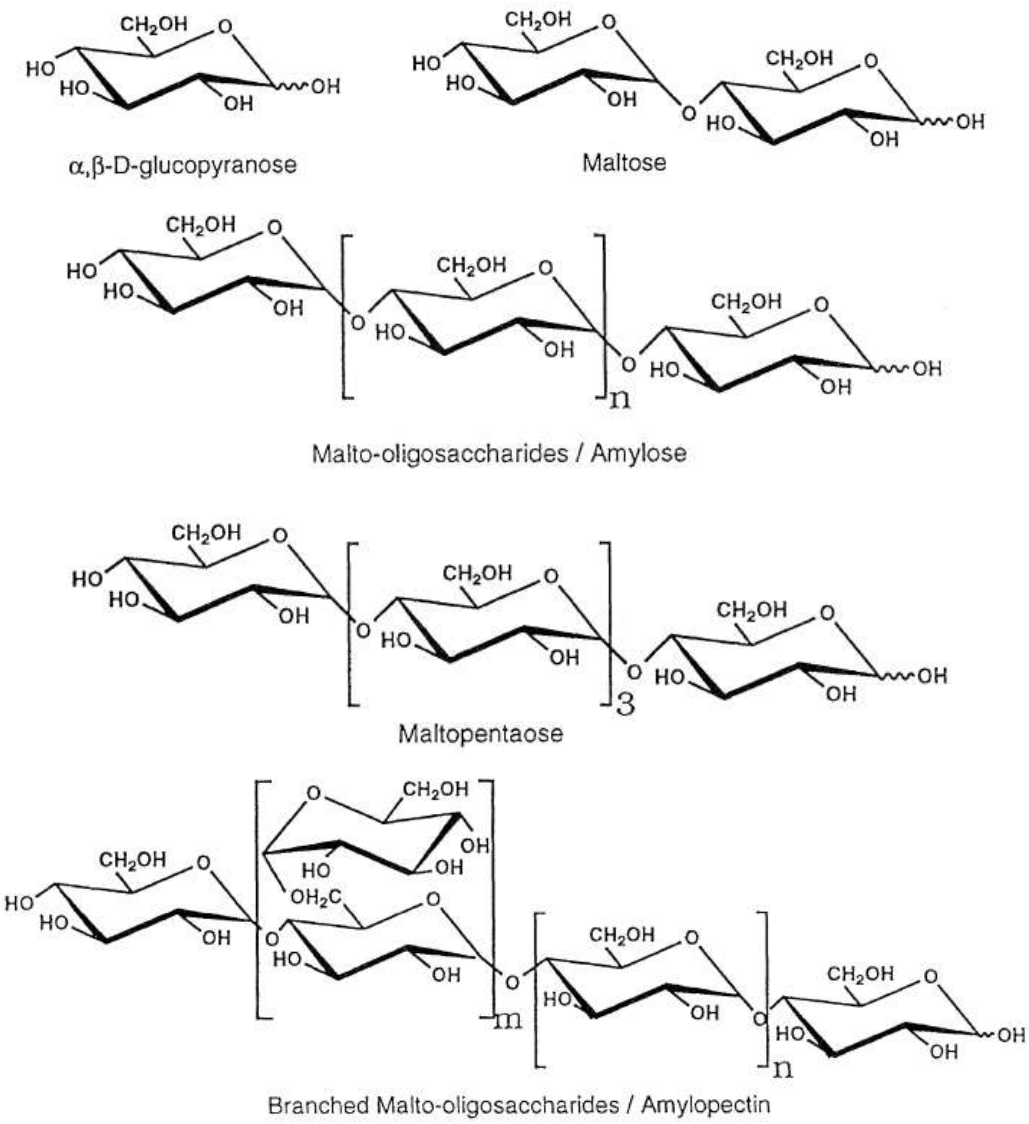

Figure 2.2: Main structural components of starch hydrolysates [3]

Commonly they are characterised by the DE value. The DE value is defined as the percentage of reducing sugar content expressed as dextrose (D-glucose) on a dry matter basis, determined using a standard method. According to this definition, pure starch has a DE value of zero, while dextrose has a DE value of 100. It indicates the various amounts of high and low molecular weight glucose polymers to which the starch has been broken down through hydrolysis, giving the syrup its unique properties. In practical terms, DE value is a way to quantify the reducing power of a syrup, providing insights into its stability and functionality. Due to the advances in enzymatic hydrolysis, syrups nowadays can have diverse carbohydrate composition, leading to variations in the properties. Consequently, other parameters such as carbohydrate composition, solid content and sulphur dioxide content are relevant in the characterisation of starch hydrolysates. [3]

The application of glucose syrups is highly versatile. One important application of course is the use as a sweetener in food and beverage industry. Further it also can be

utilised for breweries, as additives in building industry as well as an energy source for fermentation processes, i.e., to produce antibiotics or bioplastics [1]. Syrups with a low DE value are primarily employed in applications where body, cohesiveness, foam stability, prevention of sucrose crystallization, and viscosity are essential, while syrups with a high DE value are preferred when browning, fermentability, enhanced flavour, lowering of freezing point, increased osmotic pressure and sweetness are needed [15].

2.2.1 Production of Glucose Syrup

Glucose syrup production in theory can be done with any starch source. In practice factors such as the availability of the starch at a commercially acceptable price, politics considerations as well as the involved costs and technology for the production significantly influence the choice of starch source. Consequently, maise is predominantly in the United States and parts of Europe, wheat in Northern Europe, the United Kingdom and Australia, potatoes in the Netherlands and Poland, barley in Scandinavia, and tapioca as well as rice in Asia. [1]

The production of glucose syrup from starch dates back to 1811, when Gottlieb Sigismund Constantin Kirchhoff discovered that the acid hydrolysis of potato starch formed glucose [16]. Originally, acid conversion was used to produce glucose syrups [3]. Nowadays the hydrolysis of starch to glucose syrup is commonly carried out in a two-step enzymatic process consisting of liquefaction followed by saccharification, illustrated in Figure 2.3 [11].

The enzymatic hydrolysis of starch begins with a required gelatinization process to enable enzyme activity. In the first enzymatic process the major polymers, amylose and amylopectin are broke down, into oligomers called dextrins using α-amylases under starch gelatinization conditions. This process is known as liquefaction. Gelatinization and liquefaction are generally carried out in a jet cooking process at temperatures up to 105 °C. In the second step the dextrins are converted to glucose at 60 °C by the enzymes called glucoamylase and pullulanase. This conversion step referred to as saccharification results in the final glucose syrup. [11]

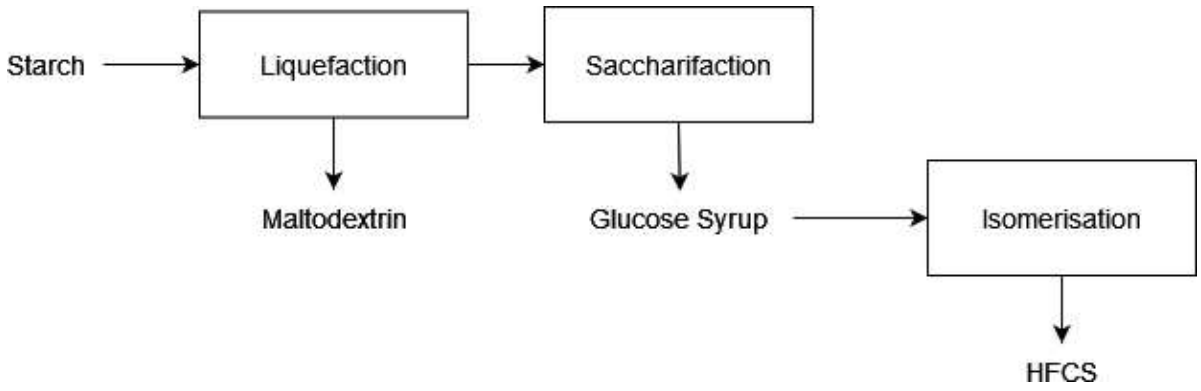

Figure 2.3: Schema of starch conversion to maltose, glucose and HFCS [11]

2.2.2 Colour Formation

Glucose syrup from starch hydrolysis typically presents a brownish to yellow colour. This coloration is primary due to colour compounds formed by caramelisation or Maillard reaction, which occur at the high temperatures used during the hydrolysis process [1]. Colour formation in glucose syrup production is crucial for sensorial properties such as appearance and flavour and give information about the purity [17]. Starch with lower quality, characterised by high protein and salt content, can promote higher colourant production and lead to poor storage properties [1].

Generally, glucose syrups are offered at the market as “water white” or colourless products [3]. This is especially important for boiled sweets where colour formations are undesirable due to unacceptable colour and development of off-flavours [18].

2.2.2.1 Maillard Reaction

The Maillard Reaction is a well-documented series of complex chemical reactions between reducing sugars, such as aldoses and ketoses, and amino groups in proteins or free amino acids [3]. Syrup with higher amount of reducing sugars, particularly dextrose and fructose, will produce significant colour when heated [1].

Proteins in the syrup are residues from the starch as the main sources wheat and maise starch contain around 0.3 % protein and residual amino acids. Therefore, it is important to remove such impurities during the manufacturing process to obtain a colour-stable glucose syrup. Additonally, demineralisation of the syrup removes charged proteins and amino acids beside inorganic compounds. [3]

2.2.2.2 Caramelisation

Caramelisation is a chemical reaction that occurs when carbohydrates are excessively heated, especially in the presence of an alkali. This process is commonly used to produce caramel colours used in foods like cola beverages, beers, and gravy browning. The final-coloured compounds generated during caramelisation are somewhat similar to those produced in Maillard reactions, although proteins are not directly involved in caramelisation. Caramelisation primarily revolves around free aldehyde or ketone groups, making it more likely to occur in higher DE value glucose syrups. Ketone groups, in particular, are more reactive than aldehydes, and syrups containing fructose can start caramelising at around 70 °C. In glucose syrup manufacturing, caramelisation reactions are less prominent than Maillard reactions, although they can potentially occur if there are localised "hot spots" in the process. [3]

2.3 Adsorption

Adsorption is the phenomenon where molecules from a fluid phase accumulate onto the surface of a solid phase. This effect occurs due to surface forces that binds molecules from the fluid phase, known as the adsorbate, to the solid phase, called the adsorbent [19]. The reverse process, where the adsorbed substances are released and transferred back into the fluid, is referred to as desorption [20]. The whole process is illustrated in Figure 2.4. Depending on the dominant mechanism, adsorption can be classified into physical adsorption (physisorption) and chemical adsorption (chemisorption) [21]

In the Physical adsorption the attractive forces are relatively weak and governed by van der Waals and electrostatic forces. This process is generally exothermic and can easily be reversed by heating or in the case of gases by decreasing the pressure of the adsorbate. In contrast chemical adsorption is governed by chemical bonding and tends to be irreversible. While chemisorption has been explored recently for separation and purification processes, most applications are based on physisorption. [21]

The most important characteristic of adsorption is the selectivity of the adsorbate that accumulates on the adsorbent and the relatively weak occurrence of surface forces. The second allows for simple physical desorption processes through heating or pressure reduction. Consequently, adsorption is an important separation process for small concentrations in fluids phases. [19]

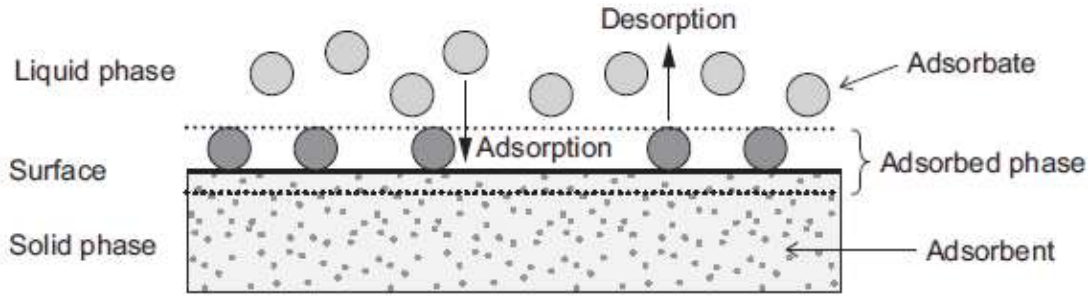

Figure 2.4: Basic terms of adsorption [20]

The adsorption process can be classified into three principal mechanisms: Steric, kinetic and equilibrium effects. In the steric mechanism small molecules enter the pores of the solids, while larger molecules are excluded from entry due to their size. The equilibrium mechanism relies on the selectivity of the solid, prioritising the removal of molecules with stronger adsorption tendencies. The kinetic mechanism is based on varying diffusion rates of different species into the pores. By controlling the exposure time, the solid can preferentially remove the species that diffuse faster. [22]

Given the topic of this thesis the focus will be on adsorption in the liquid phase. However, many of these principles can also be applied to the gas phase.

2.3.1 Application of Adsorption

Application of adsorption can be dated back to 200 B.C., when wood char was used for water purification [23]. Modern utilisation of adsorption began with the discovery that charcoal could remove colour from solutions [24]. Today adsorption covers a wide range of application in the field of separation, synthesis, storage, and purification of gases and liquids, demonstrating great versatility in thermal and chemical engineering science [25]. Some of the main uses of adsorption in both liquid- and gas-phase are presented in Table 2.1.

Table 2.1: Modern applications of adsorption [24]

liquid-phase adsorption	gas-phase adsorption
• Decolouring, drying, or degumming of petroleum products • Removing dissolved organic species from water supplies • Removing odour, taste, and colour from water supplies • Advanced treatment of wastewater (domestic and industrial) • Decolouring of crude sugar syrup and vegetable oils • Recovery and concentration of proteins, pharmaceuticals, and bio-compounds from dilute suspensions • Bulk separation of paraffin and isoparaffins	• Recovering organic solvent vapours • Dehydration of gases • Removing toxic agents and odour for personal protection • Air separation • Separating normal paraffins from isoparaffin aromatics • CO2 capture for addressing climate change

In chemical processes, adsorption is gaining recognition as a viable alternative to traditional separation methods like rectification, absorption, condensation, drying, extraction, membrane processes, and catalysis. This transition is facilitated by the use of diverse and finely tuned adsorbents. There is a substantial overlap between these thermal separation techniques and the fields of surface science and nanotechnology. Therefore, the term "technical adsorption" can be specifically applied to processes that involve highly porous media to avoid confusion and to help delineate the unique characteristics and applications of adsorption in these contexts. [25]

Liquid phase adsorption is primary used for purification purposes, such as clarification of sugar syrups with AC and the bleaching and decolourisation of mineral, vegetable, and animal oils with activated alumina. This process typically involves adding a powdered

adsorbent to the liquid phase and mixing by intense stirring until equilibrium is reached. Following, the adsorbent and the liquid are separated by filtration. Continuous processes such as those used in gas adsorption, where the liquid flows through a granulate bed for purification, are also suitable. In contrast to gas adsorption, regeneration of the adsorbent does not occur often. [19]

2.3.2 Adsorbents

Adsorption is fundamentally a surface-related phenomenon. Thus, the surface area of the adsorbent plays a crucial role, which is realised by highly porous materials allowing large surfaces as internal surfaces via the pore walls, leading to surface areas in the range between 10^2 and 10^3 m^2/g [20]. The kinetic and equilibrium are determining parameters of the performance, meaning the molecules should quickly reach the particle interior together with a high adsorbent capacity [22]. Other important characteristics of the adsorbent include selectivity, regeneration method and capability, chemical and mechanical resistance as well as the costs [19], [25].

To achieve a large surface area, meaning high capacity, as well as fast transport of molecules to the interior a combination of micropore and macropore ranges is required [22]. The following classification recommended by IUPAC [22] is often used, which is illustrated in Figure 2.5:

- Micropores $r < 1$ nm
- Mesopores $1 < r < 25$ nm
- Macropores $r > 25$ nm

Bart and von Gemmingen [25] categorise the most important adsorbents used in industry into two groups: First are those composed of oxygen-containing compounds, generally showing hydrophilic properties, such as

- silica gel,
- activated alumina,
- zeolites and molecular sieves,
- clay minerals, and
- pillared clays.

Second are adsorbents with carbon as the major component, which are hydrophobic in nature, including:

- Activated carbon,
- activated coke,
- carbon molecular sieves,
- carbon nanotubes, and
- polymeric resins.

Due to the importance of activated carbon in decolourisation, the following chapter will provide details about it.

2.3.2.1 Activated Carbon (AC)

AC is one of the most complex and versatile practical solids used in industries, thanks to its extremely high surface area and micropore volume. It exhibits bimodal and sometimes trimodal pore size distribution, allowing good access for molecules into its interior. AC has a complex amorphous and a graphite-like microcrystalline structure, with the latter providing space for molecules in the form of slit shaped channels, which is important for its capacity. [22]

AC features a ramified pore system, as presented in Figure 2.5, where mesopores, micropores and sub micropores branch off from macropores. [26]

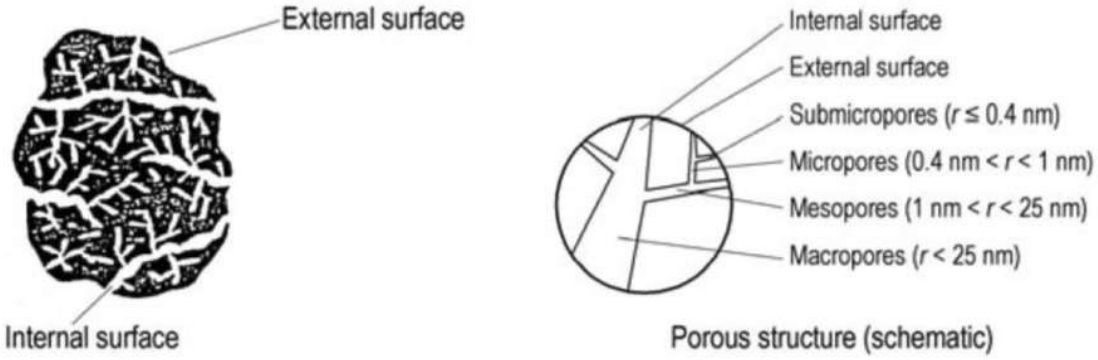

Figure 2.5: Schematic model of activated carbon [26]

Macropores are greater than 50 nm in size, with a volume ranging from 0.2 to 0.5 cm^3/g. The area macropores contribute to the adsorption is usually very small, in the order of 0.5 m^2/g, which is negligible compared to the area contributed by the micropores. While macropores do not significantly impact adsorption capacity, they are important for transporting adsorbate molecules from the bulk into the particle interior. [22]

Mesopores range in size from 2 to 100 nm, with volumes between 0.1 to 0.4 cm^3/g and a surface area of 10 to 100 m^2/g. At low concentrations, mesopores contribute marginally to the capacity, but play a significant role at higher concentrations. With low concentrations, they act like transport pores same as macropores. [22]

Micropores, defined as pores smaller than 2 nm, are slit-shaped and provide the space for the storing of most adsorbed molecules through volume filling mechanism. [22]

The chemical nature of the AC surface is more complex than its pore network and depends on many factors, such as the carbon source and the activation method. Commonly, it is made from oxygen rich raw material, resulting in many functional groups with oxygen. Oxygen can also be introduced, during the preparation, for example by activating coal by air or gasification with water vapour. Functional groups on AC can be increased by treatment with some oxidizing agents or decreased by exposing it to a vacuum environment at very high temperatures. Commercial AC exhibits a broad range of properties tailored to specific applications. In liquid-phase applications, AC tends to feature larger

mesopore volumes and average pore radius, for easier diffusion of molecules into its interior due to the larger molecules of the adsorbate. [22]

Commercial AC generally has specific inner surface areas ranging from 500 m^2/g to 1500 m^2/g. Its hydrophobic nature makes AC ideal for adsorption of nonpolar organic compounds, contributing to its wide use in air pollution control and water treatment. Moreover, AC surfaces show catalytic properties, making it valuable in commercial applications as a catalyst or catalyst support. [26]

For AC exists no comprehensive nomenclature or standardization, due to its wide variation in the properties. However, it can be characterised by its appearance, pore radius distribution, or by typical applications, as shown in Table 2.2. [26]

Table 2.2: Characterisation of activated carbon [26]

Classification	Types
Appearance	• Powdered activated carbon (PAC) • Granular activated carbon (GAC) • Cylindrical pellets • Spherical pellets • Activated carbon fibres (ACF) • Activated coke

Pore radius distribution	• Activate coke
	• Activated carbon
	  ○ fine-pore
	  ○ medium-pore
	  ○ wide-pore
	• Carbon molecular sieves (CMS)

Application	• Carbon molecular sieve (CMS) • Decolourising carbon • Water-treatment carbon • Catalyst carbon

2.3.3 Adsorption Process Configurations and Regeneration

The main objective in adsorption process design is to ensure contact between the fluid and the adsorbent. Various methods to achieve this are presented in Figure 2.6 and described below. [24]

A) ***Batch adsorption in agitated vessel***: A specific amount of adsorbent is brought into contact with a solution of known adsorbate concentration. Stirrers ensure complete suspension of the particles and homogenisation of the solutions. While batch reactors are not suitable for treating of large volumes of solution, they are often used for characterising new adsorbent applications. [24]

B) ***Fixed-bed adsorption***: The solution passes through a column packed with adsorbents. This method is usually applied for removing trace contaminants from liquid solution, or toxic and volatile vapours from gas streams. [24]

C) ***Adsorption in continuous flow tanks***: Adsorbents in powdered form are added directly to a specific treatment step with the purpose of removing a particular contaminant. This method is often used in wastewater treatment. [24]

Another technology to obtain a continuous process is moving bed adsorption as presented in Figure 2.6 (D), (E) and (F). Thereby, the solid (adsorbent) and fluid phases are in motion during the process, which can move in parallel, counter-current, or perpendicular (cross-flow) directions. [24]

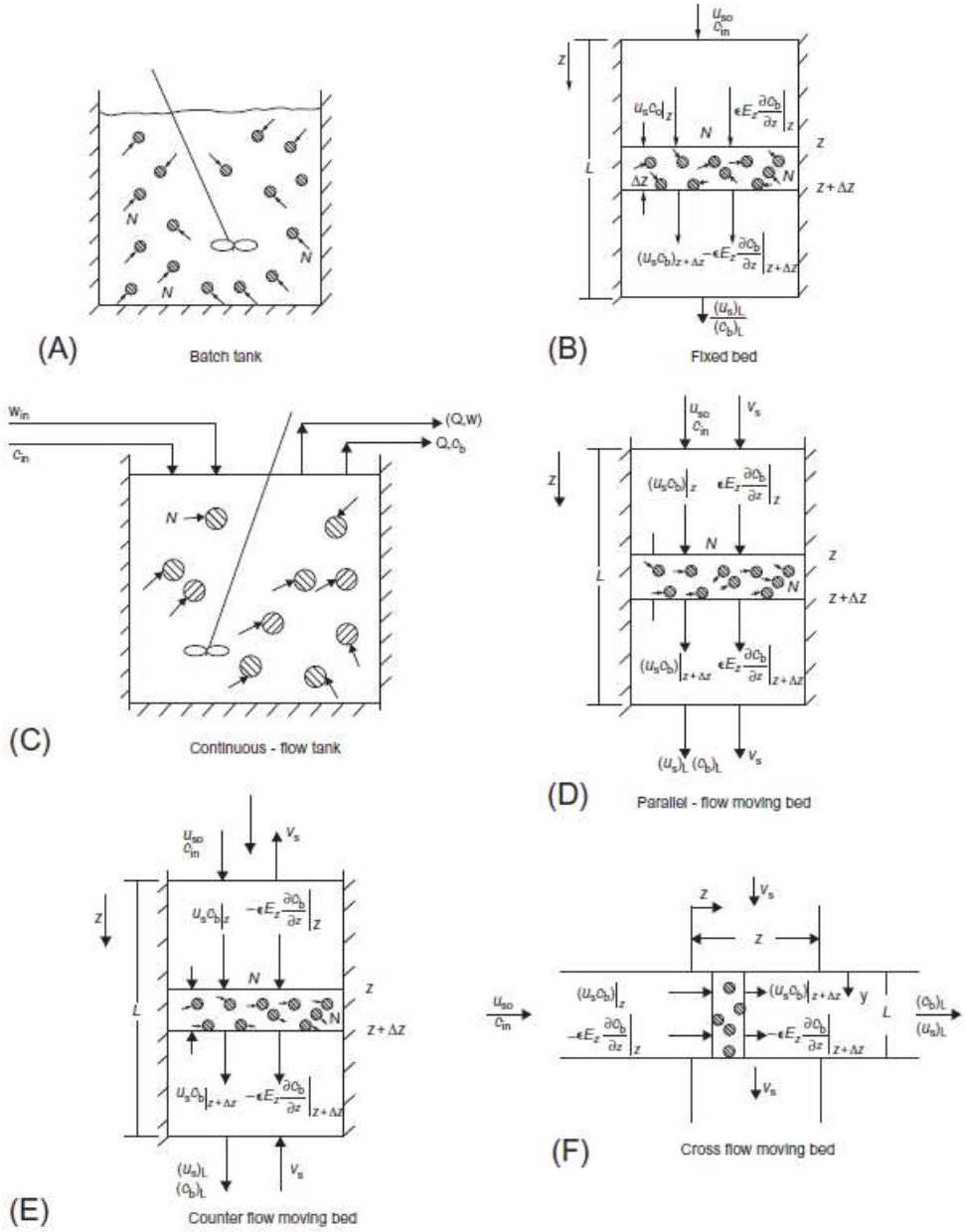

Figure 2.6: Different configurations of adsorption processes [24]

Fixed bed adsorption is a batch process starting with a fresh or newly regenerated adsorbent and lasting until the bed is saturated and regeneration is required [24]. The regeneration can be carried out by changing of temperature and/or pressure, by displacement of the adsorbed molecules, or, in some cases, by extraction of the adsorbate from the adsorbent [25]. Sometimes the pores become plugged, making reactivation necessary [25]. For continuous operation of the process various number of columns are used, arranging adsorption and regeneration at different columns at the same time [24]. These processes are also well known as temperature swing adsorption (TSA), pressure swing adsorption (PSA) or (VSA), and concentration swing adsorption (CSA) [25].

For regeneration of used AC usually pressure swing, thermal desorption, extraction or thermal reactivation processes are used. In liquid adsorption removing adsorbates and recovering them generally requires a higher energy of desorption (30 – 60 kJ/mol) compared to gases (10 – 30 kJ/mol). Usually, for this superheated steam or hot inert gas is passed through the carbon. Through this also the substances from the intergranular spaces are removed. Besides the thermal desorption also extraction with solvents can be used for AC regeneration. [26]

Complete reactivation of spent AC containing many organic substances is usually not possible, as these substances decompose at temperatures lower than required for desorption. Due to decomposition the pyrolysis products and carbon deposits remain on the internal surface of the AC. Therefore, reactivation of this AC requires temperatures of 800 – 850 °C, similar to the production process. During this process, the AC is treated with the water gas shift reaction, which restores the original surface structure and adsorption performance. [26]

2.3.4 Adsorption Equilibria

As mentioned in Chapter 2.3.2 effective adsorption presumes a solid with great micropore volume to achieve substantial adsorbate capacity as well as low diffusional resistance towards molecular flow, to ensure the interior surfaces are quickly reached. These two aspects are within the domain of equilibria and kinetics, which requires to be explored for proper understanding of the adsorption processes [22]. This chapter covers adsorption equilibrium, while the kinetic process will be addressed in Chapter 2.3.5.

The objective of investigating adsorption equilibria is to identify the most appropriate equilibrium correlation, required for prediction of adsorption parameters and quantitative comparison of adsorbent behaviour across different adsorbent systems or varying experimental conditions. [27]

The equilibrium state of adsorption is defined by the adsorbate concentration c_e, the adsorbed amount (adsorbent load) q_e of fluid on the adsorbent, and the temperature T. For single solute system this relationship can be described as follows:

$$q_e = f(c_e, T) \tag{2.1}$$

In practice it is common to keep the temperature constant, leading to adsorption isotherms (see Figure 2.7) where previous equation transforms to: [20]

$$q_e = f(c_e), \qquad T = constant \tag{2.2}$$

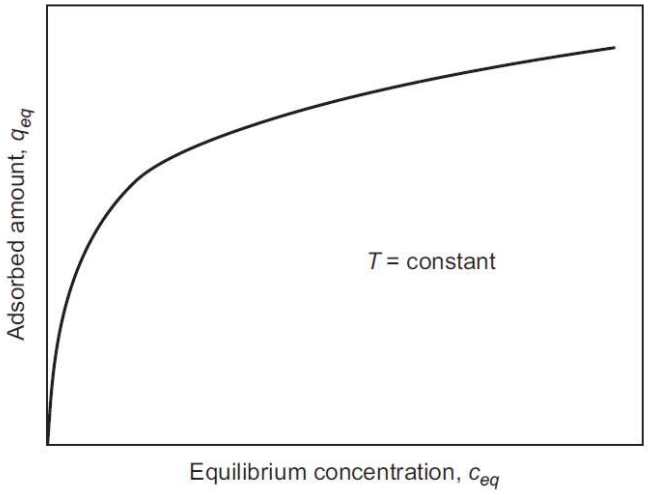

Figure 2.7: Adsorption isotherm [20]

2.3.4.1 Experimental determination of equilibrium data

The determination of equilibrium data according to Worch [20] can be carried using the bottle-point method as described in following. Thereby, a set of bottles is used to obtain multiple isotherm points in parallel. A minimum of 8 to 10 points is recommended to acquire data for subsequent isotherm fitting. Each bottle is filled with a known volume V_L and a known initial concentration c_0 of the adsorbate solution. Then, a specified mass of adsorbent m_A is added and the solution is shaken or stirred until the state of equilibrium is achieved, as illustrated in Figure 2.8. Time required to achieve equilibrium typically ranges from few hours to few weeks. The equilibration time notably is influenced by factors such as the type of adsorbent, adsorbate as well as the particle diameter of the adsorbent.

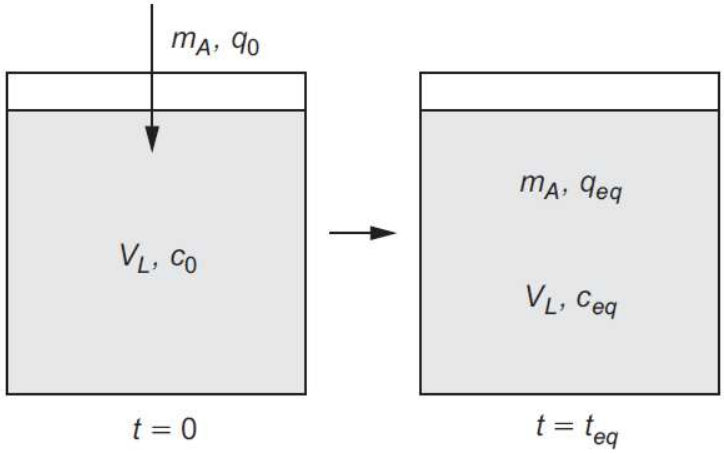

Figure 2.8: Experimental determination of adsorption equilibrium data [20]

Once equilibrium is reached, the residual concentration c_e in the liquid can be measured, from which the adsorbed amount q_e can be determined using the material

balance equation for the batch adsorption process. Assuming that other elimination processes can be ruled out and only adsorption onto the adsorbent particles takes place, the mass Δm^l removed from the liquid phase must be equal to the mass adsorbed onto the adsorbent Δm^a:

$$\Delta m^l = \Delta m^a \tag{2.3}$$

Explicitly expressed with the starting and the end values (subscripts *0* and *e*):

$$m_0^l - m_e^l = m_e^a - m_0^a \tag{2.4}$$

The mass concentration c and the adsorbent loading q are defined as:

$$c = \frac{m^l}{V_L} \tag{2.5}$$

$$q = \frac{m^a}{m_A} \tag{2.6}$$

With these the material balance can be written as

$$V_L(c_0 - c_e) = m_A(q_e - q_0). \tag{2.7}$$

The adsorbent in equilibrium measurements usually is fresh and thus not preloaded meaning $q_0 = 0$, which reduces the balance equation to

$$q_e = \frac{V_L}{m_A}(c_0 - c_e). \tag{2.8}$$

This method allows the calculation of the equilibrium loading corresponding to the equilibrium concentration, by knowing the adsorbent dose $\frac{m_A}{V_L}$ and measuring the concentration difference. This process identifies a single point on the isotherm. By variation of the adsorbent dose or the initial concentration additional points on the isotherm can be generated.

This described procedure can be illustrated using diagrams that present the equilibrium curve together with the operating line of the adsorption process. The material balance applies not only to the equilibrium state but also holds true for each concentration c and adsorbent loading q at each step of the process, generalising the equation as follows:

$$q = \frac{V_L}{m_A}(c_0 - c) \tag{2.9}$$

or

$$q = \frac{V_L}{m_A}c_0 - \frac{V_L}{m_A}c \tag{2.10}$$

This equation represents the equation of the operating line when plotted on the q-c diagram presented in Figure 2.9. The process initiates at $c = c_0$ and $q = 0$, progressing towards the equilibrium state with $c = c_e$ and $q = q_e$. The slope of the operating line is the negative reciprocal value of the adsorbent dose, $-\frac{V_L}{m_A}$. From the diagrams in Figure 2.9 it

can be seen that different isotherm points can be found by variation of the adsorbent dose at constant c_0 (a) or by changing of c_0 at constant adsorbent dose (b).

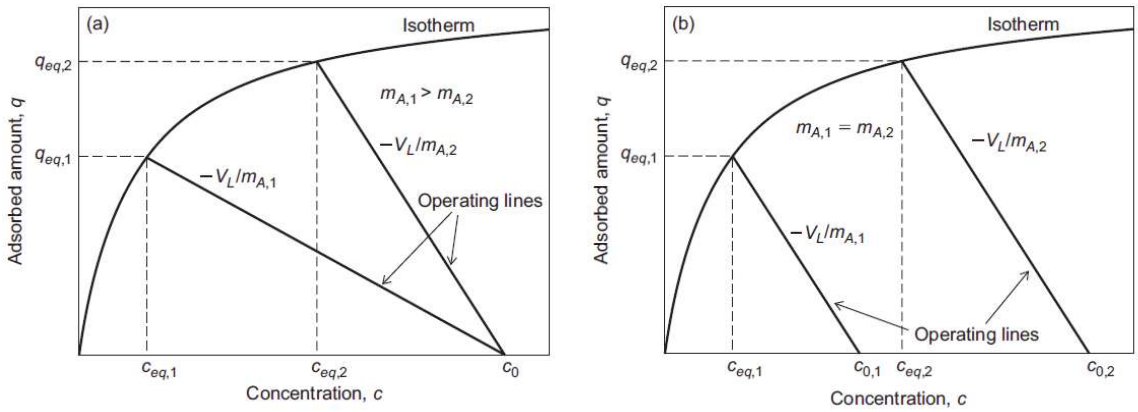

Figure 2.9: Determination of adsorption isotherms by variation of (a) an adsorbent dose and (b) initial concentration [20]

The material balance can be expressed in both molar and mass concentrations. By substituting the mass m in equations (2.3) and (2.4) with the number of moles n and applying the definitions of molar concentration $c = {n^l}/{V_L}$ and molar adsorbent loading $c = {n^a}/{m_A}$, the material balance takes on the same form as presented in Equation (2.8). Therefore, there are no limitations regarding units, and the material balance, along with resulting isotherm equations, can be utilised with either mass-related or mole-related units.

The adsorption isotherms obtained by these methods can be plotted in a diagram $q_e = f(c_e)$, and subsequently fitted to an adsorption isotherm model, which is discussed in Chapter 2.3.4.3. Often isotherms are displayed in a double logarithmic diagram when measurements are carried out over a wide concentration range.

2.3.4.2 Classification of Isotherms

Categorisation of isotherms for gas phase adsorption leaded to the BDDT (Brunauer, Deming, Deming, Teller) classification [28], resulting in five types of isotherms [22]. IUPAC expanded this classification to the six isotherm types presented in Figure 2.10 with following characteristics [29]:

Type I: Present at microporous solids with relatively small external surfaces, such as AC, molecular sieves zeolites and certain porous oxides. The amount adsorbed approaches a limiting value, which is caused by the accessible micropore volume rather than the internal surface area. Enhanced interaction between adsorbent and adsorbate in narrow micropores cause the sharp uptake at very low relative pressure. Type I(a) is characteristic with materials with predominantly narrow micropores, while I(b) is more common with a broader pore size distribution. [29]

This type can be described by Langmuir isotherms type, meaning monolayer coverage. [22]

Type II: Occurs at physisorption of most gases on nonporous or microporous adsorbents. It is characteristic for monolayer-multilayer adsorption. A sharp knee at point B usually occurs due to completion of monolayer coverage. A gradual curvature indicates that multilayer already occurs, while monolayer coverage is still in process. The adsorbed multilayer generally increases without limit at saturation pressure [29].
This shape is predesignated for description with BET isotherm model. [22]

Type III: This type shows no point B, meaning no monolayer formation. It indicates relatively weak adsorbent-adsorbate interactions, and the adsorbed molecules are clustered around the most favourable sites on the surface of a nonporous or macroporous solid. Unlike type II the amount adsorbed remains finite at the saturation pressure. [29]

Type IV: This type occurs at mesoporous adsorbents, such as many oxide gels, industrial adsorbents and mesoporous molecular sieves. Same as type II this type shows monolayer-multilayer adsorption but followed by pore condensation. This leads to a final saturation plateau. Type IV(a) occurs at pores which exceeds a certain critical width resulting in the hysteresis. Type IV(b) is shown when the mesopores are smaller in width, resulting in a completely reversible curve. [29]

Type V: This shape is similar to type III at low ranges, which can be attributed to relatively weak adsorbent-adsorbate interactions. At higher relatively pressure the molecular clustering is followed by pore filling. This type is common for water adsorption on hydrophobic microporous and mesoporous adsorbents. [29]

Type VI: This adsorption type is shown when layer-by-layer adsorption on highly uniform nonporous surface is present. Thereby, the steps show the capacity of each adsorbed layer, and the sharpness is dependent on the system and the temperature.

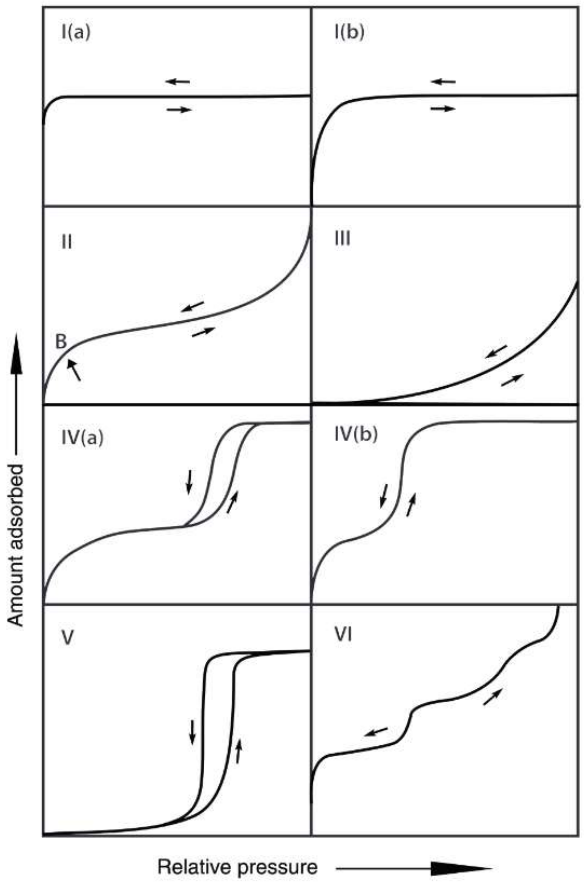

Figure 2.10: Classification of physisorption isotherm [29]

Beside describing of the mechanism, the shape of the isotherm is also an important performance indicator, see Figure 2.11. An isotherm with a convex shape shows large amount of adsorption at low pressure, favourable for adsorption. In contrast an isotherm with a concave shape requires very high concentration, unfavourable for adsorption. An irreversible isotherm with maximum adsorption already at lowest pressure would be the most favourable for adsorption. For desorption this characteristic is reversed, the concave shape would be favourable and vice versa. [30]

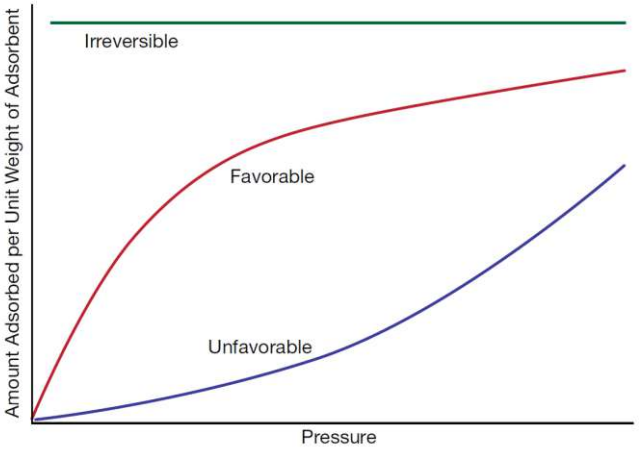

Figure 2.11: Favourable and unfavourable adsorption isotherm [30]

2.3.4.3 Adsorption Isotherms Models

As stated above, the adsorption equilibria behaviour is commonly characterised at a fixed temperature resulting in the so-called adsorption isotherms. This equilibrium correlation is usually described with the help of an equation, describing the amount of adsorbate adsorbed, q_e, as a function of concentration in the liquid, c_e [30]. The mathematical correlation of the equilibrium is usually achieved from measured data by graphically expressing the solid phase against its residual concentration in the bulk fluid phase, which then is correlated to adsorption isotherm models [27].

Different adsorbates and adsorbents require different equations and mathematical treatment due to different equilibrium relationships, which led to the development of many isotherm models [31]. There is no universal isotherm equation that can describe all experimental isotherm curves with the same accuracy known so far [20]. Three fundamental approaches are used for the development of most common adsorption isotherm models, which are

- kinetic, where adsorption equilibrium is defined as a dynamic equilibrium, with equal adsorption and desorption,
- thermodynamics, this is the base for several forms of adsorption isotherm models, and
- potential theory, which usually conveys the main idea in the generation of characteristic curve [27].

Most models using more than one approach, which leads to the difference in the physical interpretation of the model parameters [27].

Often, linearised approaches of isotherm equations are applied, which then are used for determination of parameters of isotherm equations and finding of the most fitting model by the linear least squares method [27]. These transformed data are producing slightly different results compared to nonlinear regression [20]. Depending on the model and the way of application the error could change worse and have a significant impact on the results [27]. Thus, nonlinear application should be favoured for analysing of adsorption isotherms.

Most isotherm models having two or three parameters. The only single parameter isotherm models are the irreversible and the Henry isotherm. Two of the most widely used isotherms, the Langmuir and Freundlich isotherm, are two parameter isotherms. Commonly used three parameter isotherms are Toth and Sips, which are kind of extensions of Freundlich and Langmuir isotherms. A special role plays the BET isotherm, describing multilayer physisorption based on the Langmuir theory. The most important adsorption isotherm models are described further in the following. [20], [27]

2.3.4.3.1 Single Parameter Isotherms

Irreversible isotherms represent an adsorption independent from concentration, which is typically observed for the saturation range achieved at very high concentrations, see Figure 2.12 (a). A stronger curvature of the isotherm means the irreversible isotherm extends to lower concentrations. [20]

$$q = constant \tag{2.11}$$

The Henry isotherm is the simplest form of all isotherms and describes adsorption as a linear relationship between liquid and adsorbed phases, which is commonly proportional to the partial pressure of the adsorbate. With the Henry constant K_H the relationship is defined with following equation. [31]

$$q = K_H \cdot c \tag{2.12}$$

The Henry constant K_H commonly is expressed in the unit l/g. The Henry equation represents the thermodynamically required limiting case of isotherms for very low concentrations. [20]

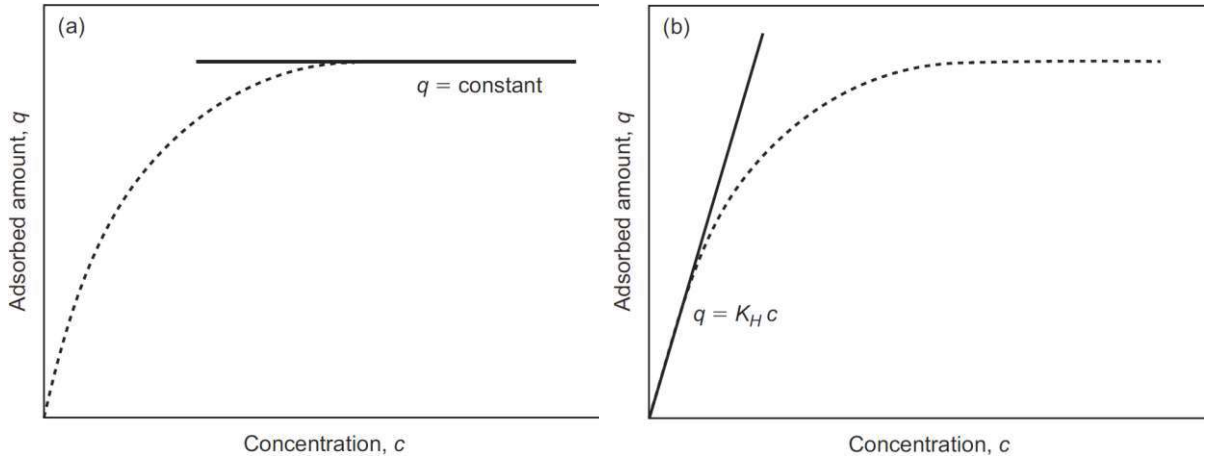

Figure 2.12: Limiting cases of adsorption isotherms: (a) irreversible isotherm and (b) linear isotherm [20]

2.3.4.3.2 Langmuir approach

One of the first theories for explanation of the adsorption phenomena was done by Langmuir [32]. Langmuir explained adsorption based on kinetic arguments, as a continual process of molecules strike onto the surface and a corresponding evaporation (desorption) of molecules from the surface with the same rate at equilibrium as presented in Figure 2.13 [22]. Thereby, following assumptions are made at describing of this process: Homogeneous surface with constant adsorption energy over all sites, adsorption is localised, and each site can accommodate only one molecule or atom [22].

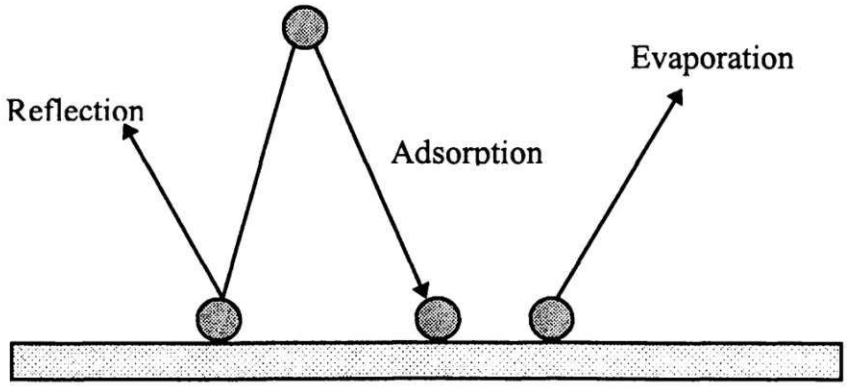

Figure 2.13: Schematic diagram of Langmuir adsorption mechanism on a flat surface [22]

This approach leads to following well known Langmuir Equation:

$$\theta = \frac{\sigma \cdot \mu}{1 + \sigma \cdot \mu} \tag{2.13}$$

Thereby θ is the fraction of sites covered with molecules and μ the number of molecules in mass striking the area per second. σ is the quotient of the fraction that condenses when unoccupied surface is struck by a molecule and the rate of molecules that evaporate on the completely covered surface. [32]

For gas adsorption the number of striking molecules is derived from the kinetic theory of gas, leading in pressure being the only variable when temperature is constant. Resulting in

$$\theta = \frac{bP}{1 + \mathrm{bP}} \tag{2.14}$$

with the constant b and the pressure P. [22]

Defining the covering fraction with the adsorbent loading we get $\theta = q/q_{max}$. Furthermore, using the equilibrium concentration of absorption in the solution instead of pressure, Equation (2.14) can be defined for liquids as:

$$q = q_{max} \frac{K_L c}{1 + K_L c} \tag{2.15}$$

In Equation (2.15) it can be noticed, that for very low concentrations with $K_L \cdot c \ll 1$, the Langmuir equation reduces to Henry isotherm

$$q = q_{max} \cdot K_L \cdot c = K_H \cdot c \tag{2.16}$$

while at very high concentrations the with $K_L \cdot c \gg 1$ the saturation capacity will be achieved, resulting into a constant loading due to complete coverage of all adsorption sites with adsorbate molecules (called monolayer coverage). [20], [22]

$$q = q_{max} = constant \tag{2.17}$$

As we can see the Langmuir isotherm shows plausible limiting cases. However, despite these limiting cases it is often not suitable to describe the experimental isotherm data of aqueous solutions. The cause is probable the fact that the Langmuir isotherm is

theoretically derived from assumptions that are often not fulfilled. Especially mono layer coverage of the adsorbent surface and energetic homogeneity of the adsorption sites. This is especially true for the most important adsorbent AC. Nonetheless, there are cases where the Langmuir isotherm showed applicability despite clear deviations from the underlying assumptions. [20]

2.3.4.3.3 BET (Brunauer, Emmett, Teller) Theory

The BET theory, first developed by Brunauer, Emmett and Teller [33], describes adsorption with multiple layers, see Figure 2.14. It uses the same assumption as used in the Langmuir theory of an energetically homogeneous surface and no interaction among the adsorbed molecules. Due to its simplicity, it is the most important equation for the characterisation of mesoporous solids. [22]

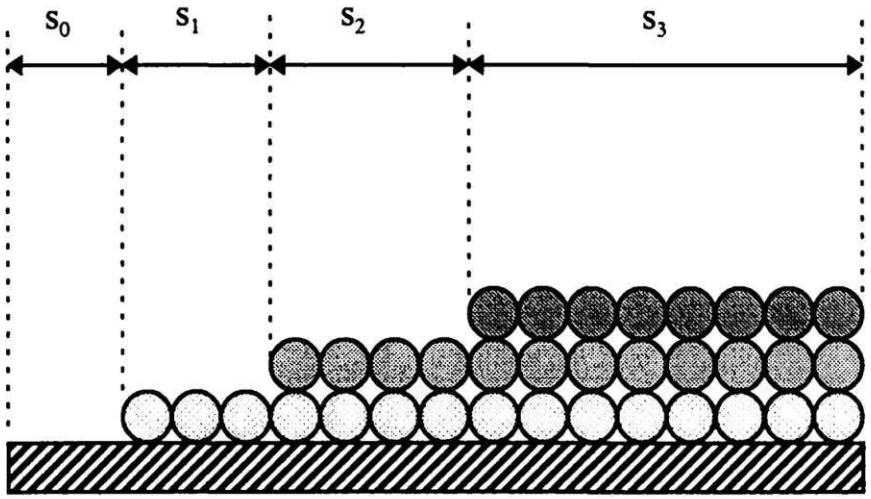

Figure 2.14: Multiple layering in BET theory [22]

For simplification, this theory has two assumptions. First that the heat of adsorption is equal for all upper adsorbed layers and it is equal to the heat of condensation. Second, the ratio of rate constants of adsorption and desorption are equal for these layers. This leads to the classical form of the BET equation: [34]

$$\frac{q}{q_m} = \frac{C \cdot x}{(1-x)(1-x+Cx)} \tag{2.18}$$

Thereby q_m is the adsorbed amount when completely covered by one unimolecular layer. The constant C is the result from the equilibrium constant of the first layer C_S divided by the second layer C_L. [34]

$$C = {}^{C_S}/_{C_L} \tag{2.19}$$

For gas adsorption it is assumed that q will be infinite when the partial pressure P of the adsorbate equals its saturation pressure P^S. This means that x must be 1 when $P = P^S$ resulting in $x = {}^{P}/_{P^S}$. Furthermore, ${}^{1}/_{C_L}$ can be replaced by P^S, simplifying the equation by reducing the unknown to the two q_m and C. This assumption is not possible in liquid

phase, where it is possible that no layers are adsorbed even at saturation concentration, or a high adsorption already can be present at very low concentrations. Therefore, for liquid adsorption the classical BET equation cannot be used. However, it can be modified by replacing of P^S by $1/C_L$ and P by c, resulting in the equation for liquid phase adsorption as: [34]

$$q = q_m \frac{C_S \cdot c[1-(n_{BET}+1)(C_L \cdot c)^{n_{BET}} + n_{BET}(C_L \cdot c)^{n_{BET}+1}]}{(1-C_L \cdot c)(1+\left(\frac{C_S}{C_L}-1\right)C_L \cdot c - \left(\frac{C_S}{C_L}\right)(C_S \cdot c)^{n_{BET}+1})} \tag{2.20}$$

Here n_{BET} is the number of adsorbed layers. One layer, meaning $n_{BET} = 1$, results in the Langmuir equation. Assuming a number of infinite layers ($n_{BET} = \infty$), we get the BET equation for liquid phase adsorption: [34]

$$q = q_m \frac{C_S \cdot c}{(1-C_L \cdot c)(1-C_L c + C_S \cdot c)} \tag{2.21}$$

The BET equation is able to describe isotherm types I, II, and III. Type III can be created when the forces between adsorbate and adsorbent are smaller than that between adsorbate molecules in the liquid state. The type IV and type V isotherms cannot be described by the BET theory since it assumes infinite layers of molecules to build up on top of the surface. To achieve a limit number of layers the equation must be modified resulting in the n-layer BET equation. [22]

2.3.4.3.4 Freundlich Isotherm

The Freundlich isotherm is the oldest known used empirical equation dating back to the end of the 19th century. It is named after Freundlich due to his extensive use of it. The isotherm equation was commonly used to describe the equilibrium of gas adsorption by a heterogeneous adsorbent and is written as follows. [31]

$$q = K_F \cdot c^{n_F} \tag{2.22}$$

The adsorption coefficient K_F, characterises the strength of adsorption, a higher value of K_F leading to a higher possible adsorbent loading. The heterogeneity of the adsorbent surfaces is described by the Freundlich exponent n_F. Lower values of n_F are favourable since they lead to a more concave curve, which means relatively high adsorbent loadings at low adsorbate concentrations. On the other hand, higher values of n_F leading to a convex curve and are unfavourable. [20]

The Freundlich isotherm is originally an empirical equation, however it can be derived from a solid theoretical basis. It can be obtained by assumption of a heterogeneous surface, where the adsorption energy is distributed and the surface topography is patchwise, meaning sites with same adsorption energy are grouped together. Thereby, the adsorption energy is the energy of interaction between adsorbate and adsorbent. Each patch is independent from each other and there is no interaction between them. Furthermore, it is assumed that on each patch adsorbate molecule only adsorbs onto one

adsorption site as in Langmuir equation. This means that for the description of equilibria of each patch the Langmuir equation is applicable. [22]

In contrast to the Langmuir isotherm, the Freundlich isotherm cannot describe the saturation effect at very high concentrations and the linear behaviour at very low concentrations, which is why it is best applicable at medium-range adsorbate concentrations [20]. The Freundlich isotherm is widely used to analyse the adsorption of aqueous solutions [20], especially the adsorption of organics from aqueous systems on AC [22]. Applications in gas phase systems with heterogeneous surfaces is also possible, but the range of pressure is not as wide as in Langmuir due to lack of proper limits for very low and high pressure [22].

2.3.5 Adsorption Kinetics

Adsorption processes commonly do not reach equilibria instantaneously, especially when dealing with porous adsorbents. The movement of mass from the solution to the adsorption sites inside the adsorbent particles is hindered by factors known as mass transfer resistances, which dictate the time it takes to reach the state of equilibrium. The progression of this time-dependent adsorption process is known as adsorption kinetics. Generally, the rate at which adsorption occurs is restricted by diffusion processes happening both towards the external surface and within the porous adsorbent particles. Analysing that adsorption kinetics becomes necessary to evaluate the rate-limiting mechanisms of mass transfer and to determine characteristic mass transfer parameters. These parameters, in conjunction with equilibrium data, are crucial input factors used to determine the necessary contact times in slurry reactors and to design fixed-bed adsorbers. [20]

2.3.5.1 Mass Transfer Mechanisms

As stated by Weber & Smith [23] in the case of microporous adsorbents, e.g., AC, the adsorption process is characterised by four consecutive steps illustrated in Figure 2.15:

1. Mass transfer from the bulk liquid phase to the hydrodynamic boundary layer surrounding the adsorbent particle.
2. Diffusive film transport through the boundary layer to the surface of the adsorbent, termed “film diffusion” or “external diffusion”.
3. Transport into the interior of the adsorbent particle termed “intraparticle diffusion” or “internal diffusion by **a** diffusion through the pore liquid of the internal pores or by **b** diffusion along the pore wall in the adsorbed state.
4. Adsorption or attachment of the molecule at a suitable “site” due to energetic interaction between the molecule and the adsorption site.

In generally it can be assumed that the first and the fourth step are very fast, thus the total rate of adsorption process is characterised by film and/or intraparticle diffusion. The

slower of these two processes determines the total absorption rate, as film and intraparticle diffusion act in series. Therefore, it is very important to look at the impact factors on these two diffusion rates. [20]

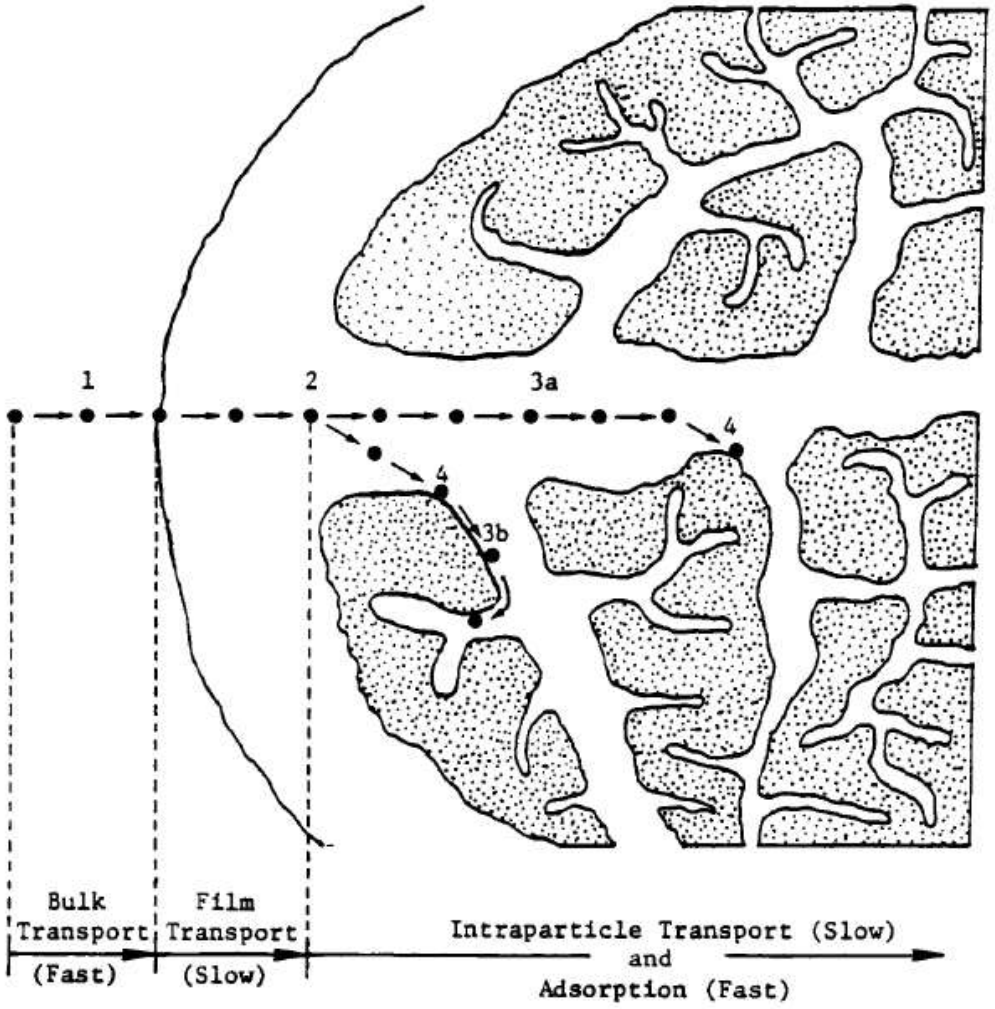

Figure 2.15: Transport processes in adsorption by porous adsorbents [23]

A fundamental distinction between film diffusion and intraparticle diffusion lies in their reliance on hydrodynamic conditions, such as the stirrer velocity in slurry reactors or the flow velocity in fixed-bed adsorbers. This distinction allows us to differentiate them and makes it possible to influence their relative contribution to the overall adsorption rate. Increasing the stirrer or flow velocity reduces the boundary layer thickness and thereby increasing the rate of film diffusion, while intraparticle diffusion remains unaffected. Furthermore, the particle's radius has an impact on both film and intraparticle diffusion due to alterations in surface area and diffusion pathways. [20]

Mass transfer within the adsorbent particle typically occurs through both pore diffusion and surface diffusion simultaneously (3a and 3b of the previous listed steps), making it challenging to separate their respective contributions. As a result, it is often assumed that one intraparticle diffusion mechanism predominates, which is then incorporated into the kinetic model. For many adsorption processes involving porous adsorbents and aqueous

solutions, the intraparticle diffusion can be accurately described using a surface diffusion approach. [20]

2.3.5.2 Experimental determination of kinetic curves

To investigate adsorption kinetics, a specific volume V_L is brought into contact with the mass of adsorbent m_A, and the subsequent change in concentration over time is recorded. Direct real-time concentration measurements are often challenging, so samples must be collected at predefined intervals, disrupting the kinetic measurement by removing a portion of the liquid from the system each time. This issue can be mitigated by using a sufficient large solution volume, making the loss of volume and adsorbate negligible compared to the total volume. While it is theoretically possible to calculate the impact of changes in solution volume and adsorbate mass using mathematical calculations, this approach is often deemed impractical in practice. [20]

Kinetic experiments will lead to a kinetic curve in the form of

$$c = f(t) \tag{2.23}$$

where c is the concentration and t the time. [20]

During the adsorption process the concentration of adsorbate with an initial concentration c_0 will decrease until the equilibrium concentration c_e is reached. Hereby, the material balance equation

$$\bar{q}(t) = \frac{V_L}{m_A}[c_0 - c(t)] \tag{2.24}$$

holds for each time during the process. Consequently, the kinetic curve can also be expressed as

$$\bar{q} = f(t) \tag{2.25}$$

With $\bar{q}$ representing the mean solid-phase concentration (adsorbed amount). Figure 2.16 presents typical kinetic curves. [20]

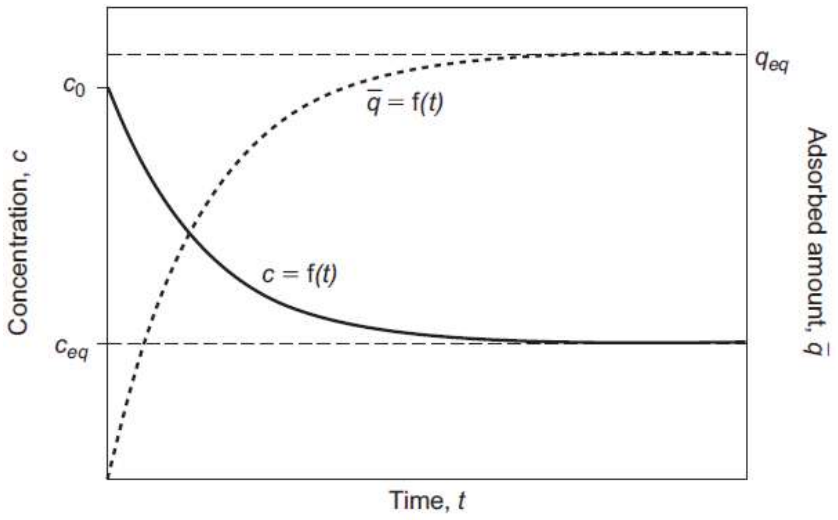

Figure 2.16: Progress of concentration and adsorbent loading with time [20]

The experimentally obtained kinetic curve serves as the dataset for a fitting process with a kinetic model (see Chapter 2.3.5.3), where the fitting parameters are the mass transfer coefficients. For selection of a specific kinetic model, assumption regarding the dominant transport mechanism needs to be done in prior, called the transport hypothesis. The transport hypothesis is verified by comparing the calculated and experimental kinetic curves, providing insights into the relevant kinetic mechanisms and values for transport parameters. [20]

The experimentally determined film diffusion mass transfer coefficients are only valid for the specific given experimental setup and cannot be applied to other experimental conditions or technical adsorbers, as film diffusion depends on hydrodynamic conditions. In slurry reactors, film diffusion impacts only the very early stages of the adsorption process and can thus be neglected. However, in fixed-bed adsorbers, film diffusion plays a role in shaping the breakthrough curve and should be factored in the curve model, which can be done by estimation of mass transfer coefficients from hydrodynamic parameters using empirical correlations. [20]

As a result, most kinetic experiments aim to determine mass transfer parameters exclusively for internal diffusion processes, which are independent of hydrodynamic conditions and can be applied to different process conditions. Therefore, kinetic experiments are often designed in a way that film diffusion becomes fast enough to be excluded from the mathematical model. This simplifies the experimental determination of the mass transfer coefficient, but it is crucial to consider the requirements in the choice of the reactor for the experiment. [20]

Typical reactors used for the kinetic experiments include slurry batch reactors, basket reactors, and differential column batch reactors, as shown in Figure 2.17 and Figure 2.18. [20]

Slurry batch reactors are commonly used to determine equilibrium data but can also serve for conducting kinetic experiments. These reactors consist of a tank equipped with an electric stirrer, which minimises the impact of film diffusion by high stirrer speeds. However, increasing the stirrer velocity risk damaging the adsorbent particles, introducing errors due to the size-dependent nature of mass transfer coefficients. This issue can be prevented by securing the adsorbent in baskets, which can be positioned either directly on the stirrer shaft, known as a spinning basket reactor or Carberry reactor, or on the walls of the vessel. [20]

In a differential column batch reactor, the solution flows through a fixed bed of limited height with high flow velocities, eliminating the influence of film diffusion. The arrangement of adsorbent particles within the fixed bed protects them from damage. The solution is recirculated, allowing the reactor to function similarly to a batch reactor and enabling the application of batch adsorption models to fit kinetic curves and determine mass transfer coefficients. Samples are extracted from the reservoir. [20]

Determining of the minimum stirrer or flow velocity requires elimination of impact by film diffusion, which is done by measuring several kinetic curves with increasing stirrer or flow velocities. When the adsorption rate is no longer influenced by film diffusion, the shape of the kinetic curve remains consistent. [20]

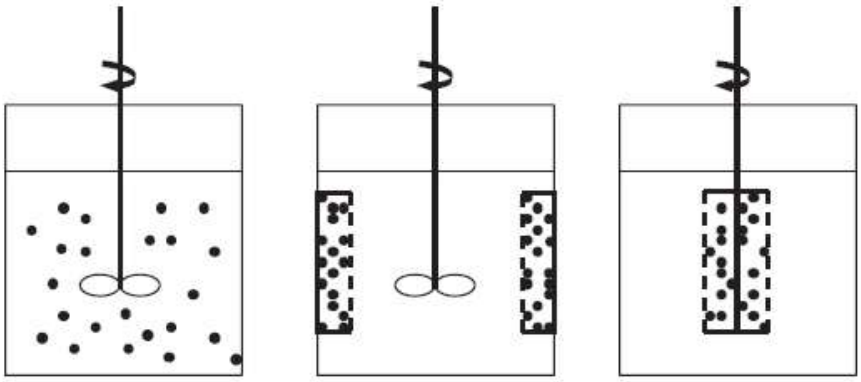

Figure 2.17: Slurry batch reactor (left) and different types of basket reactors (middle and right) for kinetic experiments [20]

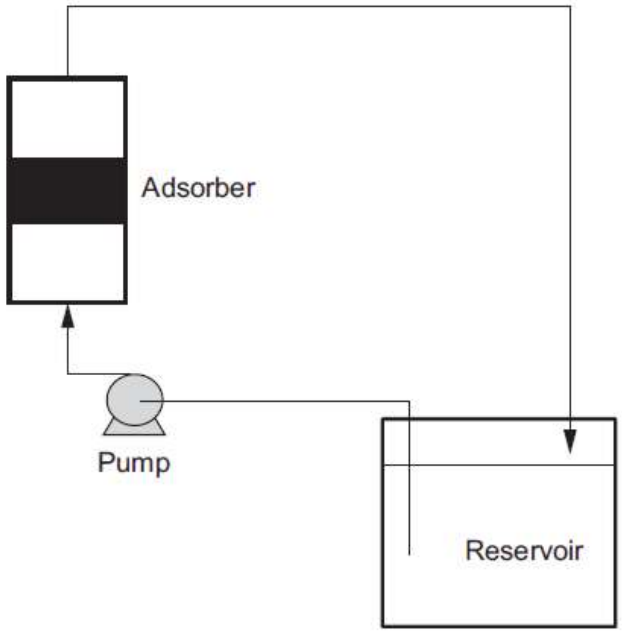

Figure 2.18: Differential column batch reactor for kinetic experiments [20]

2.3.5.3 Mass Transfer Models

Fundamental for understanding of the adsorption process is the knowledge of the mechanism of adsorbate uptake by adsorbents, including an equation describing the process under different operating conditions. As previously mentioned, the adsorption process involves external diffusion (or film diffusion), internal diffusion (or intraparticle diffusion), and the adsorption of the molecule onto active sites of the solid [20]. Usually, these mechanisms contribute to the adsorbate uptake in different extends, resulting in one rate limiting mechanism.

Literature provides a great variety of kinetic models describing the uptake process for all kinds of applications, all using different assumption and simplifications. Mostly they describe only one rate limiting transport mechanisms, assuming others proceed faster and are negligible in the modelling. Determination of the limiting process can be carried out by fitting various models. The model fitting the kinetic data best is considered the optimal model, giving information of the adsorbate uptake process. Some of the most common used and best suitable for the present process in this study are discussed below.

2.3.5.3.1 External Mass Transfer

The external mass transfer, transport of the adsorbate from the bulk liquid to the external surface of the adsorbent particle, can be described by the film diffusion. Thereby, it is assumed that the diffusion inside the particle is very fast and the diffusion through the film with the thickness δ surrounding the particle is the rate limiting factor. The concentration at the external surface, c_s, of the adsorbent is always lower as in the bulk fluid phase, c, until equilibrium is achieved, resulting in a concentration gradient as the driving force. This is illustrated in Figure 2.19, where the adsorbent loading at the external surface, q_s, is the equilibrium loading related to the concentration at the surface c_s. [20]

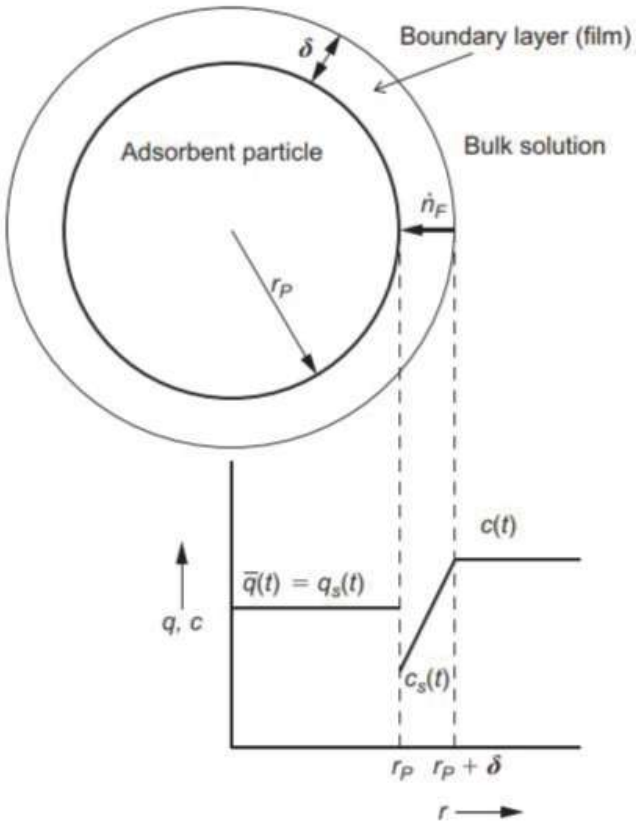

Figure 2.19: Concentration profiles in the case of rate-limiting film diffusion [20]

The mass transfer equation for film diffusion can be derived using Fick's law. Assuming a linear gradient within the boundary layer and using the material balance equation the film mass transfer equation can be expressed: [20]

$$\frac{d\bar{q}}{dt} = k_F a_m (c - c_s) \tag{2.26}$$

Thereby k_F is the film mass transfer coefficient, which is defined with the diffusion coefficient in aqueous phase, D_L, and the film thickness as: [20]

$$k_F = \frac{D_L}{\delta} \tag{2.27}$$

The specific particle surface, a_m, related to the adsorbent mass available, m_A, in the reactor is defined with the total surface area, A_s, as $a_m = A_s/m_A$. Other definitions related to adsorbent or the reactor volume are also possible. Alternatively, the film mass transfer equation can also be expressed for the concentration decay: [20]

$$\frac{\mathrm{d}c}{\mathrm{d}t} = -k_F a_m \frac{m_A}{V_L}(c - c_s) \tag{2.28}$$

The film mass transfer equation can be solved together with

- the material balance equation,
- the initial conditions: $c = c_0$ and $\bar{q} = 0$ at $t = 0$, and
- the equilibrium relationship: $q_s = \bar{q} = f(c_s)$.

These set of equations generally must be solved numerically. An analytical solution only exists for the case of a linear isotherm. [20]

2.3.5.3.2 Intraparticle Diffusion

Mass transport inside the particle is affected by the two mechanisms of surface and pore diffusion. The general approach for description is to assume both mechanisms are operative at the same time. With the surface diffusion coefficient, D_S, and the pore diffusion coefficient, D_P, the macroscopic conservation equation is:

$$\varepsilon_p \frac{\partial c}{\partial t} + \rho_p \frac{\partial q}{\partial t} = \frac{1}{r^2}\frac{\partial}{\partial r}\left[D_p r^2 \frac{\partial c}{\partial r}\right] + \frac{\rho_p}{r^2}\frac{\partial}{\partial r}\left[D_s r^2 \frac{\partial q}{\partial r}\right] \tag{2.29}$$

Where ε_p is the porosity and ρ_p the density of the particle. r is the radial distance measured from the centre of the adsorbent pellet. [20], [35]

Solution of this equation requires the specification of the relationship between q and c. Since the adsorption step commonly is much faster than the mass transfer step, these two parameters are assumed to be in equilibrium $q = f(c)$, with $f(c)$ being the isotherm equation. Furthermore, the initial and boundary conditions are necessary for solution of the conservation equation. [35]

Is only one of the two mechanisms dominating Equation (2.29) reduces to

$$\varepsilon_p \frac{\partial c}{\partial t} + \rho_p \frac{\partial q}{\partial t} = \frac{1}{r^2}\frac{1}{r}\left(D_P r^2 \frac{\partial c}{\partial r}\right) \tag{2.30}$$

for pore diffusion, or

$$(\varepsilon_p/\rho_p)\frac{\partial c}{\partial t} + \frac{\partial q}{\partial t} = \frac{1}{r^2}\frac{\partial}{\partial r}\left(D_S r^2 \frac{\partial q}{\partial r}\right) \tag{2.31}$$

for surface diffusion [35]. Simplification to only a single mechanism showed to be an appropriate approach for practical cases, especially the surface diffusion when neglecting the term $\left(\varepsilon_p/\rho_p\right)\frac{\partial c}{\partial t}$, also known as the homogeneous surface diffusion model (HSDM), was proved to be suitable for strongly adsorbable substances on porous adsorbents [20]. Generally, equations for intraparticle diffusion need to be solved with numerically methods and analytical solutions are only available for the special case of linear isotherms [20].

In the case of a linear isotherm the molecules in the pores and the adsorbed molecules at any point within the particle are in equilibrium with each other, despite the presence of concentration gradient within the particle exist, see Figure 2.20 [22]. Thus, an effective diffusion coefficient $(D_S)_e$ can be defined as

$$(D_S)_e = D_S + \frac{D_P}{\rho_p K_H} \tag{2.32}$$

with the relationship

$$(D_P)_e = \rho_p K_H (D_S)_e \tag{2.33}$$

which shows that in case of a linear isotherm each effective diffusion coefficients can be converted to each other [20]. This means that surface as well as pore diffusion models can be used for describing of the kinetic curve with identical solutions and distinction between the two mechanisms is not possible [20]. This and neglecting the molecule concentration in the pores ($\frac{\varepsilon_p c}{\rho_p} \ll q$) simplifies Equation (2.29) to as follows [36]:

$$\frac{\partial q}{\partial t} = \frac{1}{r^2}\frac{\partial}{\partial r}\left[r^2 (D_S)_e \frac{\partial c}{\partial r}\right] \tag{2.34}$$

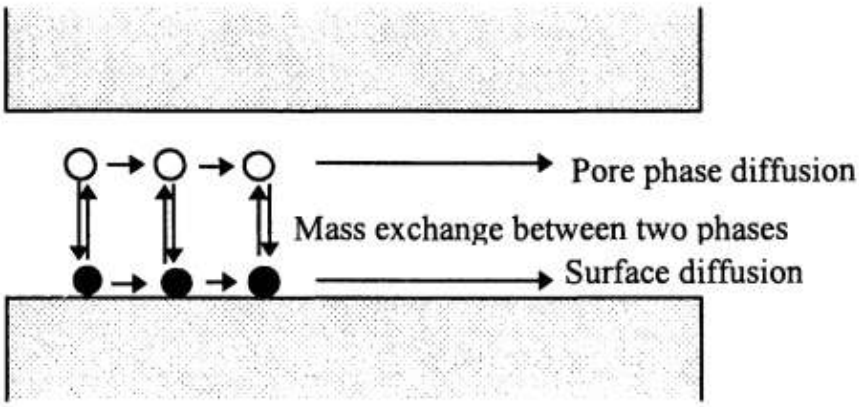

Figure 2.20: Schematic of parallel pore and surface diffusion at linear isotherm [22]

For the common case of a finite bath batch adsorption and linear isotherm an analytical solution by Clark [37] can be used. Thereby, Equation (2.43) is solved with the macroscopic conservation equation for a batch adsorption

$$V_L \frac{\partial c}{\partial t} + \frac{m_A}{\rho_p \left(\frac{4}{3}\right)\pi a_p^3} N = 0 \tag{2.35}$$

Together with the boundary conditions of $q = 0$ for $0 < r < a_p$ and $t < 0$ and the initial concentration, c_0, this will lead to the final equation of the kinetic curve as follows:

$$\frac{\bar{q}}{\bar{q}_\infty} = 1 - \sum_{n=1}^{\infty} \frac{6\alpha(\alpha+1)}{9(1+\alpha)+\gamma_n^2\alpha^2} \exp\left[-\frac{(D_S)_e \gamma_n^2 t}{a_p^2}\right] \tag{2.36}$$

with the parameters α and $\bar{q}_\infty$ defined as

$$\alpha = \frac{V_L}{m_A K_H} \tag{2.37}$$

and

$$\bar{q}_\infty = \frac{(V_L/m_A)c_0}{1+\alpha} \tag{2.38}$$

The value γ_n is calculated by

$$\tan\gamma_n = \frac{3\gamma_n}{3+\alpha\gamma_n} \tag{2.39}$$

and the series has to be solved for all nth nonnegative solutions of γ_n. [36]

Another widely applied equation for intraparticle mass transport is the Weber and Morris model. Thereby, batch adsorption is assumed to be carried out with an infinite bath, meaning V_L/m_A is infinitely large and c remains to be constant c_0. Assuming a linear adsorption equilibrium relationship, a negligible external mass transfer and the same initial and boundary conditions as before, Equation (2.43) can be solved for the fraction of adsorption uptake as follows:

$$\frac{\bar{q}}{q_e} = 1 - \frac{6}{\pi^2}\sum_{n=1}^{\infty}\frac{1}{n^2}\exp\left[\frac{-(D_S)_e\, n^2\, \pi^2\, t}{a_p^2}\right] \tag{2.40}$$

This equation can be simplified for a small time to a more useful form:

$$\frac{\bar{q}}{q_e} = 6\left(\frac{(D_s)_e\ t}{a_p^2}\right)^{\frac{1}{2}} \cdot \left[\frac{1}{\sqrt{\pi}} + 2\sum_{n=1}^{\infty} i\,\mathrm{erfc}\left(\frac{n\,r}{\sqrt{(D_s)_e\ t}}\right)\right] - 3\frac{(D_s)_e\ t}{a_p^2} \tag{2.41}$$

Furthermore, for $\bar{q}/q_e < 0.3$, this equation can be simplified to

$$\frac{\bar{q}}{q_e} = \frac{6}{\sqrt{\pi}}\left[\frac{(D_s)_e\ t}{a_p^2}\right]^{\frac{1}{2}} \tag{2.42}$$

leading to the widely used Weber and Moris Model [38] expressed by the linear relationship between the adsorbent loading and the square root of time

$$\bar{q} = k_{W\&M}\, t^{\frac{1}{2}} \tag{2.43}$$

where $k_{W\&M}$ is a constant with a relationship to the effective intraparticle diffusion coefficient $(D_S)_e$ as follows:

$$k_{W\&M} = \frac{3.385}{1+\alpha}\left(\frac{V_L}{m_A}\right)c_0\frac{[(D_S)_e]^{1/2}}{a_p} \tag{2.44}$$

For $\bar{q}/q_e > 0.7$ the infinite series of Equation (2.40) converges rapidly for large values of $(D_S)_e\,\pi^2\,t/a_p^2$. Thus, only the leading term of the series suffices, leading to the following equation:

$$\frac{\bar{q}}{q_e} = 1 - \frac{6}{\pi^2}\exp\left[\frac{-(D_s)_e\,\pi^2\,t}{a_p^2}\right] \tag{2.45}$$

This indicates another linear relationship between $\ln\left(1-\frac{\bar{q}}{q_e}\right)$ and $\frac{(D_s)_e\,\pi^2\,t}{a_p^2}$ for the latter part of the adsorption. [36], [39]

As mentioned, Equation (2.37) is only applicable for $\bar{q}/q_e < 0.3$. For application of the Weber and Morris model for the entire adsorption process, which often is the case in literature, Wang and Guo [39] suggests dividing of the kinetic data in two groups. For the first group, until time t_1, Equation (2.37) is used. For the second group starting from t_1 until t_2 the equation as follows is suggested:

$$\bar{q} - q_{t_1} = k_{W\&M}\,(t - t_1)^{\frac{1}{2}} \tag{2.46}$$

2.3.5.3.3 Simplified intraparticle diffusion model

Solving of equations for intraparticle diffusion (Equation (2.29), (2.30), and (2.31)) generally requires high mathematical effort. To reduce the effort the linear driving force (LDF) model was developed, first introduced by Glueckauf and Coates [40] and Glueckauf [41]. This model assumes that the decrease in adsorbent loading occurs within a fictive solid film, which is comparable to the solution-side film in the film diffusion model. Thereby, the concentration gradient in Fick's law of the surface diffusion model is replaced by a linear concentration difference between the equilibrium loading at the outer particle surface, q_s, and the mean loading of the particle, $\bar{q}$:

$$\dot{n}_S = \rho_P D_S \frac{\partial q}{\partial r} \rightarrow \dot{n}_S = \rho_P k_S (q_s - \bar{q}) \tag{2.47}$$

where ρ_P is the particle density and k_S the intraparticle mass transfer coefficient. The concentration gradient is illustrated in Figure 2.21 left in the case of film diffusion and right without external film diffusion. [20]

Using the material balance equation and Equation (2.47), the equation for the adsorbate uptake can be defined as

$$\frac{\mathrm{d}q}{\mathrm{d}t} = k_S^*(q_S - \bar{q}) \tag{2.48}$$

where k_S^* is the modified intraparticle mass transfer coefficient, which depends on the definition of the specific surface area (see film diffusion). The specific surface area related to the adsorbent mass is defined as:

$$a_m = \frac{A_S}{m_A} \tag{2.49}$$

This results in the definition of the modified intraparticle mass transfer coefficient as:

$$k_S^* = k_S\,a_m\,\rho_P. \tag{2.50}$$

For spherical adsorbent particles, the relationship between the mass transfer coefficient and the surface diffusion can be defined as

$$k_S^* = \frac{3\,k_S}{r_P} = \frac{15\,D_s}{r_P^2} \tag{2.51}$$

with the surface diffusion coefficient D_s. [20]

To solve Equation (2.48), the initial and boundary conditions are:

$$\bar{q} = 0, \quad c = c_0 \quad at \quad t = 0 \tag{2.52}$$

and

$$\rho_P k_S (q_s - \bar{q}) = k_F a_m (c - c_s) \quad at \quad t > 0 \tag{2.53}$$

Boundary conditions of Equation (2.53) only have to be considered if film diffusion is also relevant for the adsorption kinetics. [20]

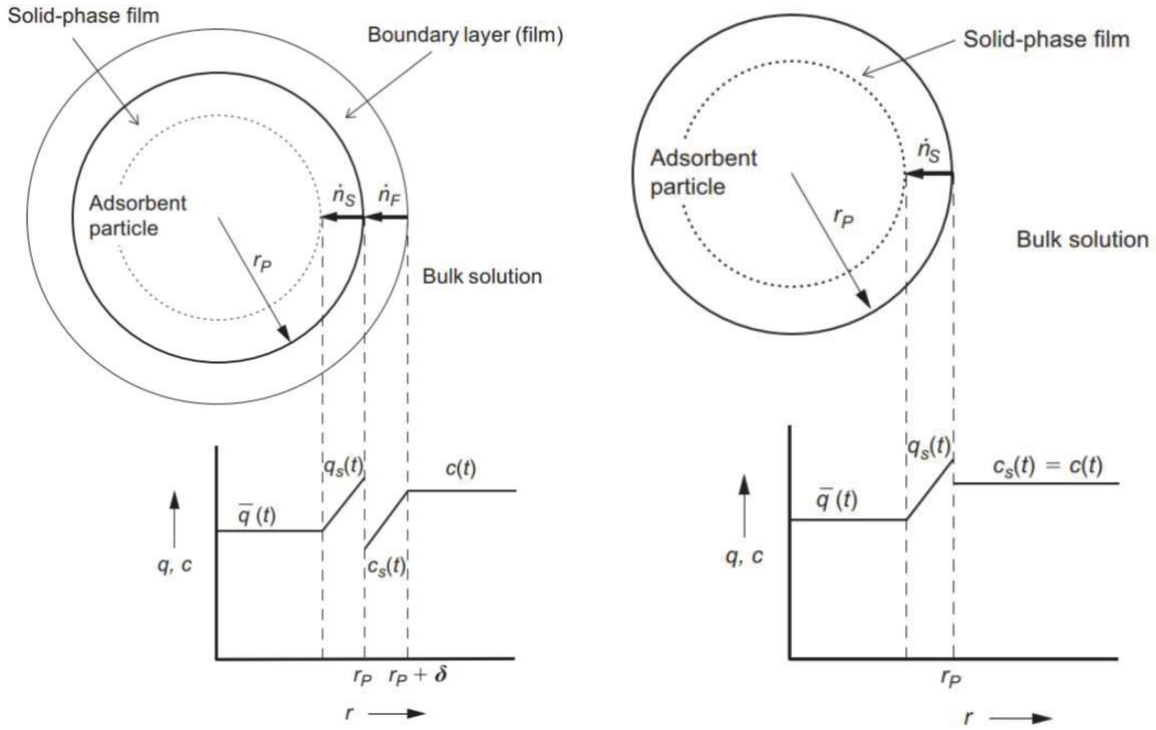

Figure 2.21: Concentration profiles of the LDF model with external mass transfer resistance left and without external mass transfer resistance right [20]

2.3.5.3.4 Empirical Models

Beside previous diffusion models also simple empirical models based on chemical reaction kinetics are widely used in recent publications for analysis of adsorption kinetics. The most common are the Lagergren and the pseudo second-order Model. These are applied to different adsorbates, including organic substances and heavy metals, adsorbed mainly onto alternative adsorbents (biosorbents, low-cost adsorbents) as well as AC. For several reasons discussed below, these models must be viewed very critically. [20], [36]

The Lagergren model or first order model, first suggested by Lagergren [42], assumes that the adsorbate uptake follows a first-order rate law, leading to the following equation:

$$\frac{d\bar{q}}{dt} = k_1(q_e - \bar{q}) \tag{2.54}$$

Thereby k_1 is the first order rate constant. Integration with the conditions $\bar{q} = 0$ at $t = 0$ leads to

$$ln\frac{(q_e - \bar{q})}{q_e} = -k_1 t \tag{2.55}$$

By plotting the data according to this equation, k_1 can be easily estimated under the condition that equilibrium loading is available from the isotherm and material balance. [36]

Equation (2.54) and the LDF model are very similar. However, at the LDF model the driving force is the difference between the equilibrium adsorbent loading at the outer surface and the mean adsorbent loading, while in the Lagergren model the driving force is the difference between the (final) equilibrium loading and the loading at time t. Therefore, the mean adsorbent loading $\bar{q}$ is the only time dependent value, while in the LDF model, both loadings q_s and $\bar{q}$ change with time, resulting in a slightly different kinetic curve. [20]

The pseudo second-order law is described by the following basic equation:

$$\frac{d\bar{q}}{dt} = k_2(q_{eq} - \bar{q})^2 \tag{2.56}$$

where $k_2\ is$ the second-order rate constant, similar to the first equation. Integration with the same initial condition as in Equation (2.54) leads to:

$$\frac{t}{\bar{q}} = \frac{1}{k_2 q_e^2} + \frac{t}{q_e} \tag{2.57}$$

The rate constant k_2 can be determined using this equation by linear regression. Given the equilibrium adsorbent loading q_e from the isotherm, the linear regression can be carried out with t/q_e as the independent variable. [20]

As mentioned earlier, reaction kinetic models must be viewed critically. First, it is well known from long-term experience that intraparticle diffusion plays a key role in the adsorption process with porous adsorbents and is typically the rate limiting factor. The final adsorption step being much faster compared to diffusion is a widely accepted assumption. Also, the intraparticle diffusion model can be extended to account for the additional impact of film diffusion, which is not possible for the reaction kinetic models. Furthermore, the rate coefficients lack theoretically founded relationships to the process conditions making the models only applicable to specific conditions present in the studied batch adsorption process. This weak theoretical background of the models and the inability to transfer rate constants to other conditions make these models empirical equations, which must be considered when applying them. [20]

Generally, reaction kinetic models are suitable only for weakly porous adsorbents, where slow surface reaction dominates the process and film diffusion resistance does not exist. The increasing application of reaction kinetic models is likely due to the simpler structure compared to the diffusion models. [20]

2.4 Membrane Technology

A membrane can be understood as an interim phase that separates two homogeneous phases from each other and selectively resists the transport of different chemical components between these phases [19]. It consists of a discrete, thin interface that moderates permeation of chemical species with which it is in contact, similar to normal filters [43]. However, the term filter generally is used for structures that retain particles with diameters larger than about 1 to 10 µm [43].

Membranes used for separation technologies are commonly synthetic. Furthermore, there are also membranes of biological structures, which are not the topic here since they are usually not used in separation technology. Synthetic membranes are made up of polymers and can be homogeneous, referred to as symmetric or isotropic, or heterogeneous, referred to as asymmetric or anisotropic. Symmetric membranes are uniform in composition and structure, while asymmetric membranes are containing holes or pores of varying dimensions or consisting of some form of layered structure, see Figure 2.22. Special types of isotropic or anisotropic membranes also can be charged membranes, supported liquid membranes, and mixed matrix membranes. [43]

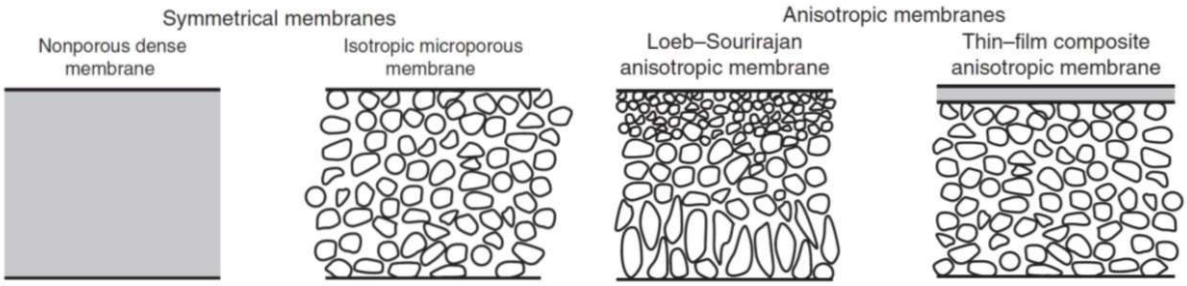

Figure 2.22: Cross section of symmetric/isotropic membranes on the left and asymmetric/anisotropic on the right [43]

Membranes are used for various separation processes, which are separation of mixtures of gases and vapours, miscible liquids such as organic mixtures and aqueous/organic mixtures, suspensions, emulsion as well as for dissolved solids and solutes from liquids [44]. Due to the lower energy consumption, the environmental friendliness and the clean and easy operation of membranes, they often offer remarkable advantages compared to conventional processes like filtration, distillation, and ion exchange [45]. As presented in Figure 2.23 Membrane is one of the most energy efficient separation technologies and requires of more than 80 % less energy compared to distillation and more than one third less energy than adsorption.

Membrane technology is widely applied in numerous industrial processes these days. It is well established in various sectors, including the food industry, in the processing of dairy products, as well as in the automotive industry, particularly in the recovery of electropainting baths. Membranes also play a crucial role in providing clean water to millions of people worldwide and are essential for the survival of numerous individuals

coping with kidney disease. Moreover, the chemical industry is experiencing a growing adoption of membrane technology, where membrane materials with exceptional stability is required often to meet the specific demands of chemical processes. [46]

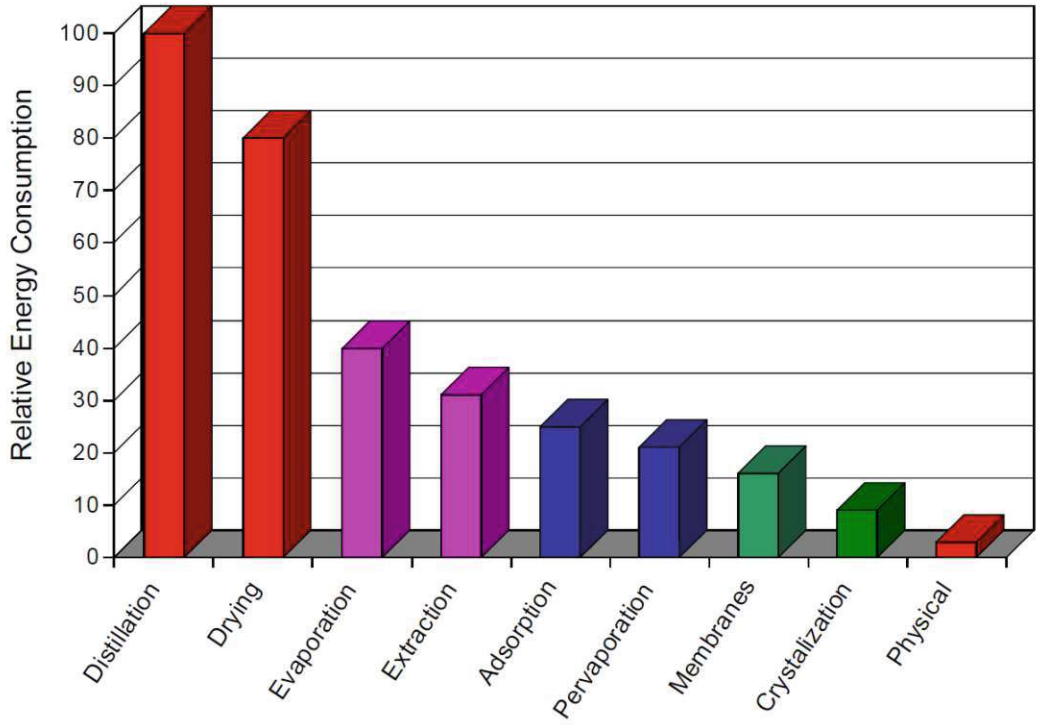

Figure 2.23: Relative energy consumption of several separation technologies compared to distillation [47]

2.4.1 Transport Theory

The main ability of membranes is that they can differentiate between closely related species. The transportation through the membranes traditionally can be described by the pore-flow model and the solution-diffusion model as presented in Figure 2.24 (a) and (b). Beside these two traditional membranes, also new once with extremely fine pores, some with diameters as small as 5 Å, have been developed over the past 20 years, see Figure 2.24 (c). These membranes have complicated mechanism of permeation, which conforms to neither traditional model. [43]

The pore-flow model explains the transport of the permeants by flow through tiny pores. The driving force is usually a pressure gradient between the feed and permeate side of the membrane and leads to a convective flow. Membranes which are following the pore-flow model separate by filtration, meaning species that are too large to pass through the membrane are selectively retained. This model is used to describe the permeation in porous membranes with pores diameters greater than 20 Å, such as ultrafiltration and microfiltration. It should be mentioned that not as shown in Figure 2.24 (a) real pores are no cylinders or uniform in size. [43]

The solution-diffusion model is used at membranes without permanent pores. Thereby, the permeate dissolve in the membrane like a liquid and, due to a concentration gradient,

diffuse through the membrane. The transport relies on the solubility of the permeant within the polymer composing the membrane and its diffusion rate once dissolved. Depending on the polymer either of former can be the limiting factor. The product of solution and diffusion is known as the permeability, which is characteristically for a given permeant. Different permeants are separated due to their difference in their permeabilities. The solution-diffusion model is applied for dense polymer membranes used for dialysis, gas separation, reverse osmosis, and pervaporation. [43]

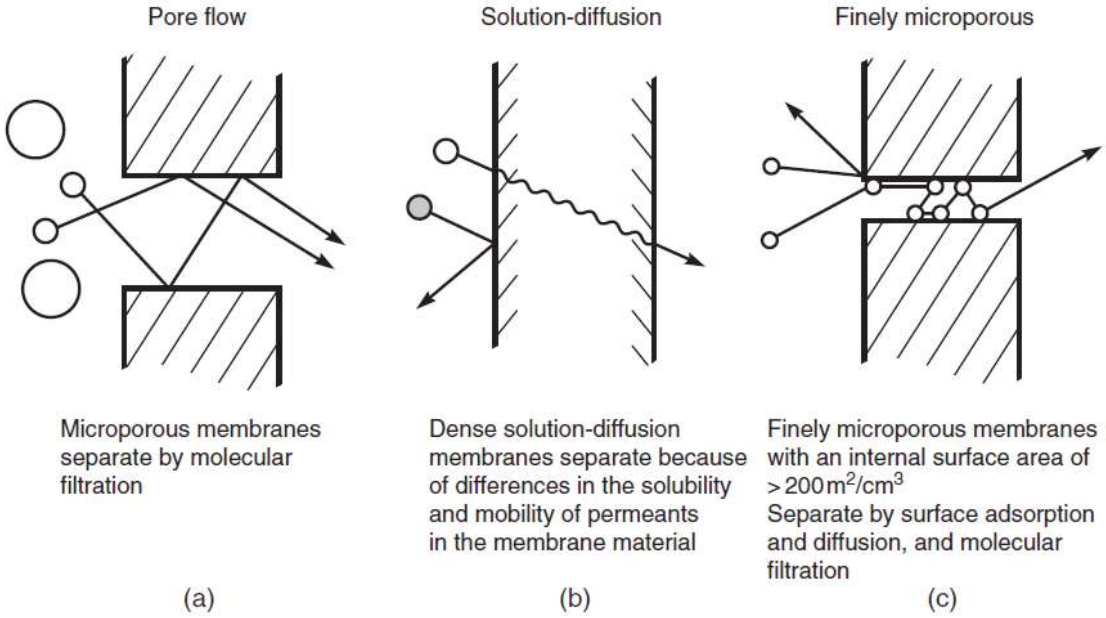

Figure 2.24: The traditional transport models for (a) porous membranes and (b) dense membranes as well as for (c) modern very finely microporous membranes [43]

The finely microporous membrane types are between the clearly nonporous solution-diffusion membranes, described by the solution-diffusion model, and the clearly microporous filtration membranes, described by the pore-flow model. Such membranes are characterised by pores of 5–25 Å diameter range and can be made from a variety of materials, such as zeolites, metal/organic hybrids, and carbonised polymers. Due to the tiny pore size, the ratio of pore surface area to pore volume is notably high, typically ranging from 100 to 1000 m^2/cm^3 of membrane material. Thus, beside of the molecular sieving, the transport though the membrane is also controlled by adsorption effects on the huge internal surface area of the pore walls. This makes the modelling of their transport behaviour more complicated than for the previous mentioned traditional membrane types. The advantage of these membranes is their exceptional permeance and selectivity, making them to the subject of much current research. [43]

2.4.2 Membrane Modules

Membrane separations are carried out in membrane modules, which includes all required components, including the body with all required openings [19]. These modules can have different configurations, commercially available ones are (a) the plate and frame

module; (b) the spiral wound module; (c) the tubular membrane module; (d) the capillary membrane module; and (e) the hollow fibre membrane module [45]. Figure 2.25 presents the basic design of such membrane modules. The inflow is referred to as feed and the part of the feed, which is retained by the membrane is the retentate. The part that is transported through the membrane is known as the permeate.

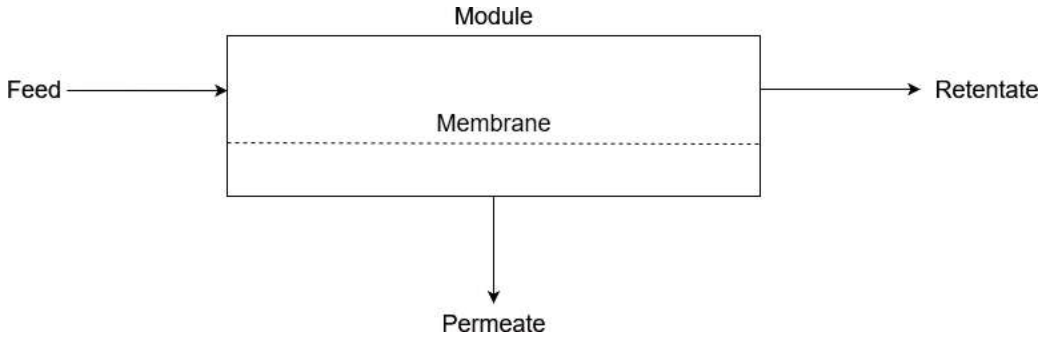

Figure 2.25: Schematic design of membrane modules (According to Grassmann et al. [19])

Such membrane modules can be operated in two different modes, which is dead-end or cross-flow. At dead-end mode the feed flows perpendicular to the membrane and all fluid passes through the membrane's surface. Thus, particles are trapped and build up a filter cake, which reduces the filtration efficiency. The filtration takes part until the permeation flux (J) reaches an uneconomical point. Membrane separation in industry is often performed with the cross-flow mode. Thereby, the solution circulates tangential to the membrane's surface, letting rejected particles continue the flow and preventing the formation of a thick filter cake. Thus, a constant flux of the fluid through the membrane and a steadier retention factor is easier to be held. [15], [19]

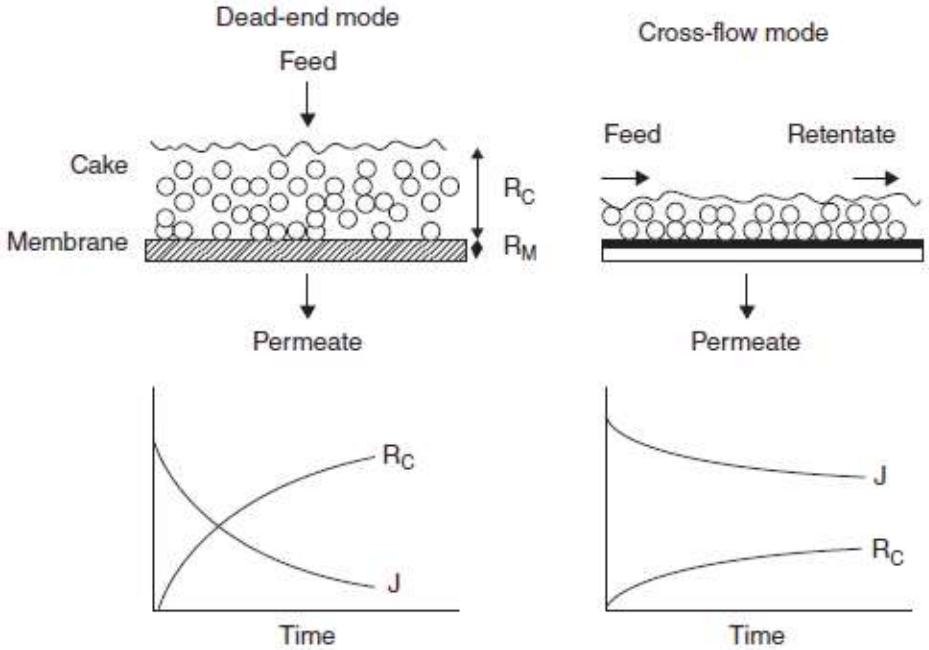

Figure 2.26: Schematic diagram of dead-end and cross-flow filtration models and their impact on permeation flux (J) and cake formation. [15]

2.4.3 Membrane Processes

Membrane can work in two possible ways, first as a barrier that rejects pollutants that may be suspended or dissolved and only allow the purified water through it. Second, to extract pollutants from the wastewater or transfer specific components into it. The most common processes are reverse osmosis (RO), nanofiltration (NF), ultrafiltration (UF) and microfiltration (MF) that are working according to the first one. Common processes of the second type, the extractive processes, are electrodialysis (ED), dialysis, pervaporation (PV), and gas transfer (GT). In these processes the membrane behaves as a selective layer, where specific components dissolved in the fluid permeate. [48]

The driving force in membrane processes can be differentiated in hydrostatic pressure, concentration, temperature or in the electric potential between the two by the membrane separated fluids [19]. In nearly all pressure-driven membrane processes the retained or rejected material is concentrated and the desired product the permeate, e.g., water. In contrast, in extractive an electrodialytic processes, the retentate is the desired product, and the permeate is the dissolved solute. [48]

Several membrane processes on the marked are listed in Table 2.3 together with their driving force and their applications. Nowadays, the most important in industry are the pressure driven processes of RO, NF, UF and MF [48]. A common rating of these membranes is the molecular weight cut-off (MWCO), which indicates the molecular weight in Dalton (Da) of the species which is rejected in a proportion of 90 – 95 % [49]. For this thesis the pressure driven membrane processes are in interest, which are explained further in the following.

Table 2.3: Membrane separation processes [44]

membrane process	driving force	applications
microfiltration	hydrostatic pressure	clarification, sterile filtration
ultrafiltration	hydrostatic pressure	separation of macromolecular solutions
nanofiltration	hydrostatic pressure	separation of small organic compounds and selected salts from solutions
reverse osmosis or hyperfiltration	hydrostatic pressure	separation of micro-solutes and salts from solutions
gas permeation	hydrostatic pressure, concentration gradient	separation of gas mixtures
dialysis	concentration gradient	separation of micro-solutes and salts from macromolecular solutions
pervaporation	concentration gradient, vapour pressure	separation of mixtures of volatile liquids

vapour permeation	concentration gradient	separation of volatile vapours from gases and vapours
membrane distillation	temperature	separation of water from non-volatile solutes
electrodialysis	electrical potential	separation of ions from water and non-ionic solutes
electrofiltration	electrical potential	de-watering of solutions suspended solids
liquid membranes	concentration, reaction	separation of ions and solutes from aqueous solutions

2.4.3.1 Microfiltration (MF)

MF shows the most similarity with normal particle filtration [19]. The membranes function through a combination of molecular sieving on the membrane surface and adsorption of particulates inside of the membrane's pores [43].

It is used for particles greater than 50 nm and works as a sieve for solutions, suspensions or emulsions. The size of MF ranges from 0.05 to 10 µm. Materials used for this type of membrane are organic or inorganic. Common applications of MF are sterile filtration for beverages, wastewater treatment and the cell retention in bio reactors, see Figure 2.27. [19]

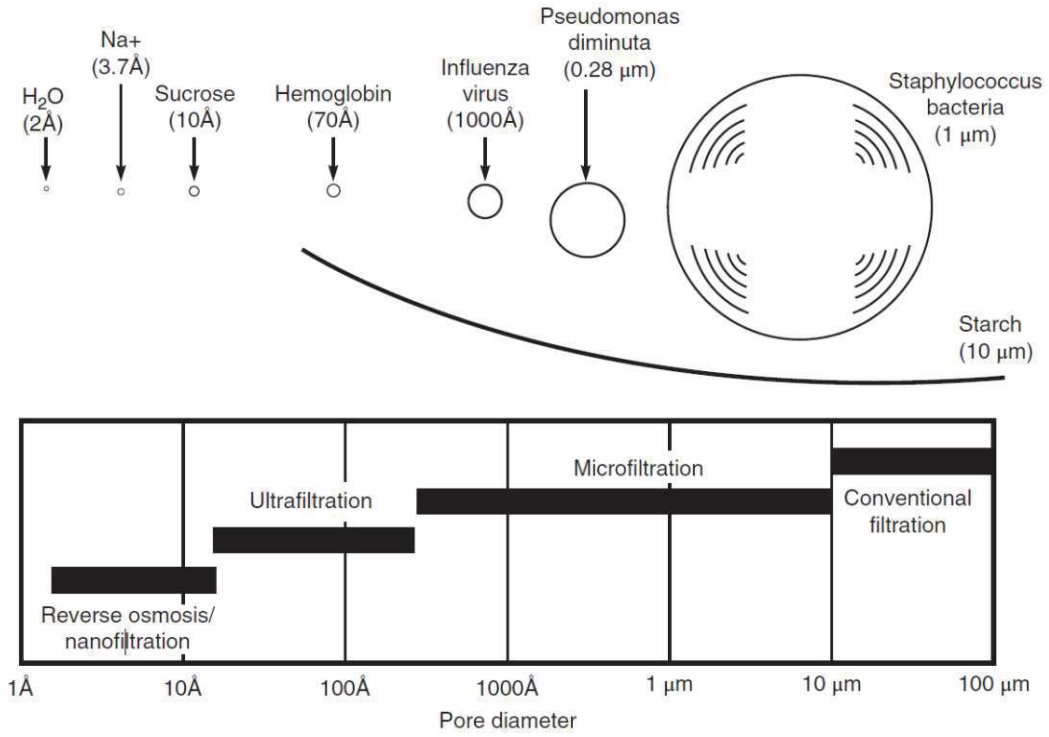

Figure 2.27: Pore sizes and the relative size of different solutes removed of the common pressure driven processes reverse osmosis, ultrafiltration, microfiltration, as well as for conventional filtration [43]

As presented in Figure 2.27 the typical pore diameter of a microfiltration membrane is about 1 µm, which is 100-fold respectively 1000-fold larger than the typical pore sizes of UF and RO. Due to the fact that the flux is proportional to the pore diameter, the permeance of microfiltration is way higher than that of UF, which in turn also is much higher than that of RO. This results in difference in the operation pressure and the way these membranes are applied in industry. Common pressures are 10 to 100 bar for RO, 0.2 to 5 bar for UF and 0.5 for MF. [43]

2.4.3.2 Ultrafiltration (UF)

UF is very similar to microfiltration but employs asymmetric membranes for tighter filtrations. The pores in the top layer of these membranes range from 0.05 µm to 1 nm, allowing for the separation of extremely small particles and dissolved molecules from fluids. Molecular size is the primary basis for separation, beside of this factor like molecule shape and charge can also influence the process. UF retain materials with molecular weights between 1 kDa and 1,000 kDa, while allowing salts and water to pass through the membrane. Also, they can retain colloidal and particulate matter. [44]

UF and MF have very similar separation characteristics, which is molecular sieving through increasingly fine pores. Figure 2.27 shows the different pore sizes of these two processes, which is the simple conventional definition of them. Ultrafiltration membranes primarily function by trapping the retained material on the membrane surface through molecular sieving or other mechanisms and shows no adsorption inside the membranes like MF. [43]

UF can be applied for purifying and collecting both, the permeate as well as the retentate. Substances smaller than the pore size rating can pass through, allowing for depyrogenation, clarification, and separation from high molecular weight contaminants. Larger substances than the pore size rating are retained and can be concentrated or separated from low molecular weight contaminants. [44]

UF membranes are often used in cross-flow mode. This maximises flux rates and filter life, since UF membranes can be repeatedly regenerated multiple times using strong cleaning agents. [44]

2.4.3.3 Reverse Osmosis (RO)

RO, sometimes referred to as hyperfiltration, is the reversal of the natural process of osmosis. Pressure greater than the osmotic pressure is applied on the salt solution side leading to reversal of the water flow. At RO the concentration of salt is increased by the flow of water (or solvent) from the concentrated solution to a dilute solution. [44]

The membranes commonly are asymmetric or composite consisting of a thin, dense top layer, which gives the membrane its separation characteristics, supported by a thick, porous sublayer [44]. Very small pore sizes, ranging from 3 to 5 Å, in the range of the

thermal motion of the polymer chains forming the membrane, meaning there are no permanent pores, and transport occurs via statistically distributed free volume areas [43]. Thus, the mechanism of permeate transport follows the solution-diffusion model, meaning separation occurs due to the difference in solubilities and mobilities [43]. Very high operating pressures are required, ranging from 30 to 100 bar, to overcome the molecular friction between permeates and membrane polymer [44].

The membrane exerts an electrostatic free energy barrier against ionic movements, leading to much less mobility of ionic species compared to water molecules. Thus, RO is mainly used for the purification of aqueous solutions with inorganic solutes, but also with macromolecules. It is applied for particle sizes of 1 to 10 Å and complete separation is achieved for solutes with molar masses greater than 300 Dalton. Applications are

- desalination of brackish water and sea water,
- production of pure water for a variety of industries,
- concentration of solutions of food products, pharmaceutical solutions and chemical streams, and
- wastewater treatment. [44]

2.4.3.4 Nanofiltration (NF)

NF is essentially a form of RO, with properties that fall in between the area of RO and UF. Other terms for NF are loose RO or low-pressure RO. NF falls in the complex area of fine micropores, where transport does not occur specifically by pore-flow and neither by solution-diffusion model and is a complex combination of surface adsorption and diffusion and molecular filtration. [43]

NF is applied, where separation capabilities between RO membranes and UF membranes are required, which is in the separation of ions from solutes such as small molecules of sugars [44]. It has lower sodium rejection than RO, but higher water permeability [43]. Therefore, it is used when high sodium rejection is not required, but other salts such as Mg and Ca are to be removed [44]. NF is also able to reject 90 % of the organic solutes above 200 Da. [43]

Most NF membranes are interfacial composites, but also some based on cellulose acetate are existing. The method used in production of these membranes may result in acid groups attached to the polymer structure. This does not affect neutral solutes like lactose, sucrose, and raffinose and their rejection increases in proportion to solute size. Nanofiltration membranes are produced with molecular weight cut-offs for neutral solutes ranging from 150 to 1500 Da. [43]

NF finds a wide range of applications in food, pulp and paper, chemical and pharmaceutical industry, as well as in metal and acid recovery. Some applications are

- water softening and removal of organic contaminants,
- concentration and demineralization of whey,

- concentration of sugar and juice in food industry,
- concentration of textile dye effluents, and
- in landfill leachate treatment [46]

2.4.3.4.1 Diafiltration

Diafiltration is an additional step at nanofiltration. In this process, the retentate is further diluted with water and then subjected to another round of nanofiltration. The primary objective is to further reduce the concentration of soluble components while simultaneously concentrating the retained components. [45]

It is commonly used when separation of two components with not very different sizes should be carried out. Thereby, a membrane that retains one component almost completely, while the other partially passes is used. The retentate is then circulated around the cross-flow ultrafiltration loop and the permeate that passes through the membrane is replaced by an equal amount of fresh solvent. [50]

3 Materials and Methods

3.1 Syrup

Organic glucose syrup from maise starch hydrolysates provided by AGRANA Stärke GmbH with DE-40 was used, see Figure 3.1. The syrup was concentrated to approximately 70 Brix for storage and required dilution with deionised water for application in the experiments. The pH of the diluted solutions ranged between 4.7 and 4.9.

Two batches with similar characteristics were used during experiments, referred to as 1st and 2nd batches. The 1st batch was used for 30 Brix dilutions at equilibrium and kinetic experiments with 0.6 g / 100 ml AC dosage. All other experiments were conducted with the 2nd batch. The diluted syrup is referred to as raw syrup, while the syrup from membrane filtration is referred to as the pre-treated syrup.

Figure 3.1: Concentrated glucose syrup

3.2 Activated Carbon Based Treatment

The powdered AC Norit GBSP was used as an adsorbent for decolourisation of the glucose syrup. The datasheet of the AC can be found in Appendix A. The dosage for the experiments was measured in gram per 100 ml solution, with an accuracy of two decimal places.

The adsorption process was conducted using a batch lab-scale experiment. A shaker with a heated water bath set to 70 °C was utilised, ensuring a shaking speed high enough so negligible influence of bulk fluid mass transfer and film diffusion is guaranteed. The experiments were performed in 100 ml Erlenmeyer flasks, pre-filled with a certain AC dosage. The adsorption process started by adding a specified diluted glucose syrup to the

flasks, which were placed in the shaker. To prevent contamination from evaporating water in the water bath, the flasks were covered with aluminium foil.

After adsorption, AC was separated from the treated solution by vacuum filtration using a Buchner funnel and Sartorius Stedim grade 391 filter paper (particle retention 2-3 µm). Filtration began immediately after removing the sample from the shaker. The funnel and the flask were subsequently cleaned with deionized water.

3.2.1 Equilibrium Experiments

The equilibrium experiments were conducted following the procedure outlined in Chapter 2.3.4.1. Based on studies with similar solutions by Atiyeh et al. [7] and information from the glucose syrup supplier (AGRANA), the adsorption process is expected to reach equilibrium after 40 minutes. Therefore, all adsorption processes were maintained for 40 minutes.

These experiments were conducted with glucose syrup of 15, 20, 30, and 40 Brix of the raw syrup and the pre-treated syrup. Seven datapoints with AC dosages of 0.1, 0.15, 0.2, 0.3, 0.4, 0.6, and 0.8 g / 100 ml solution were measured. For syrup pre-treated by UF, fewer datapoints (0.3, 0.4, 0.6, and 0.8 for lose UF and 0.2, 0.3, 0.4, 0.6, and 0.8 for tight UF) were measured due to limited availability of treated solution. Blank measurements without AC were also conducted for comparison. To ensure statistical reliability, all experiments, except for those involving solutions pre-treated by multistage setups were performed in triplicates. An overview of all experiments is presented Table 3.1.

Table 3.1: Overview of all decolourisation experiments by AC adsorption

<table>
<tr><th>Experiment</th><th>Feed</th><th>AC Dosage
in g / 100 ml</th><th>Adsorption Time</th></tr>
<tr><td rowspan="5">Equilibrium</td><td>Syrup with dilution of 15, 20, 30 and 40 Brix</td><td rowspan="2">0.1, 0.15, 0.2, 0.3, 0.4, 0.6, 0.8</td><td rowspan="5">40 minutes</td></tr>
<tr><td>Product from multistage setup 3.1, 3.2, 2.1, 2.2, 1.1, 1.2</td></tr>
<tr><td>Product from multistage setup 2.3</td><td>0.1, 0.15, 0.2, 0.3, 0.4, 0.6</td></tr>
<tr><td>Permeate from loose UF</td><td>0.3, 0.4, 0.6, 0.8</td></tr>
<tr><td>Permeate from tight UF</td><td>0.2, 0.3, 0.4, 0.6, 0.8</td></tr>
<tr><td rowspan="2">Kinetic</td><td>Syrup with dilution of 30 Brix</td><td>0.1, 0.3, 0.6, 0.8</td><td rowspan="2">5, 10, 20, 30, 40, 60, and 90 minutes</td></tr>
<tr><td>Syrup with dilution of 15, 20, and 40 Brix</td><td>0.6</td></tr>
</table>

3.2.2 Kinetic Experiments

Kinetic experiments were performed only on the raw syrup. Seven timepoints were measured at 5, 10, 20, 30, 40, 60, and 90 minutes for glucose syrup dilutions of 15, 20, 30 and 40 Brix as well as for different AC dosages of 0.1, 0.3, 0.6 and 0.8 g / 100 ml with diluted syrup of 30 Brix. An overview of the carried out kinetic experiments can be found in Table 3.1.

3.2.3 Investigation of AC separation

Beside AC adsorption also the filtration for AC separation must be evaluated for its impact on sugar content and colour. Therefore, an experiment was conducted to determine the sugar changes (reduction of Brix) and colour changes resulting from AC adsorption step versus the filtration step with filter paper. This experiment involves comparison of change in Brix and colour at decolourisation processes:

- Blank (without AC and without filtration),
- with filtration only (no AC), and
- with both AC and filtration.

3.3 Membrane Based Pre-Treatment

The membrane treatment is performed using a batch cross-flow process, as shown in Figure 3.2. The permeate was collected in a beaker for further use, while the retentate was progressively concentrated in the feed tank. After collecting a certain amount of permeate, the process is stopped, and the remaining retentate is collected from the feed tank. Due to the cleaning of the apparatus, residual water always remains in the pipes, leading to a slight dilution of the feed, as reflected in the measured values shown below.

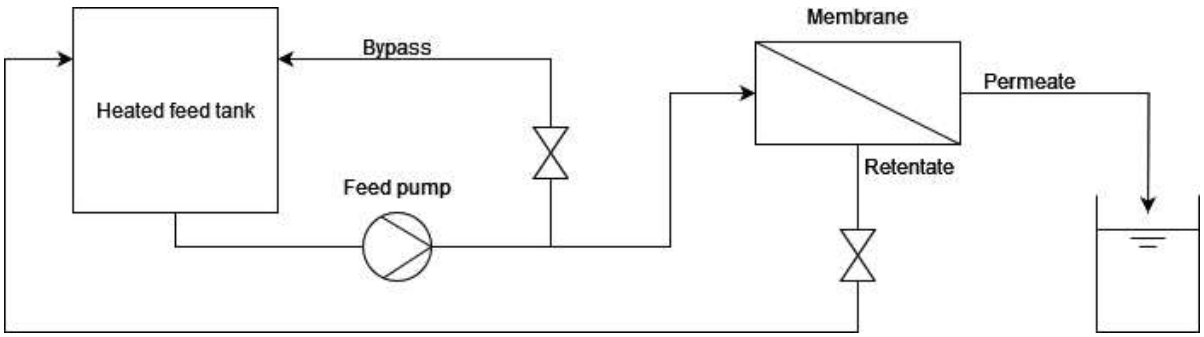

Figure 3.2: Schema of membrane separation setup with the model OSMO MemCell Classic

The pre-treatment was carried out with each of the two UF membranes as well as with different configurations including the following membranes:

- Loose UF with 100 kDa retention
- Tight UF with 5 kDa retention
- Loose NF with 150 – 300 Da retention

- Tight NF with 150 – 300 Da retention

After the pre-treatment the syrup was decolourised with AC treatment by the equilibrium experiment as shown in Chapter 3.2.1. Figure 3.3 gives an overview of the several process configurations and their steps.

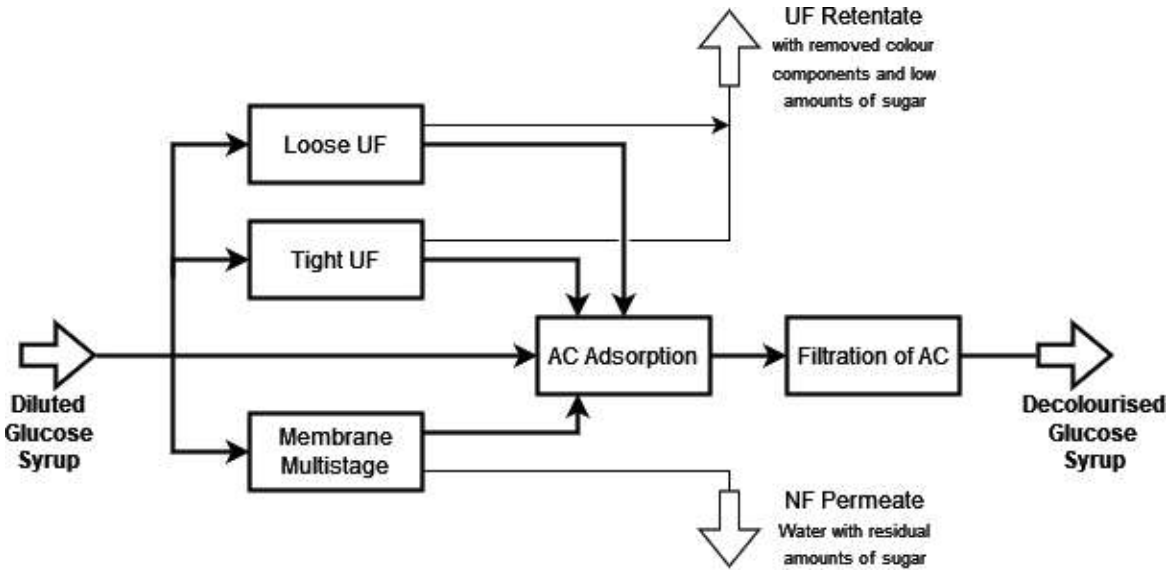

Figure 3.3: Overview of the decolourisation processes

Seven different membrane multistage configurations are tested as listed in Table 3.2 and described further in the following chapters. Each step in a multistage membrane filtration was carried out in a batch process as described above. After completion each step, the solution was frozen for stability purposes and then thawed for use in the subsequent step.

Table 3.2: Membrane multistage setups

Category	No.	Description
Multistage with three stages	3.1	With additional dilution of Feed 2
	3.2	Without dilution of Feed 2
Multistage with two stages	2.1	Feed with 20 Brix sugar concentration
	2.2	Feed with 30 Brix sugar concentration
	2.3	With loose NF instead of tight NF
Diafiltration	1.1	One stage with tight NF
	1.2	Two stages with tight UF and tight NF

3.3.1 Multistage Membrane Processes

3.3.1.1 Three-Stage Membrane-Based Pre-Treatment

Three stage multistage setup consisting of loose UF followed by tight UF and then tight NF was used as illustrated in Figure 3.5 and Figure 3.6. The retentate from the third stage (Retentate 3) is the product stream used for decolourisation by AC to obtain the final colourless product. In this setup, loose UF primarily is intended to remove large pigments from the syrup, tight UF is used for further decolourisation of the syrup. Tight NF has its purpose on concentration of the product stream. Figure 3.4 shows the syrup colours of the feed and the resulting permeate and retentate form loose and tight UF.

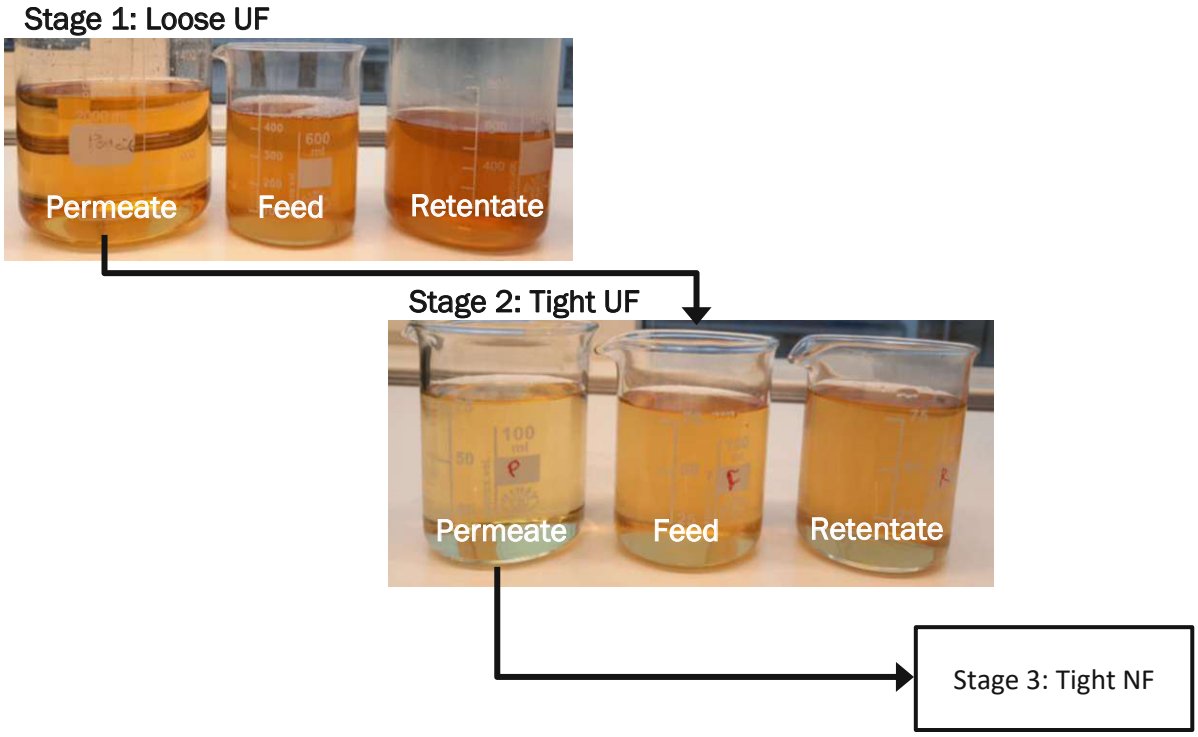

Figure 3.4: Pictures of permeate, feed and retentate from tight and loose UF

This setup was tested both with dilution (Setup 3.1), see Figure 3.5, and without dilution (Setup 3.2), see Figure 3.6, of the Permeate 1 for Feed 2, beside of the process related dilution of Permeates 1 and 2 occurred due to the residual water in the apparatus. The residual water in the apparatus resulted in a Brix reduction of approximately three of each feed.

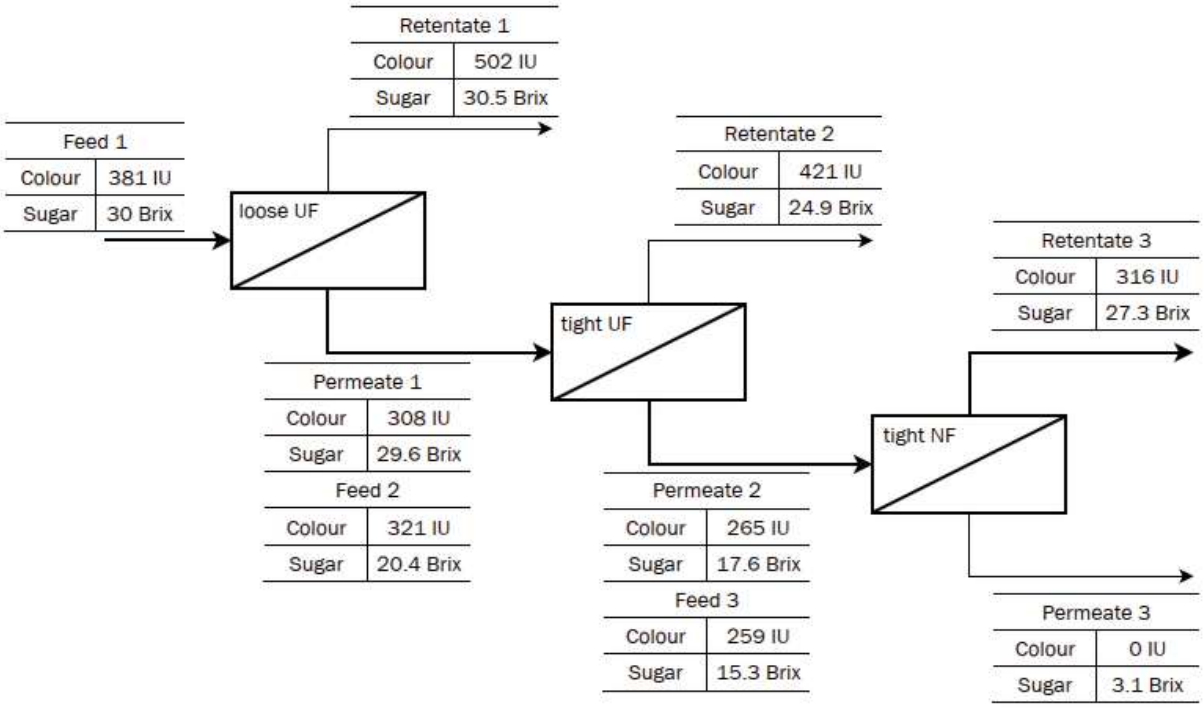

Figure 3.5: Multistage membrane process with three stages with additional dilution of Feed 2 (Setup 3.1)

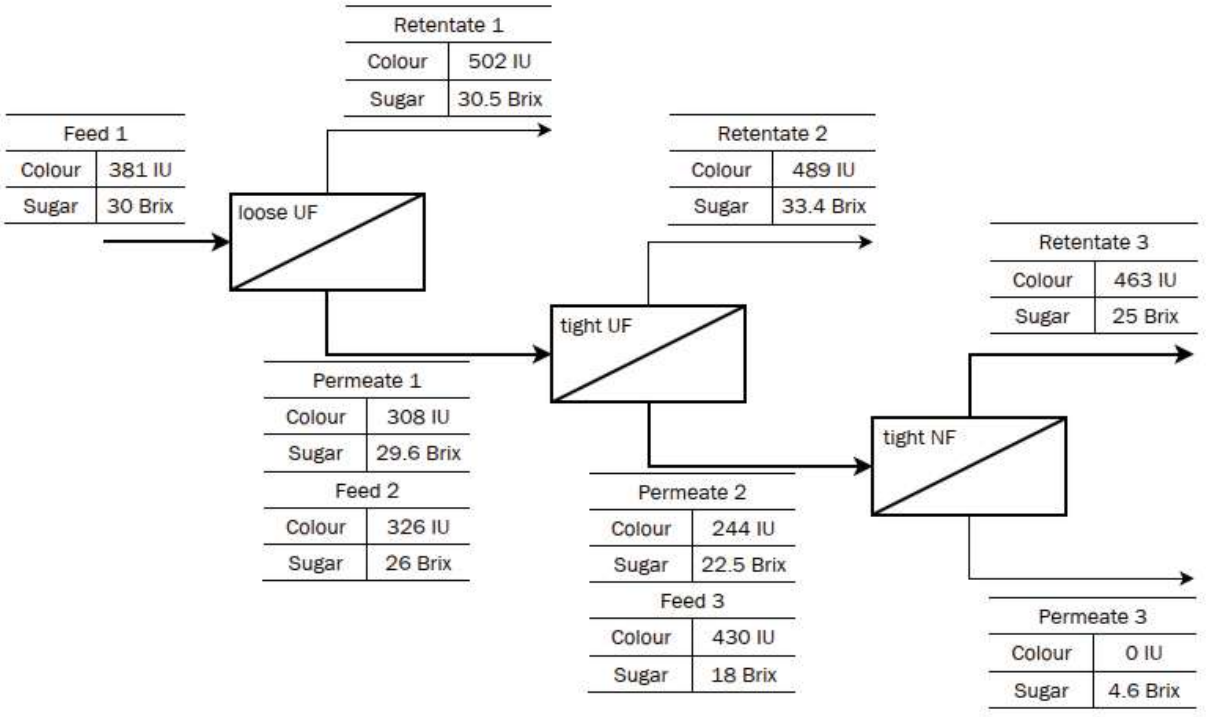

Figure 3.6: Multistage membrane process with three stages (Setup 3.2)

3.3.1.2 Two-Stage Membrane-Based Pre-Treatment

The two-stage membrane filtration setup was carried out with tight UF followed by tight NF. This process was conducted first with an initial Feed 1 of 20 Brix (Setup 2.1), see Figure 3.7 and second with an initial Feed 1 of 30 Brix (Setup 2.2), see Figure 3.8. As in

the previous setup, tight UF was used for decolourisation and tight NF was employed for concentration of the product stream. These results in the product in Retentate 2, which was subsequently used for further decolourisation with AC.

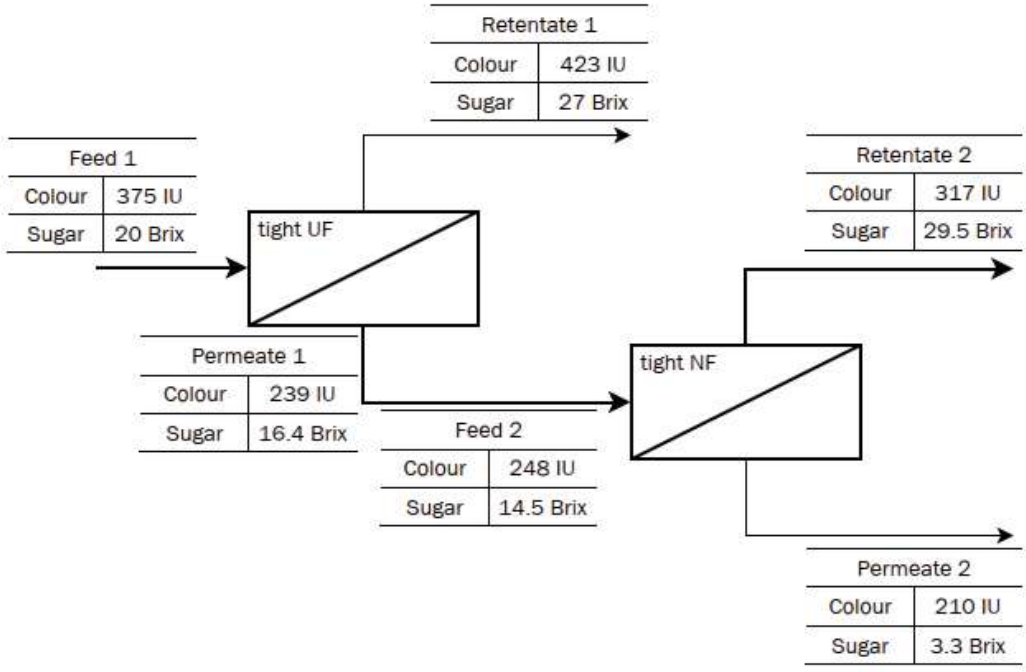

Figure 3.7: Multistage membrane process with two stages and a feed of 20 Brix (Setup 2.1)

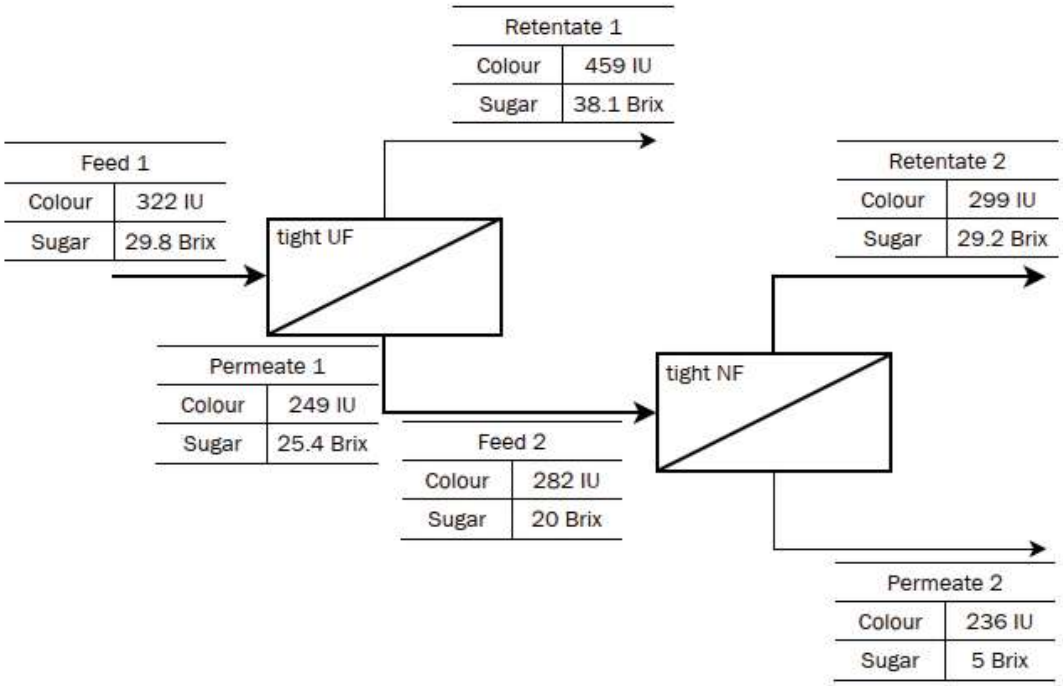

Figure 3.8: Multistage membrane process with two stages and a feed of 20 Brix (Setup 2.2)

Two stage membrane filtration with tight UF and loose NF, as presented in Figure 3.9, was conducted with an initial feed sugar concentration of 21.2 Brix. As with tight NF, the

purpose of loose NF is to concentrate the sugar-rich solution, resulting in the product stream in Retentate 2.

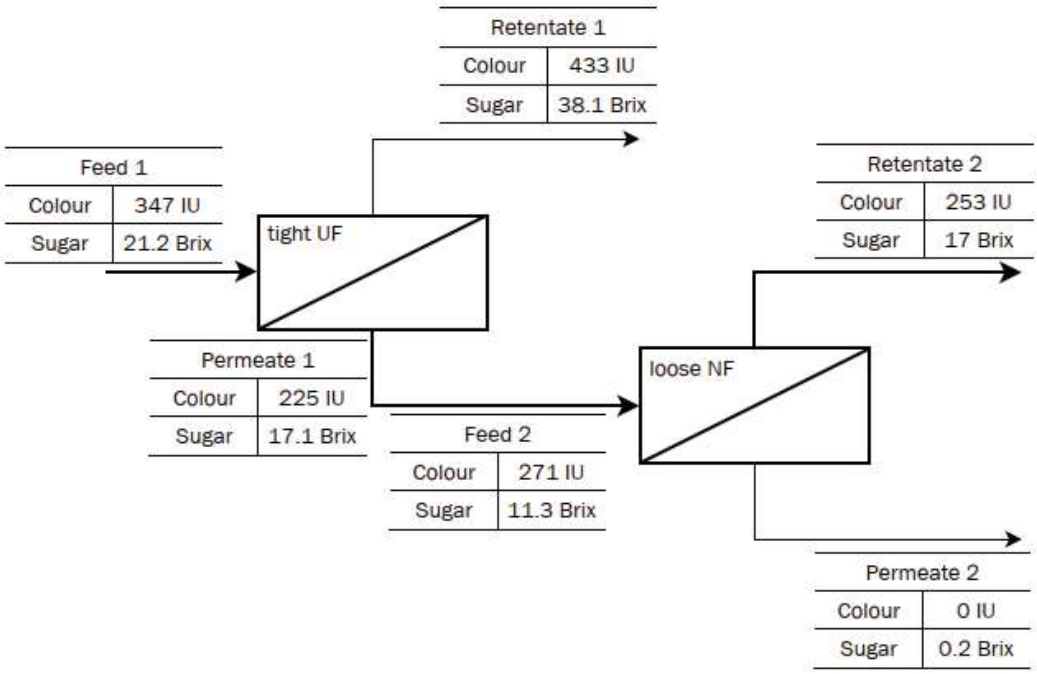

Figure 3.9: Multistage membrane process with two stages and Loose NF (Setup 2.3)

3.3.2 Diafiltration

Diafiltration was performed using tight NF only (Setup 1.1), as shown in Figure 3.10 and with tight UF followed by tight NF (Setup 1.2), as shown in Figure 3.11. After a certain amount of permeate passed the membrane, the retentate from UF and NF was diluted 3 times with a ratio of 1:1. The sugar-rich product, used for further decolourisation by AC adsorption, is the retentate of the tight NF.

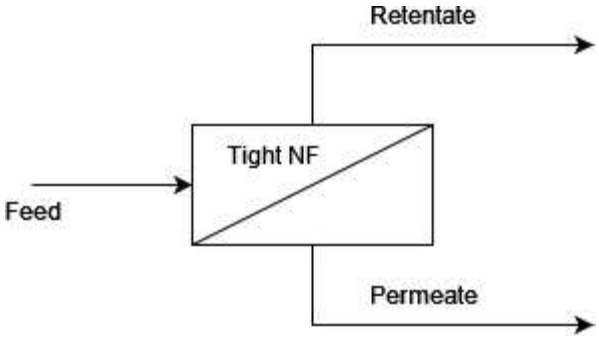

Figure 3.10: Tight NF filtration used for diafiltration (Setup 1.1)

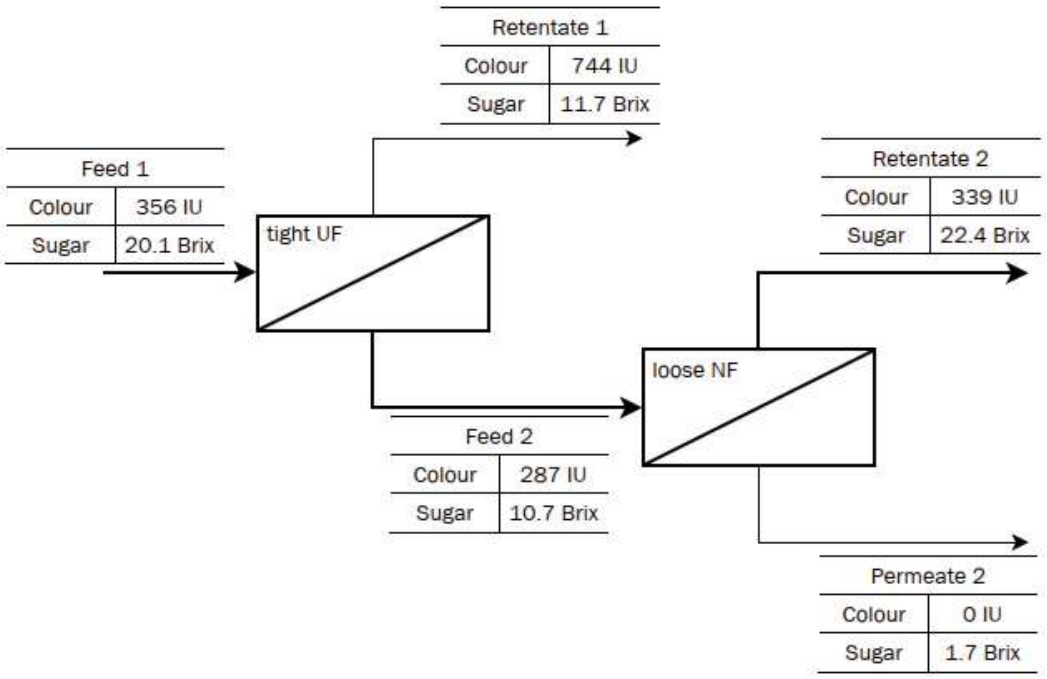

Figure 3.11: Diafiltration with two membrane stages of tight UF followed by loose NF (Setup 1.2)

3.4 Analytic Methods

The primary parameters for evaluating the syrup are colour and sugar content, as the target is to obtain a colourless sugar syrup. Therefore, it is essential to establish a proper method able to characterise both parameters accurately. Besides of these two main parameters, also pH and conductivity are important to measure, due to their informative value regarding stability of the syrup.

3.4.1 Colour

The measurement of colour in sugar syrups is standardised by the International Commission for Uniform Methods in Sugar Analysis (ICUMSA) [51]. ICUMSA defines the colour of a sugar syrup by ICUMSA Units (IU), which is calculated from the absorbance at a wavelength of 420 nm. Thereby, the following formula is used for the calculation of colour in IU:

$$Colour = \frac{1000 \cdot A}{b \cdot c} \tag{3.1}$$

Where A is the absorbance at 420 nm, b the length of the absorbing path, which is 1 cm and c the concentration of total solid in g sugar per ml. The light absorbance is measured according to the ICUMSA method [52] by the UV-vis spectrometer UV 1800 from Shimadzu with distilled water as a reference.

Relative removal of colour and sugar is determined by

$$Colour/Sugar\ reduction = \left(1 - \frac{Colour/Sugar\ after}{Colour/Sugar\ before}\right) \cdot 100\%. \quad (3.2)$$

Varying dilutions result in different sugar content, making it difficult to compare the required AC dosages across different diluted syrup. Since the goal of the decolourisation process is to obtain colourless sugar, it is not practical to determine the best conditions based on absolute AC dosages alone. Therefore, the relative AC dosage, dependent on the amount of decolourised sugar obtained, is calculated by the applied absolute AC dosage and the sugar concentration with following equation:

$$relative\ AC\ dosage = \frac{absolute\ AC\ dosage}{Sugar\ (in\ Brix)\ in\ the\ solution} \quad (3.3)$$

3.4.2 Sugar

For measurement of sugar the proportional relation between concertation of a pure substance dissolved in water to its refractive index (RI) is used. Calibration curves or tables are utilised for the conversion of the RI to try solids content in Brix. Thereby, a constant temperature is important during the measurement. Usually, modern refractometers are temperature-controlled and calibrated, allowing direct solids reading. [1], [3]

Brix is a scale for sugar measurement created by Alfred Brix and is the most used method for sugar measurement in the world. The degree Brix is defined as follows:

$$1\ degree\ Brix\ (°Bx) = \frac{1\ g\ of\ sucrose}{100\ g\ of\ solution} \quad (3.4)$$

Beside the RI also density can be used for measurement of Brix. Both methods will show the same result in a pure sucrose solution in distilled water but will have differences in other samples. Thus, only measurement with the same method could be compared and Brix is more a control value, which is easier to read than density or refractive index. [53]

Sugar content of all samples is determined with an Optronic Digital Refractometer from KRÜSS DR6200-T at 20 °C, with a direct output of Brix in g saccharose per g solution.

3.4.3 Conductivity and pH Value

For control on impurities or microbial processes conductivity and pH before and after each treatment are measured with VWR MU 6100 H multiparameter.

3.4.4 Statistical Methods

For the determination of equilibrium time and optimum dosage, analysis of variance (ANOVA) with a significance level of 5 % is used. Linear and nonlinear regression is carried out for fitting of several adsorption isotherm models and kinetic models by Origin 2023b [54] software.

4 Results and Discussion

First, analysis of the decolourisation process by AC adsorption was done by equilibrium experiments and kinetic experiments for several dilutions of the glucose syrup, see Chapter 4.1. These results from the decolourisation by only AC adsorption serve as a benchmark for determining improvements in the decolourisation by a membrane-based pre-treatment of the glucose syrup. After AC adsorption treatment the pre-treaded glucose syrups are compared to decolourisation of the raw syrup in terms of IU value, colour removal and AC dosage, as presented in Chapter 4.2.

4.1 Decolourisation by AC Adsorption

Decolourisation by AC adsorption involves all experiments where AC was applied to the diluted raw syrup without any pre-treatment of the syrup.

4.1.1 Adsorption Equilibria

The following results from adsorption equilibrium experiments were all carried out with an adsorption time of 40 minutes, as equilibrium is expected to be achieved within this time frame, as mentioned in Chapter 3.2.1. First comparison of isotherms to common applied models in the literature was carried out to figure out which mechanism the adsorption of colourants follows, see Chapter 4.1.1.1. Second, colour removal analysis by the adsorption treatment under different process conditions was done, for determination of optimal process conditions in terms of low AC dosages, presented in Chapter 4.1.1.2.

4.1.1.1 Adsorption Isotherms

The adsorption isotherms were measured for several dilutions with the method described in Section 2.3.4.1 by different AC dosages resulting in curves shown in Figure 4.1. The adsorbent loading q_e thereby was calculated based on a solution volume of $V_L = 50\ ml$ and the certain AC dosage in g / 100 ml.

Measure adsorption isotherms approach linear behaviour for lower dilutions of 30 and 40 Brix and become increasingly convex with higher dilutions of 16 and 20 Brix. These are less favourable shapes for isotherms since a higher concentration is required to achieve a high adsorbent load [30], [55]. Additionally, adsorption with lower dilutions result in lower adsorbent loading indicated by the curve being below the others with lower concentration. The cause of this is not completely clear, but may be due to the higher viscosity, which reduces the diffusivity of colour molecules into the fine pores. In addition, higher density of colour molecules in the less diluted syrup may lead to stronger interactions between them, which can reduce their tendency to accumulate onto the adsorbent. The dataset for

adsorption with a diluted syrup of 30 Brix was carried out with a different batch, the 1st batch, which shows generally lowest adsorbent loading. It had a 22 % lower colour than the other dilutions of 16, 20 and 40 Brix mixed with the 2nd batch, leading to lower adsorbent load, which explains the poorer performance.

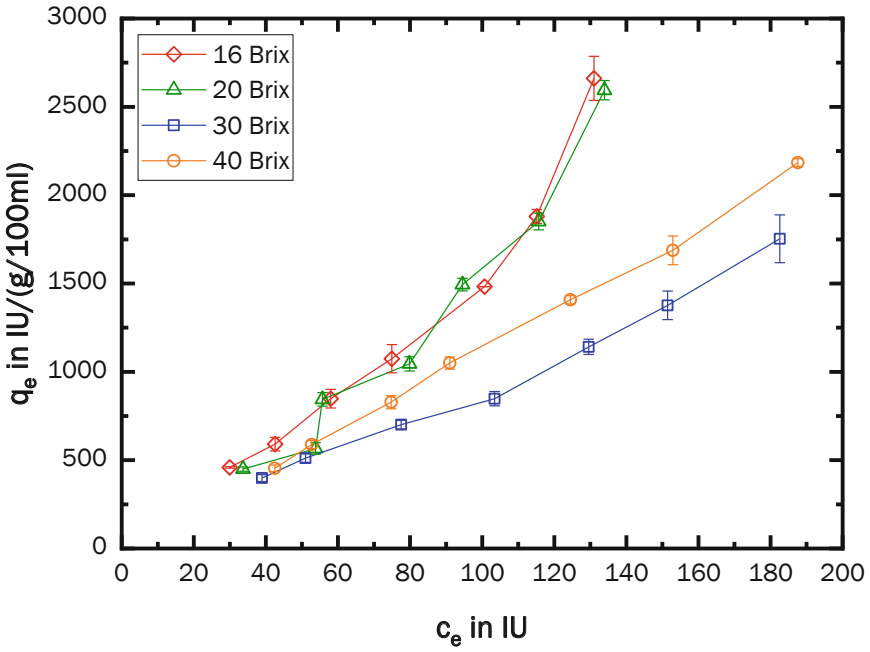

Figure 4.1: Isotherms of AC adsorption with raw syrup of different dilutions

Additionally, Henry, Langmuir, Freundlich, and BET isotherm models were fitted to the dataset of measured isotherms by non-linear fitting. The linearity of isotherms at lower dilutions resulted in a good fit with Henry isotherm, see Figure 4.3 and Table 4.1. For higher dilutions the coefficient of determination as well as residuals, see Appendix B, supports the plausibility of the Henry isotherm in describing of the adsorption process, although their nonlinear shapes is better fitting to other models.

The Langmuir isotherm model resulted in a linear curve, see Figure 4.2 and Figure 4.3. This is because of the fact that the Langmuir parameters cannot be negative due to physical senses, which would be necessary to obtain a convex curve such as obtained with dilutions of 16 and 20 Brix. Thus, Langmuir model is not able to describe the adsorption process sufficiently and monolayer adsorption can be ruled out.

The Freundlich isotherm model fits isotherm data well according to the coefficient of determination, see Table 4.1, and residuals, see Appendix B. The value of the parameter n_f close to one indicates their linearity, transforming the Freundlich equation into Henry equation for lower dilutions of 30 and 40 Brix. The decrease of K_f and increase of n_f with syrup dilution suggest the higher adsorbent loading and a less concave curve.

The BET isotherm model fits very well for all dilutions, see a coefficient of determination close to one, in Table 4.1, and residuals, see Appendix B. While lower dilutions are linear

(40 Brix) or only slightly convex (30) Brix, higher dilutions nearly follow the classical shape of BET isotherm.

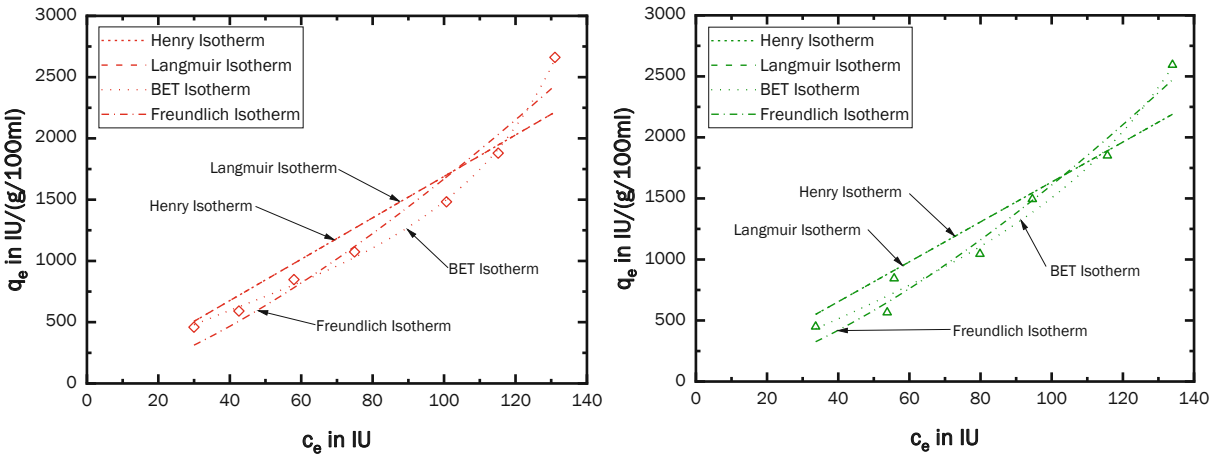

Figure 4.2: Adsorption isotherm models applied to adsorption with (a) 16 Brix syrup and (b) 20 Brix syrup

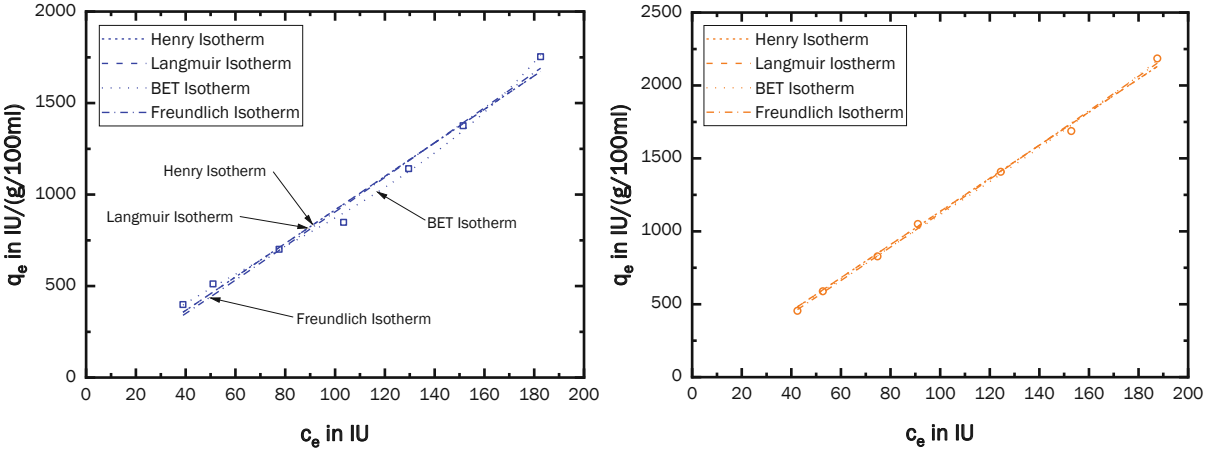

Figure 4.3: Adsorption isotherm models applied to adsorption with (a) 30 Brix syrup and (b) 40 Brix syrup

From the four fitted isotherm models, the modified BET isotherm for liquids proved to be the best fitting. This means the adsorption process follows multilayer adsorption, matching with results from other studies carried out with similar sugar-rich solutions with resin by Serpen et al. [56] and AC by Mercado & Velasco [57]. Due to the linearity of isotherms obtained with lower diluted feed syrup, the adsorption process can also be adequately described with Henry isotherm model in such cases, offering a simpler single-parameter isotherm equation.

None of the isotherm results shown above indicate a maximum of adsorbent loading, suggesting that type IV and V isotherms of IUPAC classification are unlikely [29]. Comparing of the resulting BET isotherms, see Figure 4.4, show that at higher concentrations in the bulk fluid phase, adsorbent loading increases significantly with higher dilutions, indicated by a strong rise in the curve, but does not achieve infinite adsorbent loading. Lower dilutions show a more linear trend without such an increase. This suggests that all dilutions

follow type III isotherms meaning that the interaction between molecules is stronger than between molecules and adsorbent. Thus, multilayer adsorption occurs without prior completion of monolayer adsorption. However, with increasing of dilution a small curvature for lower concentrations becomes present, visible at the curve for 16 Brix and slightly at the curve for 30 Brix, indicating that with higher dilution type II isotherms are present and monolayer adsorption occurs before multilayer adsorption starts. This change can probably be attributed to the greater distance between the colour molecules in the bulk fluid phase at higher dilutions, leading to less interaction between the molecules and relatively more interaction with the free adsorbent sites.

Table 4.1: Parameters of isotherm models

Isotherm Model	Parameter	16 Brix	20 Brix	30 Brix	40 Brix
Henry Isotherm	K_H / $100\mathrm{ml/g^{-1}}$	16.90	16.35	9.16	11.36
	R^2	0.9787	0.9763	0.9972	0.9994
Langmuir Isotherm	q_m / $10^7\ \mathrm{IU \cdot g^{-1}}$	3.99	4.59	0.836	0.778
	K_L / $10^{-7} \cdot IU^{-1}$	4.23	3.56	10.96	14.61
	R^2	0.9119	0.9017	0.9843	0.9970
Freundlich Isotherm	K_F / g^{-1}	2.75	1.88	7.61	9.61
	n_f	1.391	1.467	1.038	1.034
	R^2	0.9590	0.9729	0.9851	0.9978
BET Isotherm	q_m / $\mathrm{IU \cdot g^{-1}}$	733	1123	876	2621
	C_L /$10^{-3} \cdot IU^{-1}$	5.64	4.81	3.13	1.77
	C_S /$10^{-3} \cdot IU^{-1}$	32.86	11.84	14.86	4.43
	R^2	0.9981	0.9856	0.9972	0.9983

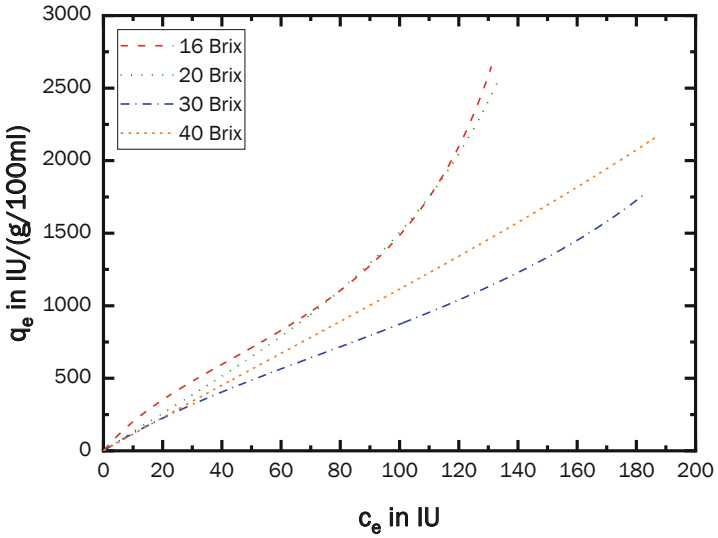

Figure 4.4: BET Isotherms for different dilutions from 16 to 40 Brix

4.1.1.2 AC Dosage Analysis

The AC was able to remove most of the colour in all dilutions, achieving 85 to 90 %. Different dilutions showed no significant difference in colour removal, as can be seen from Figure 4.5 and Table 4.2. Additionally, it is demonstrated that syrup with colour lower than 45 IU is possible to be achieved.

Figure 4.5 (a) shows that higher dilutions of 16 and 20 Brix allow higher colour removal at lower dosages, while dilutions to 30 and 40 Brix require a higher amount of AC to achieve the same colourless quality.

The optimum dosage, presented in Table 4.2, is defined as the AC dosage beyond which no further increase of colour removal occurs anymore. The optimum dosage for a lower concentration of 16 Brix is less than for higher concentrations. Thus, for lower concentrations less AC is required for the decolourisation process. It should be noted that the experiment with a dilution of 30 Brix was conducted with the 1st batch, leading to slight differences in the results.

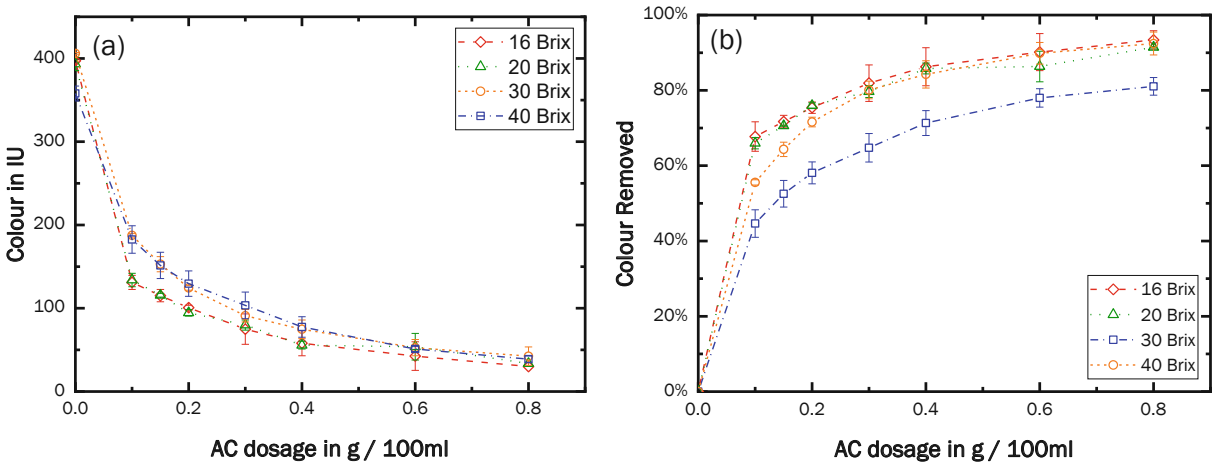

Figure 4.5: (a) Colour values and (b) colour removed in percentage after decolourisation with AC

As mentioned in Chapter 3.4.1, producing colourless sugar is the main objective. Therefore, determining the concentration that shows the best decolourisation behaviour in terms of lowest required relative AC dosage per gram of obtained sugar is essential for the process optimisation. Figure 4.6 presents the curves of decolourisation related to the relative AC dosage calculated according to Equation (3.3).

The solution with 40 Brix shows a significantly lower colour (Figure 4.6 (a)) and therefore a higher colour removal. Considering the optimum AC dosage, presented in Table 4.2, the required dosages are the same for dilutions from 16 to 30 Brix, while the 40 Brix solution required only half the amount of AC for the same amount of obtained sugar. Since the 1st batch used for the 30 Brix dilution showed generally slightly less decolourisation behaviour, it can be assumed that the relative dosage for this concentration would also be lower compared to lower concentrations.

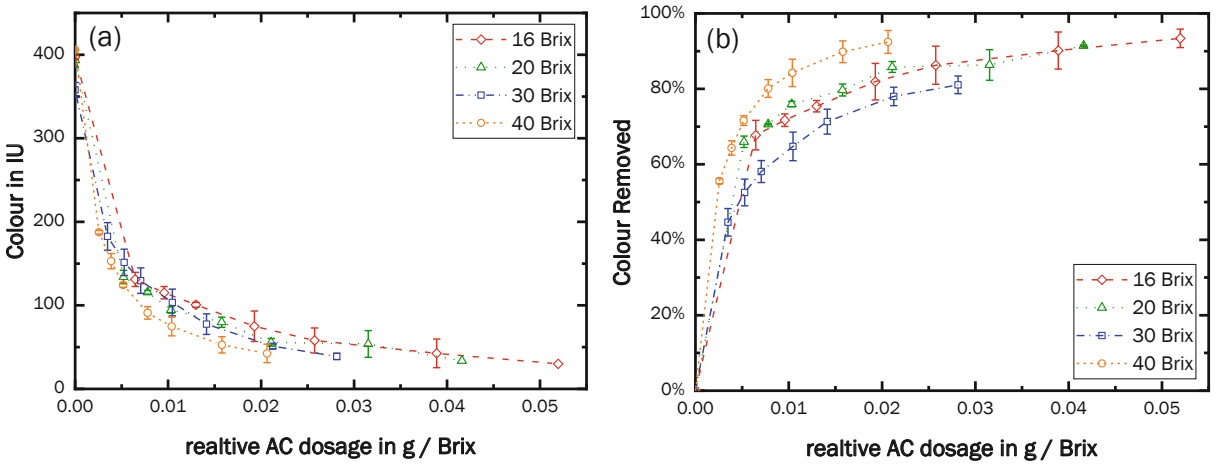

Figure 4.6: (a) Colour values and (b) colour removed in percentage after decolourisation with AC by using the relative AC dosage

Table 4.2: Optimum AC dosages for decolourisation and colour removed

Dilution	Optimum Dosage / g/100ml	Saccharose content after adsorption / g	Required g AC per g Sugar	Colour removed at optimum dosage	Remaining colour at optimum dosage / IU
16 Brix	0.3	7.54	0.020	85 %	75
20 Brix	0.4	9.37	0.021	88 %	56
30 Brix	0.6	14.39	0.021	87 %	51
40 Brix	0.4	20.03	0.010	85 %	75

During the decolourisation a noticeable colour removal was observed in the blank without any AC, especially with higher dilutions. Possible cause of this is the filtration for AC separation, which is investigated below in Chapter 4.1.3. This impacted especially the high dilutions with very low light absorbency. For the results presented in Figure 4.5 and

Figure 4.6 the reference for the removed colour is the colour in the blank, in this way only the actual colour removed by AC adsorption was considered.

When focusing on the obtained decolourised sugar, lower dilutions require less AC to remove the colour from glucose syrups. This means lower diluted syrup results in more efficient AC utilisation. However, lower dilution leads to higher viscosity, worsening the bulk fluid, film and intraparticle diffusion, as well as filtration behaviour. Therefore, a limit to the efficiency increase could be expected. Filtration of the 40 Brix solution already showed significant increase in required filtration time, meaning that the technically feasible concentration could be expected to be not far above the sugar concentration of 40 Brix.

4.1.2 Adsorption Kinetics

The first section deals with the determination of the equilibrium time, how it is affected by dilution and AC dosage, and check if previous equilibrium assumption of 40 minutes is correct, see Chapter 4.1.2.1. In the second part, kinetic models are applied on the experimental data for determination of the mass transfer mechanism dominating the decolourisation process, see Chapter 4.1.2.2 to 4.1.2.5.

4.1.2.1 Equilibrium time

As in equilibrium experiments, results from kinetic experiments with different dilutions, shown in Figure 4.7 (a), indicate that the colour removal capability is similar for all concentrations except 30 Brix. This is supported by the data shown in Table 4.3, with no significant difference between the different concentrations, except for 30 Brix dilution, which was carried out with a different batch (1st batch).

Comparing the curves of 16, 20, and 40 Brix, the latter, with significantly higher sugar concentration, requires more time to reach the maximum colour removal. The equilibrium time is achieved when no change in colour removal occurs anymore, which was determined by ANOVA analysis. Lower dilutions, therefore higher concentration of colour components, result in longer adsorption times until equilibrium, see Table 4.3. Thus, a higher dilution, meaning lower colour concentration, resulted in a significantly faster decolourisation process. Considering that the objective was decolourised sugar, the same conclusion applies: The time required for decolourisation per Brix, determined by dividing equilibrium time by sugar concentration, is 0.64 min/Brix for a highly diluted 16 Brix syrup compared to 1.55 min/Brix for a 40 Brix syrup. Thus, if a fast adsorption process is the goal, a high dilution of the syrup is favourable.

As shown in Figure 4.7 (b) and detailed in Chapter 4.1.1.2, the capacity for colour removal decreases with the reduction of AC dosages. This could be expected since higher AC dosages, provide a larger surface with more adsorption sites. The time to reach equilibrium increases with the lowering of AC dosage, as indicated by the curves in Figure 4.7 (b) and statistical analysis presented in Table 4.4.

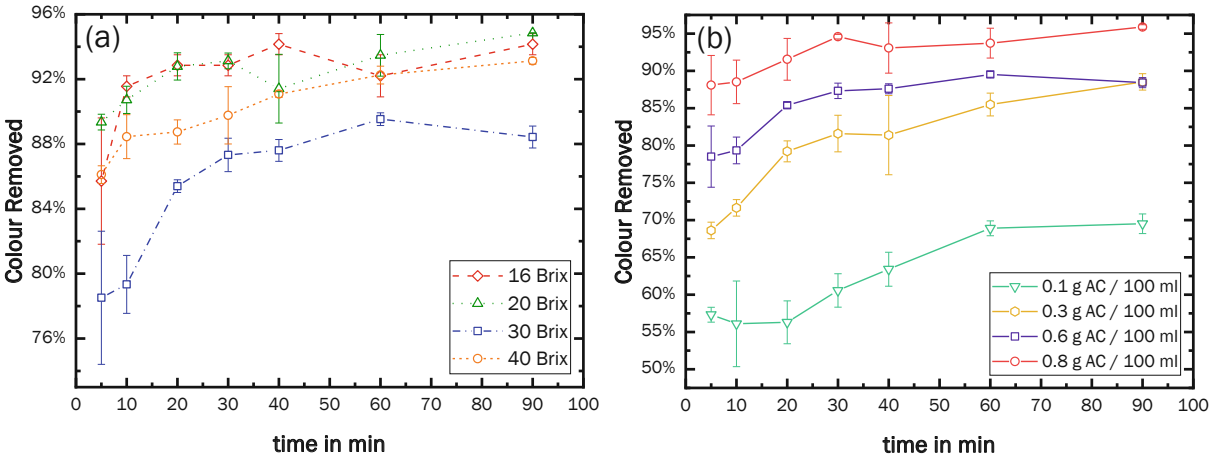

Figure 4.7: Decolourisation over time with different sugar concentration for AC dosages of 0.6 g / 100 ml in (a) and different AC dosages with dilutions to 30 Brix in (b)

Table 4.3: Equilibrium time and colour removal for several dilutions

Dilution	Equilibrium time / min	Colour removed at equilibrium	Colour removed / IU	Colour at equilibrium / IU
16 Brix	10	92 %	415	34
20 Brix	20	93 %	409	30
30 Brix	30	87 %	310	41
40 Brix	60	92 %	436	34

Table 4.4: Equilibrium time and colour removal for several AC dosages

AC dosage / g/100ml	Equilibrium time / min	Colour removed at equilibrium	Colour removed / IU	Colour at equilibrium / IU
0.1	60	69 %	333	148
0.3	30	82 %	381	71
0.6	30	87 %	310	41
0.8	5	94 %	417	35

Comparing kinetic with equilibrium results the highest efficiency in terms of kinetics is achieved with low concentrations of the feed solution and high AC dosage. However, both parameters will reach a maximum reduction in contact time, and AC dosage will have a maximum effect on colour removal. On the other hand, increasing dilution requires more water, leading to higher energy consumption for heating of the solution in the process and concentrating it through evaporation for storage purposes. Furthermore, the aim is to minimise AC dosage for waste reduction, as evaluated in 4.1.1.2. Therefore, finding the optimal conditions for the decolourisation process requires an overall evaluation, including minimum AC dosage needed to meet product quality requirements, alongside kinetic analysis in relation with energy consumption and economic aspects.

4.1.2.2 Film Diffusion Model

Solving Equation (2.28) together with the initial and boundary conditions mentioned in Chapter 2.3.5.3.1, equation for the kinetic curve of film mass transfer results as

$$\frac{c}{c_0} = \frac{1}{\left(\frac{m_A}{V_L}K_H + 1\right)} + \frac{\frac{m_A}{V_L}K_H}{\left(\frac{m_A}{V_L}K_H + 1\right)} \exp\left[-\left(\frac{m_A}{V_L}K_H + 1\right) k_F a_m \frac{1}{K_H}\ t\right] \tag{4.1}$$

The calculation steps can be found in Appendix C. Together with the median particle size of $r = 35\ \mu m$ and a density of $\rho_p = 0.43\ g/ml$ the specific particle surface leads to

$$a_m = \frac{3}{r\rho_p} = 1993.4\ cm^2/g \tag{4.2}$$

when spherical particles are assumed. The value for the AC dosage factor m_A/V_L is defined as

$$\frac{m_A}{V_L} = 0.6\frac{g}{100\ ml} \tag{4.3}$$

for a dosage of 0.6 g / 100 ml used in the experiment with different dilutions. The Henry constants are from equilibrium experiments, shown in Table 4.1.

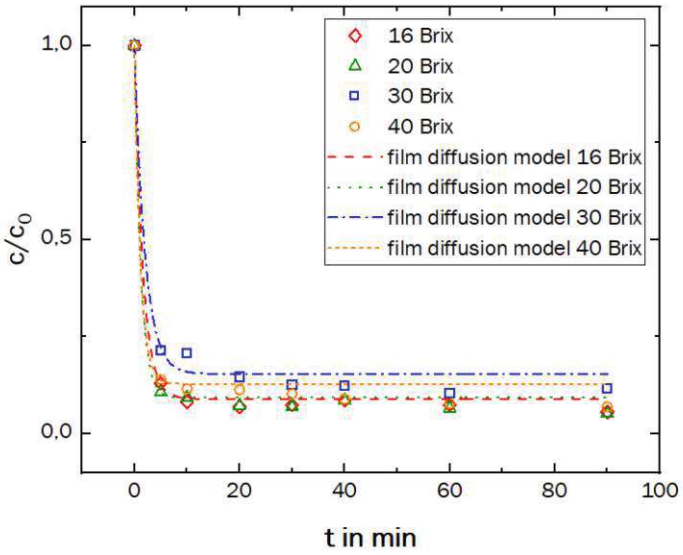

Figure 4.8: Fitting of film diffusion model to kinetic data of different dilutions

The fitted kinetic curve of film diffusion shows a very fast removal of adsorbate concentration at the initial stage of the adsorption process of approximately ten minutes, indicated by the steep negative slope at the beginning of the curve presented in Figure 4.8. This is also evidenced by the high values of the film diffusion coefficient, see Table 4.5. However, kinetic data shows an additional slow occurring adsorption process after the very fast at the first minutes and state of equilibrium can require up to 60 minutes, see Table 4.3. This especially occurs at lower dilutions, making them less fitting to the film diffusion model.

Table 4.5: Film mass transfer coefficient of different dilutions

Dilution	16 Brix	20 Brix	30 Brix	40 Brix
k_F / cm · s^{-1}	4.788 · 10^{-6}	6.350 · 10^{-6}	3.551 · 10^{-6}	6.433 · 10^{-6}
R^2	0.997	0.995	0.988	0.988

4.1.2.3 Intraparticle Diffusion Model

For solving of the intraparticle diffusion model of Equation (2.36) the values for γ_n were calculated by GeoGebra Classic [58]. Thereby, the first five terms of the series are calculated and used for the fitting. Terms of higher γ_n are neglected due to their low value. Since the adsorbent loading at the beginning is zero, $q_0 = 0$, we have $m_\infty = \bar{q}_\infty$. The calculated values used for the curve fitting can be found in Appendix D.

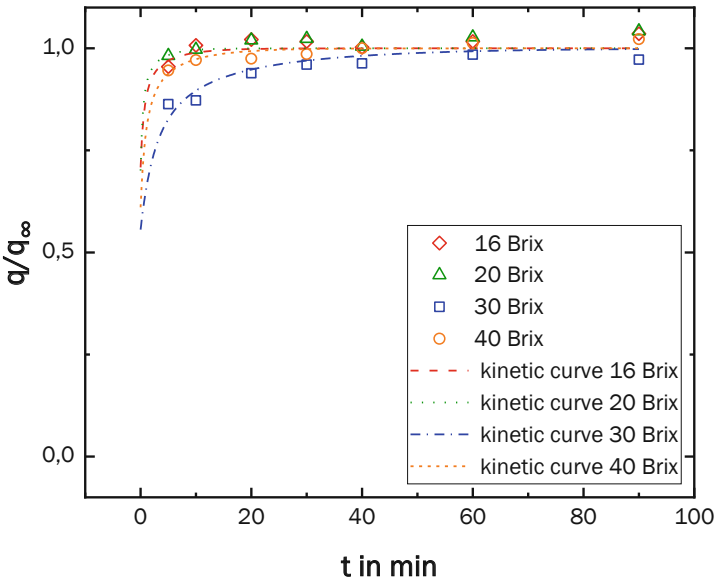

Figure 4.9: Intraparticle diffusion model fitted to kinetic data of (a) different dilutions and (b) different AC dosages

The curves of the intraparticle model are fitting kinetic data very well and can describe the initial as well as the slower adsorption process after around ten minutes, see Figure 4.9. Residuals presented in Appendix B prove the good fit of the model. The intraparticle diffusion seems to occur slower for less diluted glucose syrup, also indicated by the coefficients being slightly lower for lower dilutions, see Table 4.6.

Table 4.6: Intraparticle diffusion coefficients at different dilutions

Dilution	16 Brix	20 Brix	30 Brix	40 Brix
$(D_S)_e$ / cm^2 · s^{-1}	18.76 · 10$^{-10.}$	29.49 · 10^{-10}	4.812 · 10^{-10}	13.66 · 10^{-10}

The second intraparticle model, the Weber and Morris model, was separated in the two ranges of [t_0 = 0 min … t_1 = 5 min] and [t_1 = 5 min … t_2 = $t_{equilibrium}$]. The time $t_{equilibrium}$ corresponds to the time necessary to achieve equilibrium as estimated before, see Table 4.3. The linear fitting, Figure 4.10 (a), resulted in the constants, shown in Table 4.7 and Table 4.8, necessary to calculate the kinetic curves presented in Figure 4.10 (b). The curve in the first range of the adsorption process consists only of two measured points, making conclusion about the suitability of the model difficult. However, the curve at the second range of the process shows good fitting to the kinetic data.

The intraparticle diffusion coefficients are calculated with Equation (2.44). For the first stage of the adsorption process the intraparticle diffusivity is not affected by the dilutions, see similar diffusion coefficients in Table 4.7. The diffusivity in the second range increases with higher dilutions with a coefficient increasing by approximately the factor 10 for each further dilutions, as data in Table 4.8 shows.

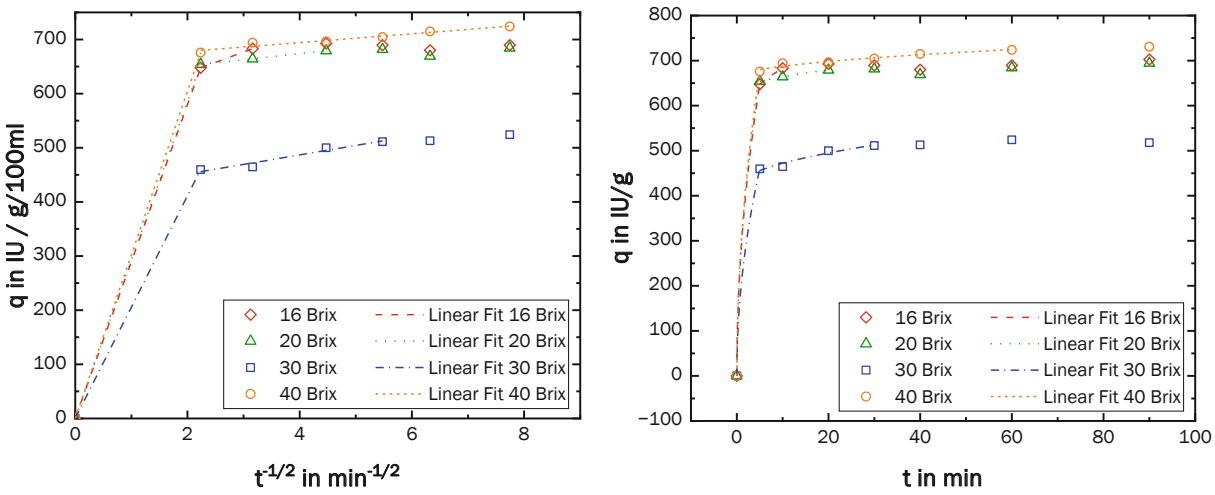

Figure 4.10: Linear fitting of Weber and Morris Model in (a) and the resulting kinetic curve in (b) for kinetic data of different dilutions

Table 4.7: The surface diffusivity and intraparticle diffusion constant by the Weber and Morris model for the first range

	16 Brix	20 Brix	30 Brix	40 Brix
K / IU (g/100ml)$^{-1}$ min$^{-1/2}$	289,63	292,46	205,57	302,18
$(D_S)_e$ / cm^2 · s^{-1}	$2.508 \cdot 10^{-8}$	$2.677 \cdot 10^{-8}$	$2.372 \cdot 10^{-8}$	$2.679 \cdot 10^{-8}$

Table 4.8: The surface diffusivity and intraparticle diffusion constant by the Weber and Morris model for the second range

	16 Brix	20 Brix	30 Brix	40 Brix
q_0	562	629	417	662
K / IU (g/100ml)$^{-1}$ min$^{-1/}$	38.27	11.27	17.51	8.094
R^2	1	0.9997	0.9501	0.9503
$(D_S)_e$ / cm^2 · s^{-1}	43.78 · 10^{-11}	3.959 · 10^{-11}	17.20 · 10^{-11}	1.922 · 10^{-11}

Applying of Equation (2.45), which is applicable for adsorbent loads above 70 %, resulted in a less sufficient fit, see Figure 4.11 and Table 4.9. The adsorbent load is close to the equilibrium at the late stage of the adsorption process. Due to deviations adsorbent load higher as the equilibrium load appears, causing negative values for the term inside the logarithm. Thus, not enough datapoints are present for dilutions of 16, 20, and 40 Brix. However, same as in the previous curves, the diffusion coefficient increases with higher dilution when comparing 20 and 40 Brix, see Table 4.9.

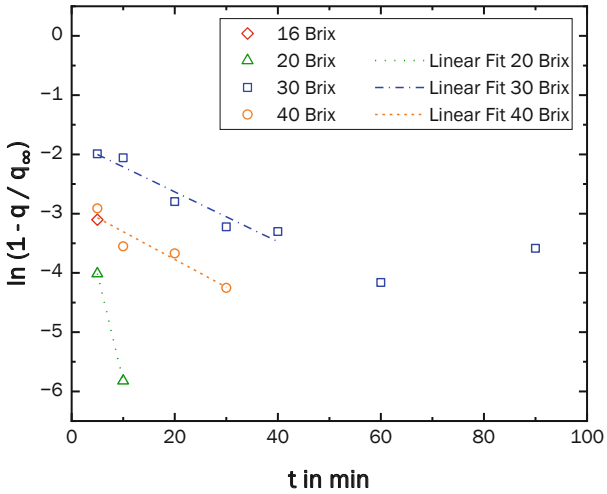

Figure 4.11: Fitting of Weber and Morris model for adsorbent load above 70 %

Table 4.9: Weber and Morris Model for adsorbent loads above 70 % according to Equation (2.45)

	16 Brix	20 Brix	30 Brix	40 Brix
$(D_S)_e$ / cm^2 · s^{-1}	-	74.82 · 10^{-10}	8.701 · 10^{-10}	9.694· 10^{-10}
R-Quadrat	-	1	0.9301	0.8932

The commonly used Weber and Morris model fits good to the two stages of the adsorption process. However, it lacks theoretical basis [39] and can be interpreted

differently and even possibly incorrect [36]. Therefore, it must be viewed carefully. Additionally, there is not enough data present for the fast initial adsorption process.

The intraparticle diffusion model suited the experimental determined kinetic data best, describing the adsorption process well. Both models, intraparticle diffusion and Weber and Morris, showed that diffusivity increases with higher dilutions. The dimensionless Biot number, Bi, according to Do [22] adapted for the present problem reads as:

$$Bi = \frac{k_F \, a_p}{(D_S)_e} \tag{4.4}$$

It measures the relative resistance of the film surrounding the particle to the internal diffusion resistance. Calculation of the Biot number with values from film diffusion and intraparticle diffusion models leads to values presented in Table 4.10. A higher Biot number indicates a higher rate of film diffusion compared to intraparticle diffusion [20]. Thus, with high values above one the adsorption rate is generally governed by intraparticle diffusion. Higher dilution leads to decreasing of the Biot number, meaning that film diffusion will also play a more relevant role when the syrup is diluted stronger. This may can be explained by a lower density of colour and sugar compounds in the bulk fluid phase, resulting in a lower concentration of molecules in the pores. This lower concentration resulting in less viscosity due to less interaction between the colour molecules and thus increases the mobility of them.

Table 4.10: Biot numbers for several dilutions

	16 Brix	20 Brix	30 Brix	40 Brix
Biot number	8.933	7.537	25.82	16.48

4.1.2.4 LDF Model

The equation for the LDF model, Equation (2.48), is solved similar as the film diffusion model together with the initial and boundary conditions of Equation (2.52). This leads to the equation for the kinetic curve as

$$\frac{c}{c_0} = \frac{1}{\left(\frac{m_A}{V_L} K_H + 1\right)} + \frac{\frac{m_A}{V_L} K_H}{\left(\frac{m_A}{V_L} K_H + 1\right)} \exp\left[-\left(\frac{m_A}{V_L} K_H + 1\right) k_S^* t\right] \tag{4.5}$$

The calculation steps can be found in Appendix E. The value for the AC dosage factor is $m_A/V_L = 0.6 \frac{kg}{100ml}$. The Henry constants are from equilibrium experiments, shown in Table 4.1.

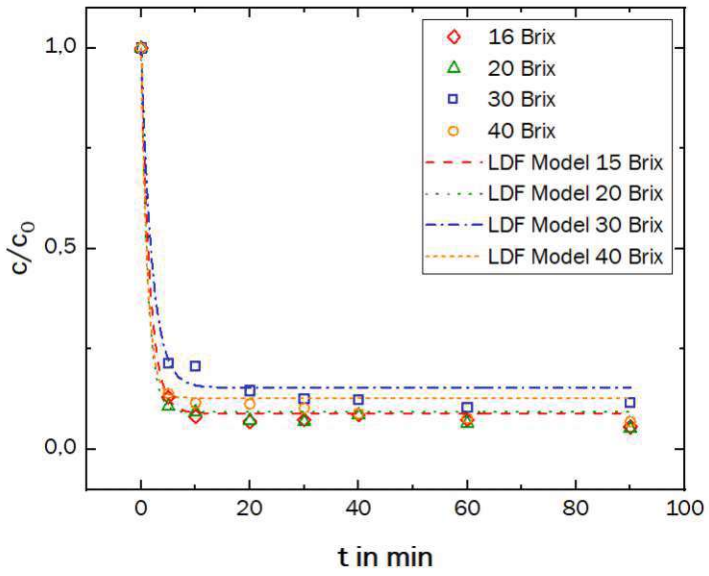

Figure 4.12: LDF model fitted to kinetic data of several dilutions

The kinetic curves of LDF model show a good fit to the data but are not able to explain the slow occurring adsorption process after the very fast initial one, similar as in the film diffusion model. The curves are comparable to the film diffusion model as expected due to their identical mathematical character. The intraparticle diffusion coefficient, calculated from the determined diffusivity coefficient by Equation (2.51) decreases slightly for higher dilutions, see Table 4.11. The good fit of the intraparticle diffusion model, which can describe the second slow adsorption process, makes the LDF model obsolete.

Table 4.11: LDF model coefficients for different dilutions

	16 Brix	20 Brix	30 Brix	40 Brix
k_S^* / min^{-1}	3.3882	4.6596	4.6368	6.7734
D_S / $cm^2 \cdot s^{-1}$	$7.686 \cdot 10^{-10}$	$10.06 \cdot 10^{-10}$	$10.52 \cdot 10^{-10}$	$15.37 \cdot 10^{-10}$
R^2	0.99707	0.99532	0.98785	0.98788

4.1.2.5 Reaction Kinetic Models

The equilibrium load, q_e, required for the linear fit by Equation (2.55) for the first order and Equation (2.57) for the second order model are calculated according to the material balance equation shown in Equation (2.9) and Equation (2.24). Thereby, the equilibrium concentration was defined by the average colour concentration in the bulk fluid phase after the equilibrium from Table 4.3.

Linear regression of the first order model resulted in a not satisfactory fit, see Figure 4.13 (a) and Table 4.12. Additionally, some datapoints, specially at a later point during the adsorption process, are not included, because their adsorbent load was higher

than the equilibrium load. This leaded to no solution for these datapoints. The resulting kinetic curve, presented in Figure 4.13 (b), does not suit the kinetic data until after approximately 30 minutes.

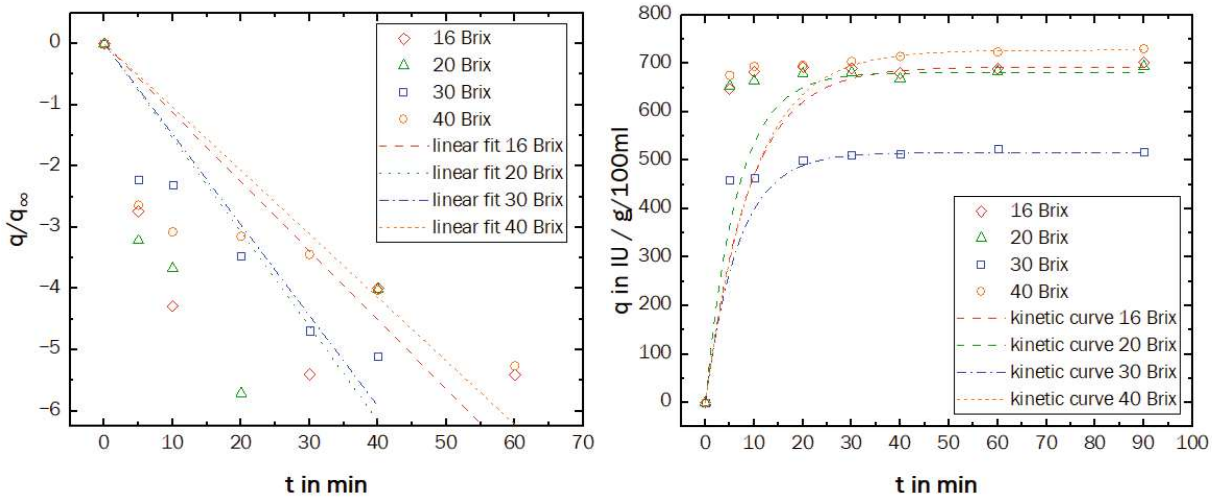

Figure 4.13: Linear regression in (a) and the resulting kinetic curve in (b) for the pseudo first-order model

Linear regression of pseudo second-order model fits well with the kinetic data, see Figure 4.14 (a) and Table 4.12. The resulting kinetic curve can describe the adsorption process in a plausible manner when compared to the kinetic data presented in Figure 4.14 (b). However, the pseudo second-order may show weakness in describing the initial stage, indicated in the first two points of the dataset being slightly at a higher adsorbent loading as the curve.

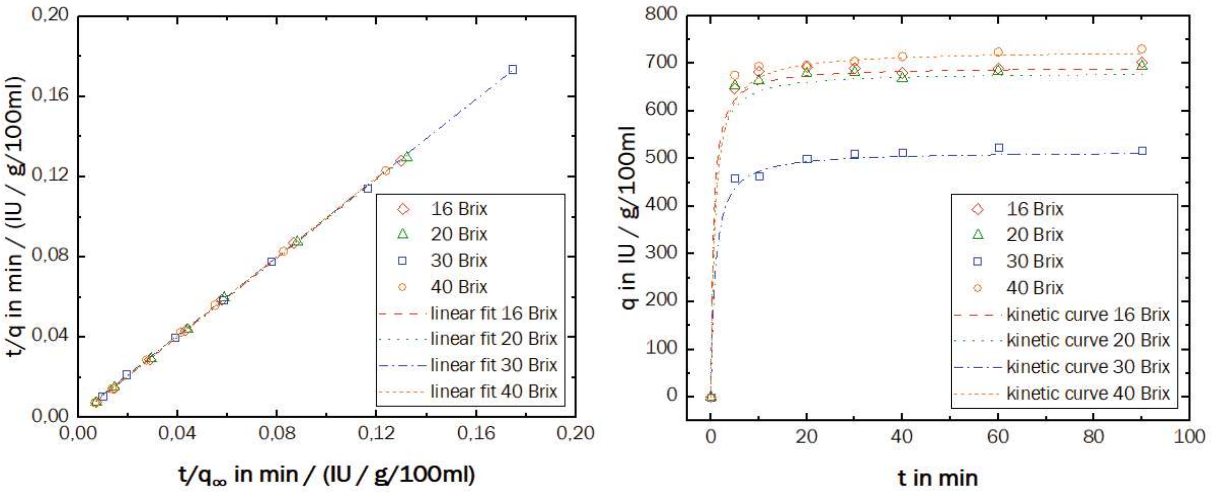

Figure 4.14: Linear regression in (a) and the resulting kinetic curve in (b) for the pseudo second-order model

From the widely used reaction kinetic models the second order fits the data sufficient, while first order model do not agree well. Similar results were obtained by Nasehi et al. [59] and Ahdno and Jafarizadeh-Malmiri [60] with date syrup. However, both models lack justification [36] and it is well known that intraparticle diffusion plays an important role at

porous adsorbents [20]. Thus, the results should be considered carefully, and a reaction dominated adsorption process is very implausible.

Table 4.12: Constants and equilibrium loading of pseudo first and second order adsorption models

Dilution	q_e / IU / g/100ml	Pseudo First Order		Pseudo Second Order	
		K_1 / s^{-1}	R^2 of linear fit	K_2 / $s^{-1} \cdot$ (IU / g/100ml)$^{-1}$	R^2 of linear fit
16 Brix	692	$1.881 \cdot 10^{-3}$	0.7917	$4.391 \cdot 10^{-5}$	0.9997
20 Brix	682	$2.569 \cdot 10^{-3}$	0.6961	$3.924 \cdot 10^{-5}$	0.9998
30 Brix	517	$2.468 \cdot 10^{-3}$	0.9452	$3.618 \cdot 10^{-5}$	0.9998
40 Brix	727	$1.728 \cdot 10^{-3}$	0.8679	$2.645 \cdot 10^{-5}$	0.9999

4.1.3 Decolourisation by AC Separation

Results in Figure 4.15 from the decolourisation experiment without AC, both with and without subsequent filtration, show that colour can be reduced by the filter paper by approx. 100 IU respectively 20 %. This indicates that more than 20 % of colour molecules are either a size greater than 2-3 µm or adsorbed by the filter material, resulting in colour removal through filtration.

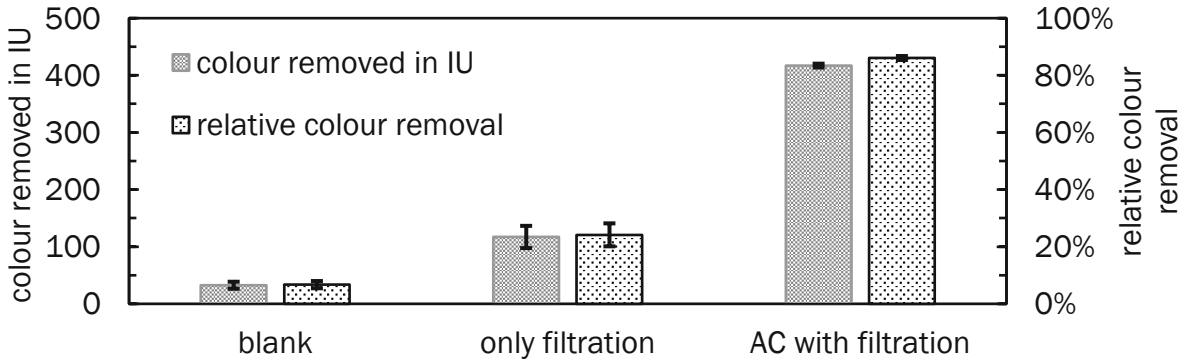

Figure 4.15: Colour removed due to filtration compared to colour removed due to AC for dilution to 30 Brix and AC dosage of 0.6 g / 100 ml

The occurrence of colour removal through AC filtration suggests that pre-treatment with filtration before AC treatment could be a promising decolourisation technology, as shown similar by Al-Farsi [61] with colour removal from 6.6 to 3.7 IU by two stage filtration with 50 µm followed by 3 µm. However, it is unclear if filtration after AC treatment improves decolourisation, as it is not determined whether the pigments filtered out were already adsorbed by AC.

4.1.4 Decolourisation and Sugar Loss

Measurement of the sugar after the decolourisation process showed sugar losses in the range of 0.5 to 1.5 Brix compared to the initial solution, as seen in Figure 4.16 for various dilutions. During the decolourisation there is no significant difference in sugar loss at equilibrium for solutions with different concentrations, with a p-value of 0.72 and 0.18, for 16 Brix and 40 Brix, respectively. Similarly, the kinetic data for different solution concentrations and different AC dosages also do not show significant difference, see Appendix F.

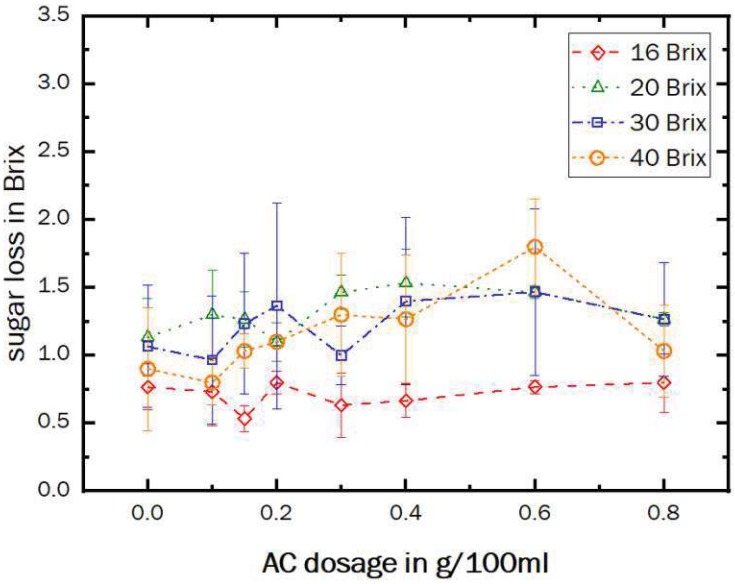

dilution / Brix	average reduction / Brix	deviation / Brix
16	0.7	0.2
20	1.3	0.2
30	1.2	0.5
40	1.2	0.3

Figure 4.16: Average sugar reduction at several AC dosages for different sugar concentrations

The constant sugar loss, regardless of process parameters, indicates that sugar loss maybe occurs due to a step other than adsorption. However, other studies show a dependency of sugar loss on the AC dosage. Deng et al. [62] reported sugar reduction of 10.2 % and 27.8 % for AC dosage of 5 % w / v respectively 10 % w / v, and a study by Preechakun et al [63] resulted in a sugar loss increase from 6.85 % to 11.65 % when AC dosage is increased from 5 to 11 % w / v. Possible cause of this disagreement is due to the applied dosages which are in a far higher range in other studies than in this study. The ranges here are very small with an increase from 0.1 to 0.8 g / 100 ml meaning 0.1 to 0.8 % w / v. Comparing results from Mustapa [64] with similar AC dosage of 1 % w / v and a pH of 5.5 identical sugar loses of 4 % are obtained. As reported by Lee et al. [65] sugar is not adsorbed by the AC but more possibly entrapped inside the AC particles and thus an increase of sugar loss for significant higher dosages can be expected.

Beside the entrapped sugar in the AC also the filtration of AC can restrain a significant amount of sugar at the decolourisation process. Thus, the effect on the sugar loss of the different process steps adsorption and filtration were observed, resulting in losses shown in Figure 4.17. Thereby, sugar losses of around 5 to 6% occurring for both cases with

filtration with no significant difference between with and without AC. This means the primary cause of sugar loss is the separation of AC through filtration and the sugar entrapped is negligible for small AC dosages as used in this study. Similar conclusion can be made from results from Al-Farsi [61] where filtration and AC have nearly similar sugar removal from 18.4 to 16.7 for filtration and 16.5 for powdered AC.

Therefore, to minimize sugar losses in decolourisation processes, the focus should be on the separation step of the AC. Investigating filter paper to identify a medium with low sugar retention could offer improvements. Alternatively, another separation process, such as centrifugation, may result in lower sugar losses.

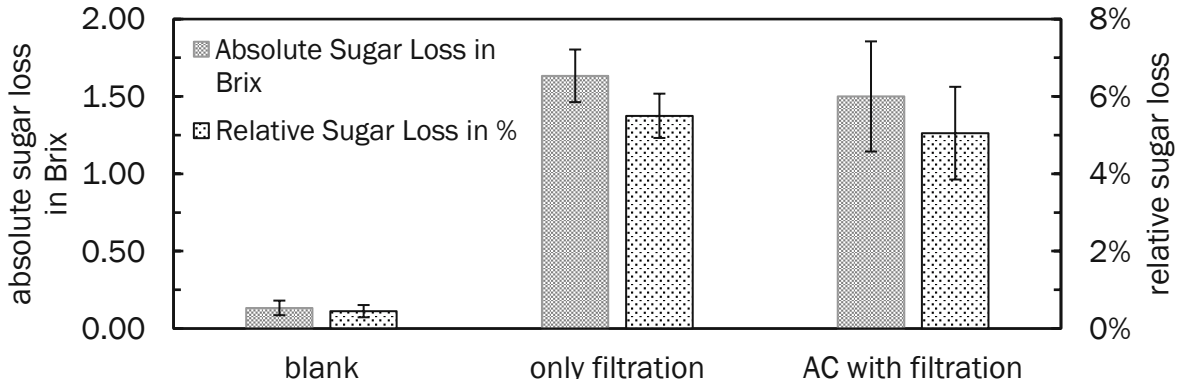

Figure 4.17: Sugar reduction due to AC in comparison due to the AC separation step for dilution to 30 Brix and AC dosage of 0.6 g / 100 ml

4.2 Decolourisation with Membrane-Based Pre-Treatment

An advantage of membrane-based pre-treatment on decolourisation is analysed by comparing the removed colour and the colour after several AC dosages of the pre-treated solution to the decolourised raw syrup with similar sugar concentration, from results presented above. Following presents first the results from UF alone, afterwards from multistage setups, and last AC savings and advantages by the pre-treatment.

4.2.1 Ultrafiltration

Decolourisation with pre-treatment by loose (100 kDa) and tight UF (5 kDa) membranes show no improvements compared to syrup without pre-treatment, see resulting curves in Appendix G. This is an unsatisfactory result since it is shown in other studies that membrane-based pre-treatment of the syrup can remove colour and thus improve the decolourisation efficiency of the AC treatment.

For example, Atiyeh and Duvnjak [7] demonstrate that filtration of fructose syrup by a membrane with 10 or 1 kDa MWCO before AC treatment resulted in higher colour removal compared to AC treatment only. Cabeza et al. [6] showed that UF by membrane with 70 kDa MWCO can remove 27 % of the colour from glucose syrups. Gyura et al. [66] using UF with 15—20 kDa and 6-8 kDa MWCO to reduced colour of syrup from sugar-beet processing by

55 % respectively 58 %. Furthermore, results below from multistage pre-treatment show that UF plays a significant role in improvement of decolourisation by AC treatment.

Causes for the bad performance with tight UF are may due to the high dilution of the permeate, leading to high deviations due to inaccuracy in measurement of light absorbance. Another possible reason for the lack of improvement is the fact that the benchmark curve of 16 Brix was carried out with the 2nd batch, which in generally showed better decolourisation behaviour. Considering this worse decolourisation behaviour, with the 1st batch the UF pre-treatment was carried out, an improvement by tight UF is plausible.

The worsening of AC decolourisation with loose UF can possibly be explained by an error due to the usage of samples with only 25 ml. As there was not enough pre-treated syrup available, the adsorption experiments were carried out with these smaller samples and not enough datapoints. This may have caused high deviations in the measurement.

4.2.2 Three-Stage Membrane-Based Pre-Treatment

The three-stage membrane filtration followed by AC adsorption resulted in a lower IU-value and a higher colour removal compared to the AC treatment of the raw syrup, see Figure 4.18 and Figure 4.19 respectively. Notably, the setup without additional dilution of feed 2 of tight UF (Figure 4.18) resulted in significantly lower colour (Figure 4.18 (a)) and higher colour removal (Figure 4.18 (b)) at the lower dosages up to 0.4 g AC / 100 ml. On the other hand, additional dilution of the tight UF feed shows a decrease in performance after 0.15 g AC / 100 ml, resulting in only slightly lower colour compared to the AC adsorption on the raw syrup, with improvements present only for AC dosages of 0.1 and 0.15 g AC / 100 ml, see Figure 4.19 (a). For colour removal, this set up provides nearly no improvement at all.

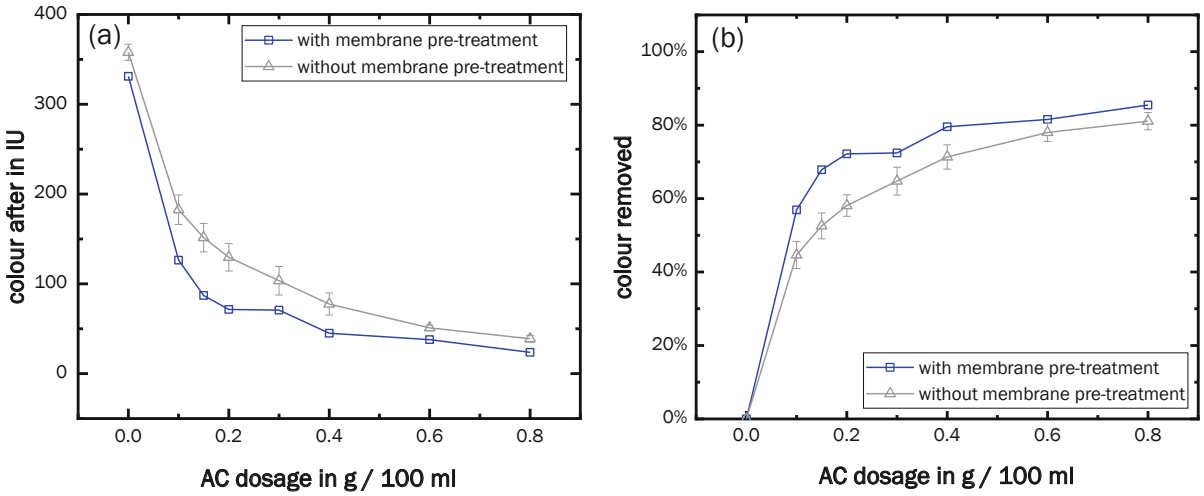

Figure 4.18: (a) Colour values after treatment with AC adsorption and three-stage membrane pre-treatment without additional dilution of feed 2 (Setup 3.2) compared to a non-pre-treated syrup and (b) colour percentage removed by the process

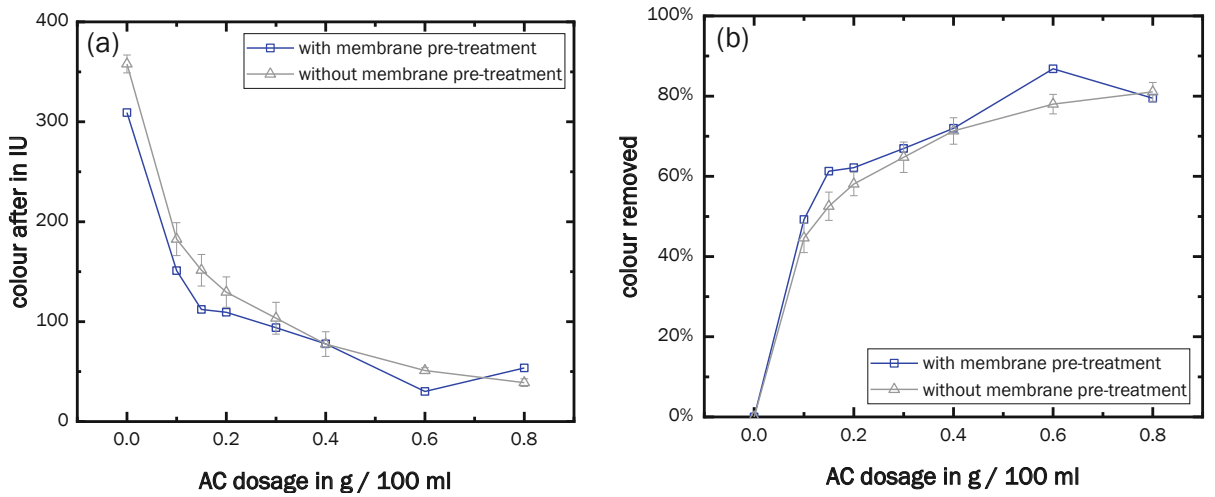

Figure 4.19: (a) Colour values after treatment with AC adsorption and three-stage membrane pre-treatment with additional dilution of feed 2 (Setup 3.1) compared to a non-pre-treated syrup and (b) colour percentage removed by the process

Freundlich isotherm models presented in Figure 4.20 demonstrate that the adsorbent loading increases significantly with pre-treatment with a tight UF feed of 30 Brix, indicated by the higher slope of the curve. This improvement by the membrane-based pre-treatment cannot be found with a 20 Brix feed at tight UF.

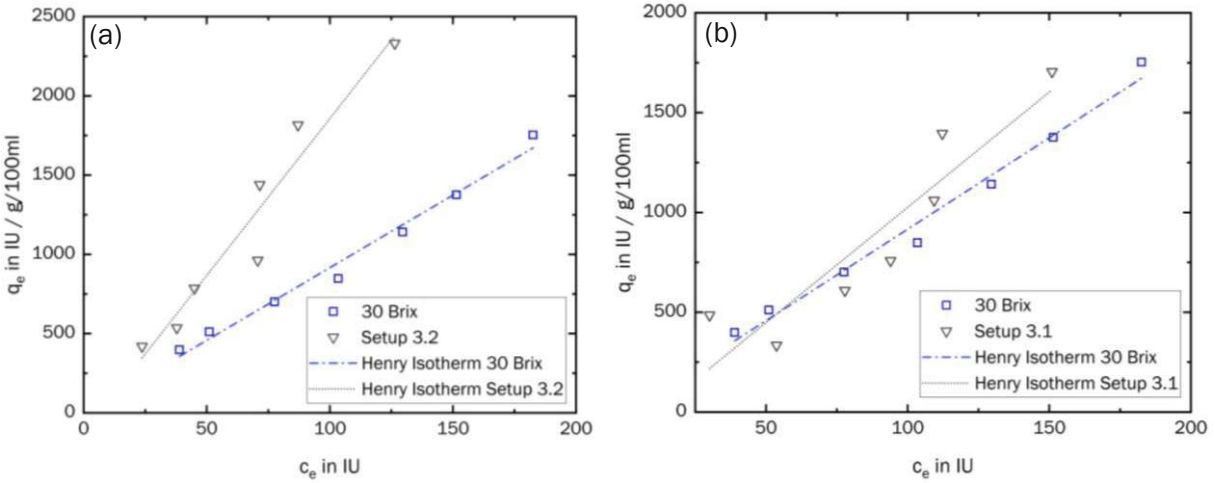

Figure 4.20: Henry isotherms of three stage membrane pre-treated syrup (a) without and (b) with additional dilution of feed 2

Summarizing, the tree stage membrane pre-treatment performed very well without additional dilution of the feed for tight UF. Additional dilution of the feed 2 to 20 Brix resulted in a performance drop with increasing dosage. Due to lack of replicates, it is unclear if this drop is due to deviations or errors. Since this drop does not fit the trend of other curves, it is more plausible that it is due to measurement inaccuracies or errors. It is clear that, in terms of colour removal, dilution does not lead to any performance improvements and should be avoided if possible.

4.2.3 Two-Stage Membrane-Based Pre-Treatment

Pre-treated syrup by tight UF followed by tight NF resulted in significant improvement in the AC decolourisation behaviour of the syrup, see Figure 4.21 and Figure 4.22. Thereby, with the two-stage membrane-based pre-treatment it was possible to achieve a very low colour below 100 IU already at the lowest dosage of 0.1 g AC / 100 ml. In general, it was possible to reduce colour by approximately 70 IU and improve colour removal by around 14 % for AC dosages in the range of 0.1 to 0.4 g AC / 100 ml.

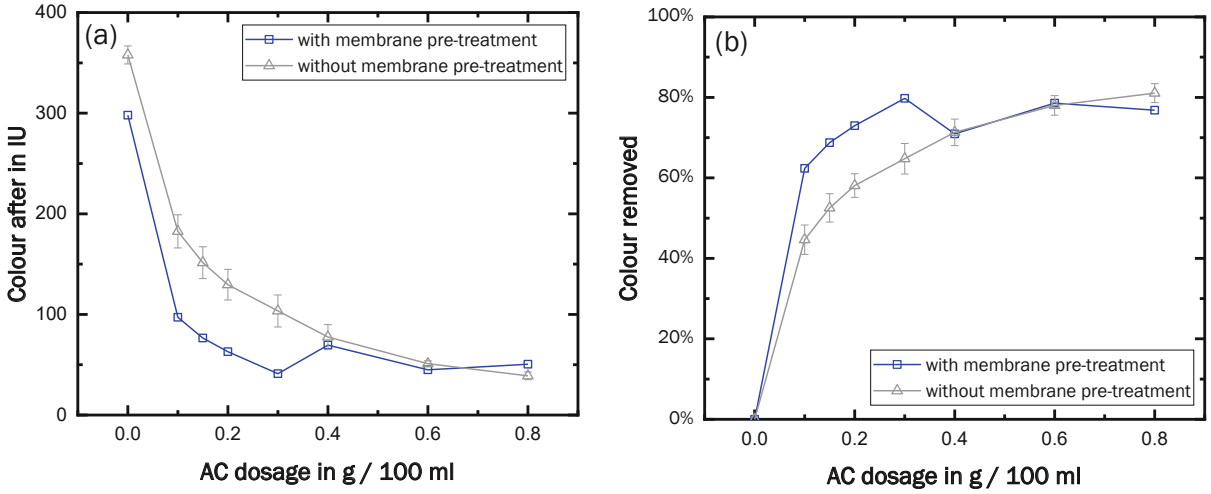

Figure 4.21: (a) Colour values after treatment with AC adsorption and two-stage membrane pre-treatment with an initial feed concentration of 20 Brix (Setup 2.1) compared to a non-pre-treated syrup, and (b) colour percentage removed by the process

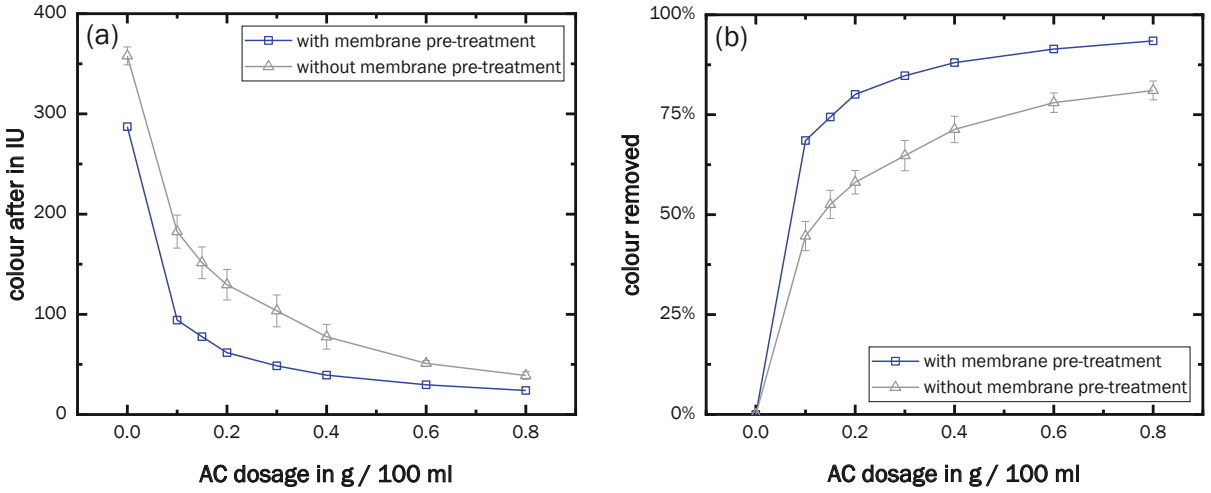

Figure 4.22: (a) Colour after treatment with AC adsorption and two-stage membrane pre-treatment with an initial feed concentration of 30 Brix (Setup 2.2.) compared to a non-pre-treated syrup, and (b) colour percentage removed by the process

The curve of the pre-treated syrup with an initial solution of 20 brix, see Figure 4.21, show a decrease in decolourisation characteristics starting at a dosage of 0.4 g AC / 100 ml, which is not a plausible trend in this adsorption process and probably can be explained by deviations in measurement.

The Freundlich isotherms of two-stage membrane-based pre-treatment show significant improvement for feed with 20 Brix as well as with 30 Brix, see Figure 4.23 (a) respectively (b). Both have distinct higher slopes meaning higher adsorbent loading for lower colour remaining in the bulk solution at equilibrium. In contrast to previous results in three-stage membrane-based pre-treatment, the higher diluted feed of 20 Brix performs slightly better or at least similar to the lower diluted feed.

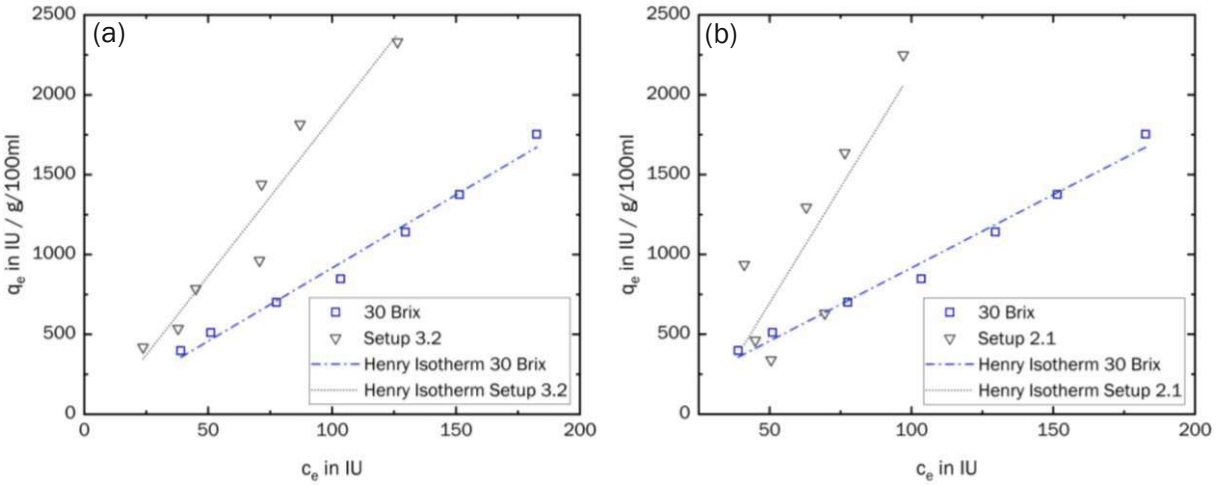

Figure 4.23: Henry Isotherms of two stage membrane setup with tight UF and NF with an initial feed of (a) 20 Brix and (b) 30 Brix compared to not pre-treated syrup with 30 Brix

Generally, two stage membrane with tight UF followed by tight NF led to significant improvement in decolourisation by AC adsorption after the pre-treatment. In contrast to the three-stage membrane-based pre-treatment, the setup with the higher diluted feed of tight UF also resulted in significant lower colour.

4.2.3.1 Two-Stage Membrane-Based Pre-Treatment with Loose NF

Results of AC adsorption on syrup which underwent tight UF followed by loose NF show very high fluctuations in the datapoints of the several AC dosages, see Figure 4.24. This is likely due to the high dilution of the syrup, resulting to substantial inaccuracies in light absorbance measurement. The initial colour of the pre-treated syrup was 23.5 % lower as the non pre-treated syrup. However, even the best dosages of 0.1 and 0.2 g AC / 100 ml only show a negligible lower colour after AC treatment for the pre-treated syrup compared to the non-pre-treated syrup. Also, in colour removal the pre-treated syrup performs only similar or worse for all dosages.

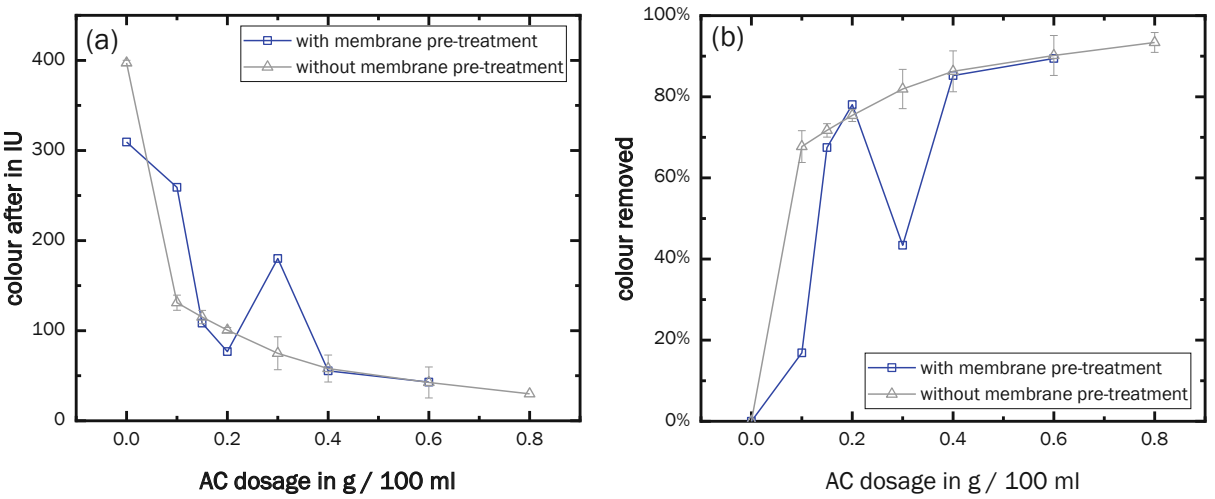

Figure 4.24: (a) Colour after treatment with AC adsorption and two-stage membrane pre-treatment with loose NF (Setup 2.3) compared to a non-pre-treated syrup, and (b) colour percentage removed by the process

Henry isotherm of pre-treated and not pre-treated syrup in Figure 4.25 show that the pre-treated curve has a slightly higher slope, indicating a better adsorption behaviour of the pre-treated syrup.

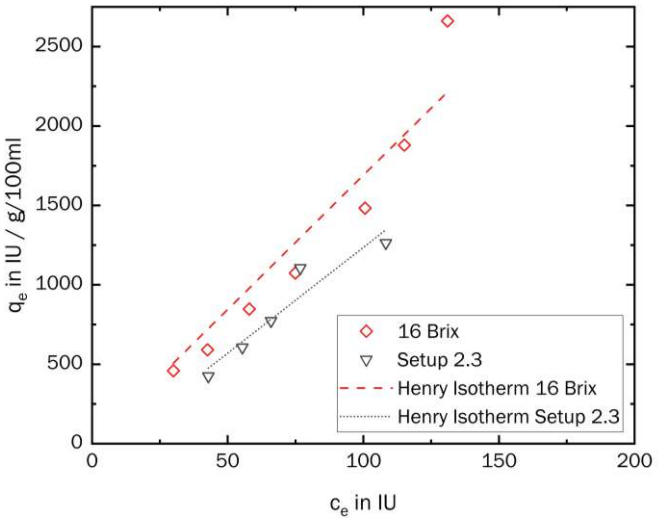

Figure 4.25: Henry isotherm of two-stage membrane pre-treatment syrup with loose NF compared to decolourisation with not pre-treated 16 Brix syrup

Due to high deviation in the results, it is difficult to draw exact conclusions from the pre-treated syrup with loose UF. However, it can be assumed that tight UF improves decolourisation performance in this set up as well. The high dilution caused by loose NF led to very low values in the absorption measurement, resulting in a strong impact at already very low measurement errors. Also, the non-pre-treated syrup of 16 Brix syrup was from the 2nd batch, so comparison of this results should be treated carefully.

4.2.4 Diafiltration

With syrup pre-treatment by tight UF followed by tight NF with diafiltration each around 50 IU lower colour was achieved after AC decolourisation for low dosages of 0.1 to 0.3 g AC / 100 ml when compared to the 20 Brix raw syrup AC decolourisation, see Figure 4.26 (a). Comparing the removed colour in Figure 4.26 (b), similar result can be seen. The pre-treated syrup removes more colour beside AC dosages of 0.3 and 0.6 g AC / 100 ml, at which pre-treated syrup shows significantly worse decolourisation performance, which appear to be outside a plausible range of deviation. This is probably due to the high dilution of the syrup, as mentioned with previous graphs. Also, the isotherm results in significantly higher adsorbent load at lower concentrations, see Figure 4.28 (a).

Comparing decolourisation improvements with the same setup but without diafiltration (Chapter 4.2.3) we obtain similar improvements. Thereby, it also has to be considered that the benchmark curve for 20 Brix was carried out with the better performing 2nd batch, suggesting that the actual improvement might be higher than indicated by the data. Thus, in terms of decolourisation the diafiltration is an unnecessary effort. However, diafiltration shows other advantages in membrane separation, such as a higher sugar recovery as demonstrated by Luo et al. [67], making it interesting for the overall process.

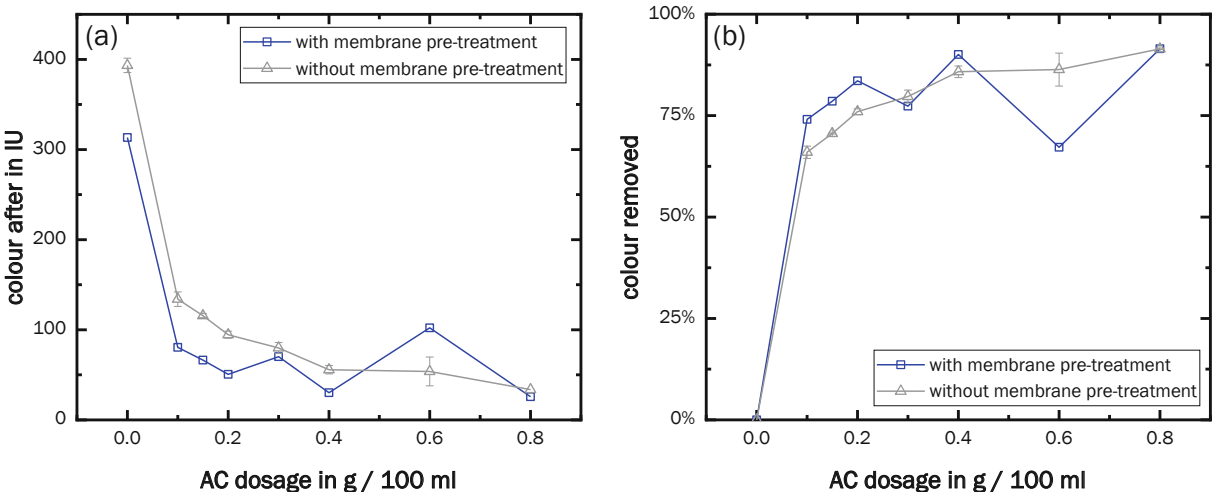

Figure 4.26: (a) Colour after treatment with AC adsorption and two-stage diafiltration pre-treatment (Setup 1.2) compared to a non-pre-treated syrup, and (b) colour percentage removed by the process

Pre-treatment with diafiltration by tight NF only shows a decline in decolourisation at dosages from 0.2 to 0.4 g AC / 100 ml, probably due to measurement errors, see Figure 4.28. If we disregard this error and assume the curve would follow a similar shape as the untreated solution, no improvement in colour after reduction or increase colour removal by tight NF diafiltration can be observed. Similar conclusion can be drawn from the Henry isotherms presented in Figure 4.28 (b). Both isotherms show the same slope and shape but distinguish in its adsorbent loading, where the isotherm of untreaded syrup

show slightly higher loading. This is probably due to the slightly lower sugar concentration of the treated syrup used for AC adsorption and deviations.

Thus, tight NF alone does not participate in improvements for the decolourisation. This could be expected since the main purpose of tight NF was the concentration of the high diluted syrup for further downstream processing.

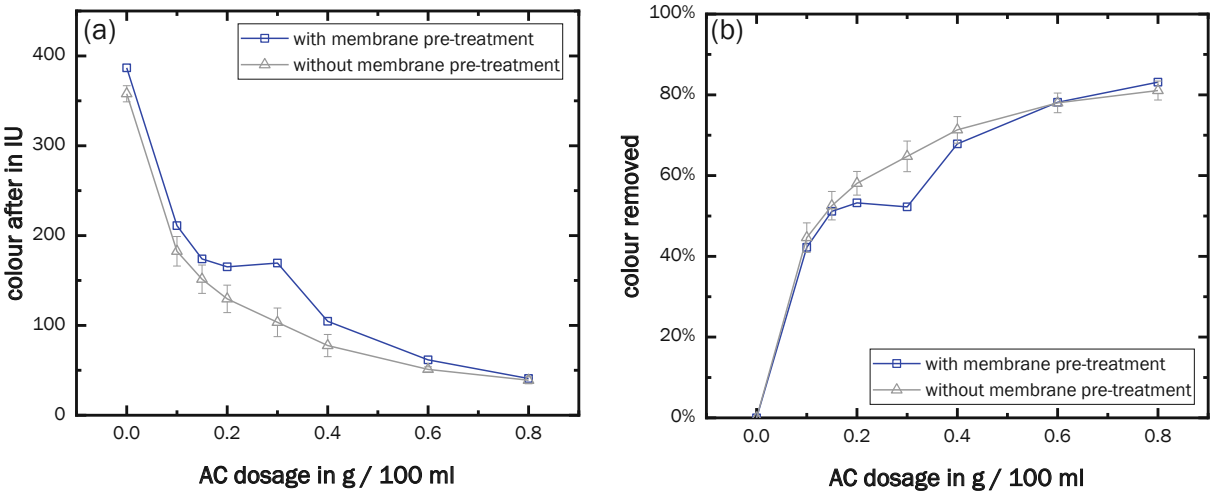

Figure 4.27: (a) Colour after treatment with AC adsorption and tight NF diafiltration pre-treatment (Setup 1.1) compared to a non-pre-treated syrup, and (b) colour percentage removed by the process

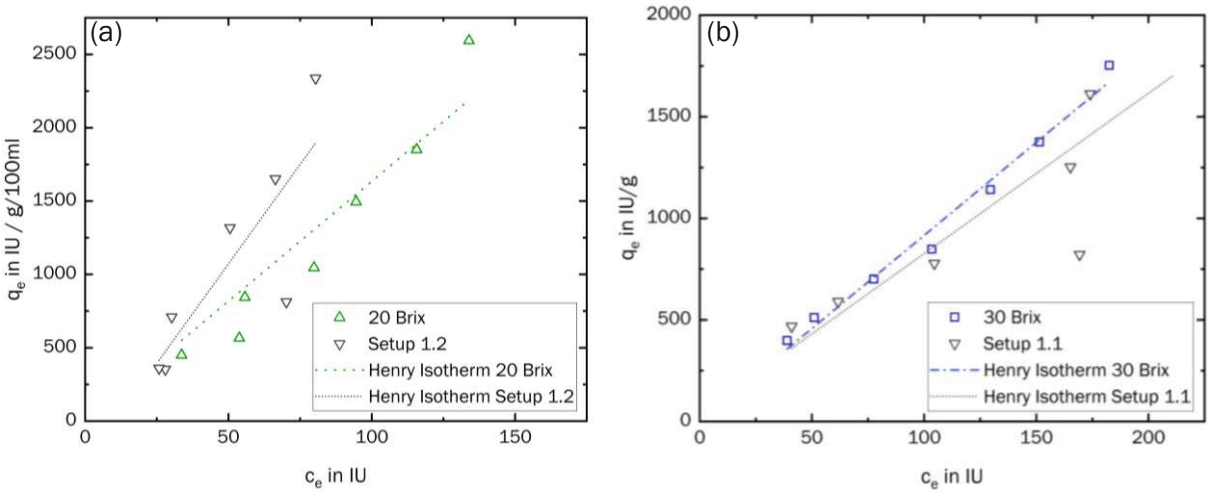

Figure 4.28: Henry isotherm with pre-treated solution by (a) two-stage diafiltration and by (b) tight NF

4.2.5 AC Dosage Savings and Best Setup

AC carbon savings due to membrane-based pre-treatment are estimated by comparing necessary AC dosages to achieve the colour requirements. The required colour of the glucose syrup is dependent on what it is utilised for and what are the certain standards. According to EU the colour of sugar solutions must be below 45 IU [14]. Same applies to glucose syrup used for the manufacture of sweetened beverages [68]. The Codex Alimentarius prescribes a value equal or below 60 IU to be considered as a white

sugar [13]. Other authors speak of colour values below 100 IU for commercial glucose syrups [69]. Thus, the AC dosages with and without pre-treatment to achieve a colour below 100 IU and 45 IU are compared.

The results presented in Figure 4.29 show that the setups with tight UF decrease the required AC significantly, beside of the three-stage configuration with an additional dilution of Feed 2. The two-stage membrane configuration with tight NF offers the best performance, reducing the required AC dosage by 74 % for 100 IU and more than 60 % for less than 45 IU. This results in an AC dosage of approximately 3.5 mg / (100ml · Brix) for 100 IU and 10 mg / (100ml · Brix) for 45 IU.

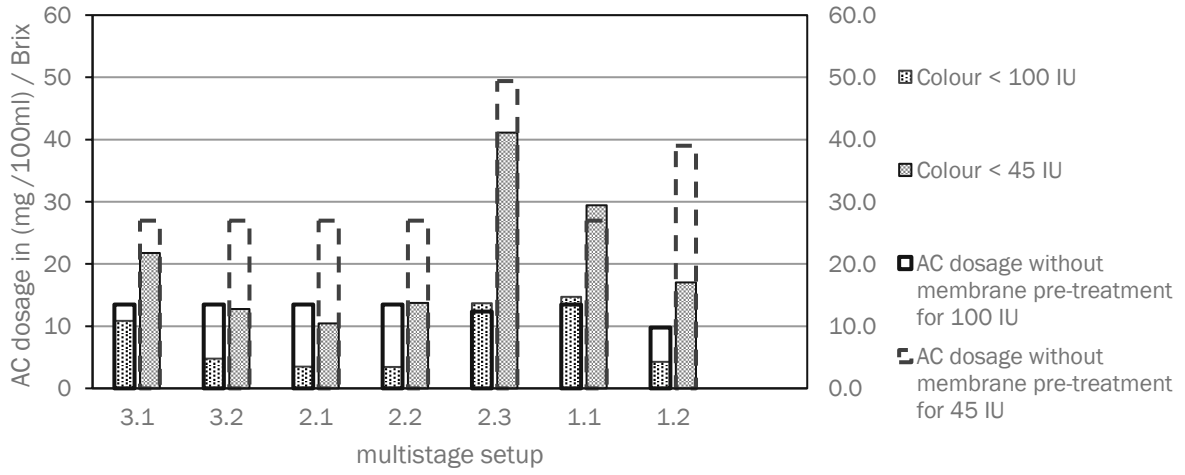

Figure 4.29: Required AC dosage to achieve decolourisation until 45 and 100 IU with and without pre-treatment

Above results show that all multistage setups containing tight UF resulted in enhanced decolourisation by following AC treatment, meaning less AC was required or the product syrup has less colour with the combination of the two treatments. On the other hand, diafiltration carried out solely with tight NF did not lead to any decolourisation improvements. This indicates that tight UF plays a significant role and improves performance in decolourisation by AC adsorption.

The performance improvements at AC decolourisation seem to be due to colour compounds being retained by the membrane and concentrated in the retentate. This results in a lower colour load of the feed for AC adsorption, reducing the amount of AC required. However, the colour difference between treated and untreated feeds is more pronounced at lower dosages, indicating that membranes not only remove colour but also improve AC adsorption capabilities, as evidenced by the steeper isotherm slopes. This may can be explained by the removal of bigger colour molecules by the membranes. These bigger molecules can plug the fine pores of the AC and prevent smaller molecules from further diffusion into the micropores. This means pre-treatment may increase the effective surface area of the AC, leading to higher adsorption capacity and higher colour removal. Furthermore, it may also improve the rate of adsorption.

The advantage in tight NF is in its concentration of the high diluted permeate, resulting in a higher concentrated solution more suitable for AC treatment, see Chapter 4.1.1. Furthermore, tight NF can replace traditional evaporation processes, which requires high energy consumption and can lower the quality of the sugar syrup and affect its colour [15].

Loose UF did not provide any advantage when applied as a pre-treatment. Although the fact that three-membrane stage configuration showed improvements, these were not due to the loose UF, evidenced by the two-stage configuration demonstrating same performance. Thus, loose UF in terms of decolourisation would be an unnecessary additional step causing additional sugar losses, when retentate is not used further. However, loose UF has other advantages such as elimination of the suspended solids and proteins from hydrolysates [68] and thus can increase the permeate flux of the following stage and overall system.

4.2.6 Sugar Loss by Membrane Technology

Despite the good improvements with membrane-based pre-treatment, the sugar loss from not used retentate needs to be considered. Although the final volumes in the retentate are minimal, the retentate has approx. 30 Brix sugar concentration after loose UF and approx. 25 to 35 Brix, depended on the feed concentration, after tight UF. Tight UF, in particular, leads to significant sugar losses of approx. 17 % due to the higher mass flow, as reported by Cabeza et al. [8].

To implement a sustainable, resource-saving process, membranes with less sugar retention must be utilised or the retentate needs to be further investigated for recovery or recycling in other applications. Possible improvement of the current process can be achieved with recycling of the retentate or diafiltration steps in the retentate side [8]. An alternative process is carbonation clarification which can resulted in 71.2 % sucrose recovery from the retentate as reported by Shi et al. [70] for non-organic applications. Other possibilities are applications, where the colour compounds are desired, for example as a possible flavour agent in vegan food [71].

5 Conclusions and Outlook

The study on decolourisation by AC adsorption showed that the optimal process conditions are between minimising AC usage and a fast adsorption process. Decolourisation with efficient AC utilisation, meaning low AC requirement, is achieved by low syrup dilutions. On the other hand, high syrup dilutions lead to a faster decolourisation.

It was shown that the AC adsorption follows a multilayer mechanism without prior monolayer coverage, best described by BET isotherm. Furthermore, it was proven that pore and surface diffusion are the limiting step. However, with increasing dilution film diffusion plays a more significant role.

The adsorption results showed that AC separation plays a critical role in the overall process, accounting for nearly all sugar losses of approximately 5 %. Therefore, to optimise AC decolourisation, a filtration medium with lower sugar retention should be utilised and carefully considered. Additionally, the filter paper was able to remove around 20 % of the colour in the syrup without involving AC adsorption, suggesting that incorporating a filtration pre-treatment could enhance the efficiency of the AC decolourisation process.

The study on a process combining membrane technology and AC adsorption showed that lower colour could be achieved at already lower dosages, and the amount of AC applied can be reduced by more than 60 %. Thereby, especially a membrane multistage configuration containing of tight UF (5 kDa) followed by tight NF (150 -300 Da) followed by AC adsorption are performing best, indicated by highest AC dosage reduction. Tight UF can restrain colour in the retentate, resulting in increasing of adsorption efficiency regarding required adsorbent. Tight NF is able to concentrate the syrup, thus can lead to improvements in the AC adsorption and can reduce energy consumption by the energy intensive evaporation process. However, the membrane separation can result in significant high sugar losses of up to 17 %, if the sugar in the UF retentate is not recovered. This loss would increase resource and energy consumption due to the need for higher feed input to achieve the same amount of colourless sugar. Therefore, exploring methods for sugar recovery or alternative utilisations of the retentate require more investigation in future studies. Additionally, potential improvements in adsorption kinetics achieved through membrane-based pre-treatment also require further investigation.

Overall, the study demonstrated that membrane-based pre-treatment is a suitable and promising technology for enhancing the decolourisation process of glucose syrups in combination with AC adsorption, leading to a more energy efficient and resource saving process. To fully realise these benefits, the integration of tight UF and tight NF processes should play a central role in further research, with a particular focus on addressing sugar losses in side streams.

List of Figures

List of Tables

List of Abbreviations and Symbols

AC ..... activated carbon
A_S ..... total surface area of the adsorbent
a_m ..... specific particle surface related to the adsorbent mass
a_p ..... adsorbent particle radius
b ..... Langmuir constant for gas adsorption
Bi ..... Biot number
C_{BET} ..... BET constant
C_L ..... equilibrium constant of the second layer
C_S ..... equilibrium constant of the first layer
c ..... concentration in the bulk fluid phase
c_0 ..... initial concentration
c_e ..... equilibrium concentration
c_s ..... external surface concentration
Da ..... Dalton
DE ..... dextrose equivalent
D_L ..... liquid phase diffusion coefficient
D_P ..... pore diffusion coefficient
D_S ..... surface diffusion coefficient
$(D_S)_e$ ..... effective diffusion coefficient
ED ..... electrodialysis
GT ..... gas transfer
HFCS ..... high fructose corn syrup
HSDM ..... homogeneous surface diffusion model
k_1 ..... pseudo first order rate constant
k_2 ..... pseudo second order rate constant
K_F ..... Freundlich constant
k_F ..... film mass transfer coefficient
K_H ..... Henry constant
K_L ..... Langmuir constant
k_S ..... intraparticle diffusion mass transfer coefficient
k_S^* ..... modified intraparticle mass transfer coefficient
$k_{W\&M}$ ..... Weber and Morris mass transfer coefficient
MF ..... microfiltration
m_A ..... mass of adsorbent

Δm^a ..... mass adsorbed onto the adsorbent
Δm^l ..... mass removed from liquid phase
N .....adsorbate uptake rate per adsorbent pellet
n .....number of moles
n^a ..... moles adsorbed to the solid
n^l ..... moles in the liquid phase
n_{BET} ..... number of adsorbed layers
n_F .....Freundlich exponent
NF .....nanofiltration
P .....partial pressure
P^S ..... saturation pressure
PV .....pervaporation
q .....adsorbent load
$\bar{q}$ ..... mean solid-phase concentration
q_e .....equilibrium adsorbent load
q_{max} ..... maximum adsorbent load (Langmuir isotherm)
q_m .....adsorbent load when completely covered with one unimolecular layer
q_s .....adsorbent loading at the external surface
r .....radial distance measured from the centre of the adsorbent pellet
RO .....reverse osmosis
RI..... refractive index
T ..... temperature
t .....time
UF..... ultrafiltration
V_L .....solution volume
α.....quantity defined by Equation (2.37)
γ_n ..... nth root of Equation (2.39)
δ .....film thickness
ε_p ..... particle porosity
θ.....fraction of sites covered with molecules
ρ_p .....particle density
μ..... number of molecules striking the area in mass per second
σ.....quotient of the condensing fraction when occupied

References

[1] H. Peter, *Glucose Syrups: Technology and Applications*, First edition. John Wiley & Sons, 2010.

[2] VGMS e.V., "VGMS: Daten und Fakten." Accessed: Feb. 27, 2023. [Online]. Available: https://www.vgms.de/staerkeindustrie/presse-service/daten-fakten

[3] M. W. Kearsley and S. Z. Dziedzic, *Handbook of Starch Hydrolysis Products and their Derivatives*, First edition. Dordrecht: Springer Science + Business Media, 1995. doi: 10.1001/918-1-4615-2159-4.

[4] European Union, "REGULATION (EU) 2018/848 OF THE EUROPEAN PARLIAMENT AND OF THE COUNCIL on organic production and labelling of organic products and repealing Council Regulation," May 30, 2018.

[5] European Commission, "Organic farming in EU - A decade of organic growth," Brussel, Jan. 2023.

[6] C. A. Cabeza, A. El-Gohary-Ahmed, M. Minauf, and M. Harasek, "Sustainable Industrial Treatment of Starch Hydrolysates," *Chem Eng Trans*, vol. 96, pp. 67–72, 2022, doi: 10.3303/CET2296012.

[7] H. K. Atiyeh and Z. Duvnjak, "Purification of Fructose Syrups Produced from Cane Molasses Media Using Ultrafiltration Membranes and Activated Carbon," *Sep Sci Technol*, vol. 39, no. 2, pp. 341–362, 2005, doi: 10.1081/ss-120027562.

[8] C. A. Cabeza, A. El Gohary Ahmed, M. Minauf, and M. Harasek, "Integration of Membrane Processes for Decolorization of Starch Hydrolysates," *Chem Eng Trans*, vol. 94, pp. 1177–1182, 2022.

[9] K. P. C. Vollhardt and N. E. Schore, *Organic Chemistry*, 6th ed. New York: Wiley-VCH, 2011.

[10] O. Türk, *Stoffliche Nutzung nachwachsender Rohstoffe*. Wiesbaden: Springer Fachmedien, 2014.

[11] K. Wagemann and K. Tippkötter, Eds., *Biorefineries*, 1st ed. Springer Cham, 2019. doi: https://doi.org/10.1007/978-3-319-97119-3.

[12] MikroMarketMonitor, "Global Glucose Syrup Market Research Report." Accessed: Sep. 10, 2023. [Online]. Available: http://www.micromarketmonitor.com/market-report/glucose-syrup-reports-9991818692.html

[13] Food and Agriculture Organization of the United Nations and World Health Organization, "Standard for Sugars. CXS 212-1999," 2022. Accessed: Sep. 10, 2023. [Online]. Available: www.codexalimentarius.org

[14] European Council, "Council Directive 2001/111/EC of 20 December 2001 relating

to certain sugars intended consumption," 2013, Accessed: Sep. 10, 2023. [Online]. Available: https://eur-lex.europa.eu/legal-content/EN/TXT/?uri=CELEX%3A02001L0111-20131118

[15] S. Clark, Stephanie. Jung, and Buddhi. Lamsal, *Food Processing : Principles and Applications.*, Second Edition. Chichester: John Wiley & Sons, 2014.

[16] R. Höfer, "Sugar-and Starch-Based Biorefineries," in *Industrial Biorefineries and White Biotechnology*, Elsevier, 2015, pp. 157–235. doi: 10.1016/B978-0-444-63453-5.00005-7.

[17] A. Bostan and D. Boyacioğlu, "Kinetics of non-enzymatic colour development in glucose syrups during storage," *Food Chem*, vol. 60, no. 4, pp. 581–585, Dec. 1997, doi: 10.1016/S0308-8146(97)00036-8.

[18] M. W. Kearsley and G. G. Birch, "The chemistry and metabolism of the starch based sweeteners," *Food Chem*, vol. 16, no. 3–4, pp. 191–207, Jan. 1985, doi: 10.1016/0308-8146(85)90115-3.

[19] P. Grassmann, F. Widmer, and H. Sinn, "Einführung in die thermische Verfahrenstechnik," 1997.

[20] E. Worch, *Adsorption Technology in Water Treatment*, 2nd Revised Edition. Berlin: De Gruyter, 2021. doi: DOI:10.1515/9783110240238.

[21] S. Ramaswamy, H.-J. Huang, and B. V. Ramarao, *Separation and purification technologies in biorefineries*, 1st ed. Chichester: John Wiley & Sons, 2013.

[22] D. D. Do, *Adsorption analysis: equilibria and kinetics*, Reprint. in Series on chemical engineering. London: Imperial College Press, 2008. doi: https://doi.org/10.1142/p111.

[23] W. J. Weber and E. H. Smith, "Activated Carbon Adsorption: The State of the Art," in *Studies in Environmental Science*, vol. 29, 1986, pp. 455–492. doi: 10.1016/S0166-1116(08)70958-0.

[24] C. Tien, "Introduction," in *Introduction to Adsorption*, Elsevier, 2019, pp. 1–6. doi: 10.1016/B978-0-12-816446-4.00001-4.

[25] H.-J. Bart and U. von Gemmingen, "Adsorption," in *Ullmann's Encyclopedia of Industrial Chemistry*, Weinheim, Germany: Wiley-VCH Verlag GmbH & Co. KGaA, 2005. doi: 10.1002/14356007.b03_09.pub2.

[26] K.-D. Henning and H. von Kienle, "Carbon, 5. Activated Carbon," in *Ullmann's Encyclopedia of Industrial Chemistry*, Weinheim, Germany: Wiley-VCH Verlag GmbH & Co. KGaA, 2010. doi: 10.1002/14356007.n05_n04.

[27] K. Y. Foo and B. H. Hameed, "Insights into the modeling of adsorption isotherm systems," Jan. 01, 2010. doi: 10.1016/j.cej.2009.09.013.

[28] S. Brunauer, L. S. Deming, W. E. Deming, and E. Teller, "On a Theory of the van der Waals Adsorption of Gases," *J Am Chem Soc*, vol. 62, no. 7, pp. 1723–1732, Jul. 1940, doi: 10.1021/ja01864a025.

[29] M. Thommes *et al.*, “Physisorption of gases, with special reference to the evaluation of surface area and pore size distribution (IUPAC Technical Report),” *Pure and Applied Chemistry*, vol. 87, no. 9–10, pp. 1051–1069, Oct. 2015, doi: 10.1515/pac-2014-1117.

[30] A. Gabelman, “Adsorption Basics: Part 1,” *Chem Eng Prog*, vol. 113, no. 7, p. 48, 2017.

[31] M. Ghaedi, *Adsorption: fundamental processes and applications*, 1st ed., vol. 33. London: Elsevier, 2021.

[32] I. Langmuir, “THE ADSORPTION OF GASES ON PLANE SURFACES OF GLASS, MICA AND PLATINUM.,” *J Am Chem Soc*, vol. 40, no. 9, pp. 1361–1403, Sep. 1918, doi: 10.1021/ja02242a004.

[33] S. Brunauer, P. H. Emmett, and E. Teller, “Adsorption of Gases in Multimolecular Layers,” *J Am Chem Soc*, vol. 60, no. 2, pp. 309–319, Feb. 1938, doi: 10.1021/ja01269a023.

[34] A. Ebadi, J. S. Soltan Mohammadzadeh, and A. Khudiev, “What is the correct form of BET isotherm for modeling liquid phase adsorption?,” *Adsorption*, vol. 15, no. 1, pp. 65–73, Feb. 2009, doi: 10.1007/s10450-009-9151-3.

[35] C. Tien, “Adsorbate Uptake and Equations Describing Adsorption Processes,” in *Introduction to Adsorption*, Elsevier, 2019, pp. 87–118. doi: 10.1016/B978-0-12-816446-4.00004-X.

[36] C. Tien, “Batch Adsorption Models and Model Applications,” in *Introduction to Adsorption*, Elsevier, 2019, pp. 119–153. doi: 10.1016/B978-0-12-816446-4.00005-1.

[37] J. Crank, *The Mathematics of Diffusion*. Clarendon Press, 1956.

[38] W. J. Weber and J. C. Morris, “Kinetics of Adsorption on Carbon from Solution,” *Journal of the Sanitary Engineering Division*, vol. 89, no. 2, pp. 31–59, Apr. 1963, doi: 10.1061/JSEDAI.0000430.

[39] J. Wang and X. Guo, “Rethinking of the intraparticle diffusion adsorption kinetics model: Interpretation, solving methods and applications,” *Chemosphere*, vol. 309, p. 136732, Dec. 2022, doi: 10.1016/j.chemosphere.2022.136732.

[40] E. Glueckauf and J. I. Coates, “241. Theory of chromatography. Part IV. The influence of incomplete equilibrium on the front boundary of chromatograms and on the effectiveness of separation,” *Journal of the Chemical Society (Resumed)*, p. 1315, 1947, doi: 10.1039/jr9470001315.

[41] E. Glueckauf, “Theory of chromatography. Part 10.—Formulæ for diffusion into spheres and their application to chromatography,” *Trans. Faraday Soc.*, vol. 51, no. 0, pp. 1540–1551, 1955, doi: 10.1039/TF9555101540.

[42] S. Lagergren, “Zur Theorie der sogenannten Adsorption gelöster Stoffe,” *Kungliga Svenska Vetenskapsakademiens*, vol. 24, no. 4, pp. 1–39, 1898, doi:

10.1007/BF01501332.

[43] R. W. Baker, *Membrane Technology and Applications*, Fourth Edition. Wiley, 2023. doi: 10.1002/9781119686026.

[44] K. Scott, *Handbook of Industrial Membranes*, 1st ed. Oxford: Elsevier, 1995. doi: 10.1016/B978-1-85617-233-2.X5000-4.

[45] A. K. Pabby, S. S. H. Rizvi, and A. M. S. Requena, Eds., *Handbook of Membrane Separations*. CRC Press, 2008. doi: 10.1201/9781420009484.

[46] S. P. Nunes and K. Peinemann, Eds., *Membrane Technology*, 2nd ed. Wiley, 2006. doi: 10.1002/3527608788.

[47] US Dept Energy, "Materials for Separation Technologies. Energy and Emission Reduction Opportunities," May 2005. doi: 10.2172/1218755.

[48] S. Judd and B. Jefferson, Eds., *Membranes for Industrial Wastewater Recovery and Re-use*. Oxford: Elsevier, 2003. doi: 10.1016/B978-1-85617-389-6.X5000-0.

[49] Lenntech B.V., "Molecular weight cutoff (MWCO)." Accessed: Oct. 04, 2024. [Online]. Available: Lenntech B.V.

[50] R. W. Baker, *Membrane Technology and Applications*, 3rd ed. Chichester: Wiley, 2004. doi: 10.1002/0470020393.

[51] H. C. S. Whalley, *ICUMSA methods of sugar analysis: Official and tentative methods, recommended by the International Commission for Uniform Methods of Sugar Analysis*. Elsevier, 1964.

[52] ICUMSA, "ICUMSA Colour." Accessed: Apr. 12, 2024. [Online]. Available: https://www.icumsa.org/definitions/general-definitions/refractometric-dry-substance-content-copy-2/

[53] Mettler Toledo, "Brix Measurement." Accessed: Apr. 12, 2024. [Online]. Available: https://www.mt.com/gb/en/home/perm-lp/product-organizations/ana/brix-meters.html

[54] OriginLab Corporation, "Origin(Pro)," *Northampton, MA*: 2023.

[55] W. J. Weber and Jr. E. H. Smith, "Simulation and design models for adsorption processes," *Environmental Science & Technololgy*, vol. 21, no. 11, pp. 1040–1050, Nov. 1987, doi: https://doi.org/10.1021/es00164a002.

[56] A. Serpen, B. Ataç, and V. Gökmen, "Adsorption of Maillard reaction products from aqueous solutions and sugar syrups using adsorbent resin," *J Food Eng*, vol. 82, no. 3, pp. 342–350, Oct. 2007, doi: 10.1016/j.jfoodeng.2007.02.048.

[57] R. Z. Mercado and D. M. L. Velasco, "Fine tuning the production of colorless sucrose syrups," *ACTA NOVA*, vol. 9, no. 2, pp. 176–189, Jul. 2019.

[58] "GeoGebra Classic," 2024. Accessed: Nov. 28, 2024. [Online]. Available: https://www.geogebra.org/classic

[59] S. M. Nasehi, S. Ansari, and M. Sarshar, "Removal of dark colored compounds from

date syrup using activated carbon: A kinetic study," *J Food Eng*, vol. 111, no. 3, pp. 490–495, Aug. 2012, doi: 10.1016/j.jfoodeng.2012.02.037.

[60] H. Ahdno and H. Jafarizadeh-Malmiri, "Clarification of date syrup by activated carbon: Investigation on kinetics, equilibrium isotherm, and thermodynamics of interactions," *International Journal of Food Engineering*, vol. 11, no. 5, pp. 651–658, Oct. 2015, doi: 10.1515/ijfe-2015-0093.

[61] M. A. Al-Farsi, "Clarification of date juice," *Int J Food Sci Technol*, vol. 38, pp. 241–245, Mar. 2003, doi: http://dx.doi.org/10.1046/j.1365-2621.2003.00669.x.

[62] F. Deng, D.-Y. Cheong, and G. M. Aita, "Optimization of activated carbon detoxification of dilute ammonia pretreated energy cane bagasse enzymatic hydrolysate by response surface methodology," *Ind Crops Prod*, vol. 115, pp. 166–173, May 2018, doi: 10.1016/j.indcrop.2018.02.030.

[63] T. Preechakun, S. Pongchaiphol, M. Raita, V. Champreda, and N. Laosiripojana, "Detoxification of hemicellulose-enriched hydrolysate from sugarcane bagasse by activated carbon and macroporous adsorption resin," *Biomass Convers Biorefin*, vol. 14, no. 13, pp. 14559–14574, Jul. 2024, doi: 10.1007/s13399-022-03596-6.

[64] S. M. M. Kamal, N. L. Mohamad, A. G. L. Abdullah, and N. Abdullah, "Detoxification of sago trunk hydrolysate using activated charcoal for xylitol production," *Procedia Food Sci*, vol. 1, pp. 908–913, 2011, doi: 10.1016/j.profoo.2011.09.137.

[65] J. M. Lee, R. A. Venditti, H. Jameel, and W. R. Kenealy, "Detoxification of woody hydrolyzates with activated carbon for bioconversion to ethanol by the thermophilic anaerobic bacterium Thermoanaerobacterium saccharolyticum," *Biomass Bioenergy*, vol. 35, no. 1, pp. 626–636, Jan. 2011, doi: 10.1016/j.biombioe.2010.10.021.

[66] J. Gyura, Z. Šereš, G. Vatai, and E. Békássy Molnár, "Separation of non-sucrose compounds from the syrup of sugar-beet processing by ultra- and nanofiltration using polymer membranes," *Desalination*, vol. 148, no. 1–3, pp. 49–56, Sep. 2002, doi: https://doi.org/10.1016/S0011-9164(02)00652-5.

[67] J. Luo *et al.*, "Refining sugarcane juice by an integrated membrane process: Filtration behavior of polymeric membrane at high temperature," *J Memb Sci*, vol. 509, pp. 105–115, Jul. 2016, doi: 10.1016/j.memsci.2016.02.053.

[68] G. Daufin, J. P. Escudier, H. Carrère, S. Bérot, L. Fillaudeau, and M. Decloux, "Recent and emerging applications of membrane processes in the food and dairy industry," *Food and Bioproducts Processing: Transactions of the Institution of of Chemical Engineers, Part C*, vol. 79, no. 2, pp. 89–102, 2001, doi: 10.1205/096030801750286131.

[69] I. Çelebi and N. S. Kincal, "Color formation in wheat starch based glucose syrups and use of commercially available and laboratory-prepared agricultural waste-based activated carbons for decolorization," *Sep Sci Technol*, vol. 42, no. 8, pp. 1761–1773, Jun. 2007, doi: 10.1080/01496390601174232.

[70] C. Shi *et al.*, “Sugar and value-added products derived from retentate concentrate of sugarcane juice,” *J Clean Prod*, vol. 278, p. 123915, Jan. 2021, doi: 10.1016/j.jclepro.2020.123915.

[71] P. Kale, A. Mishra, and U. S. Annapure, “Development of vegan meat flavour: A review on sources and techniques,” *Future Foods*, vol. 5, p. 100149, Jun. 2022, doi: 10.1016/j.fufo.2022.100149.

Appendix A - AC Datasheet

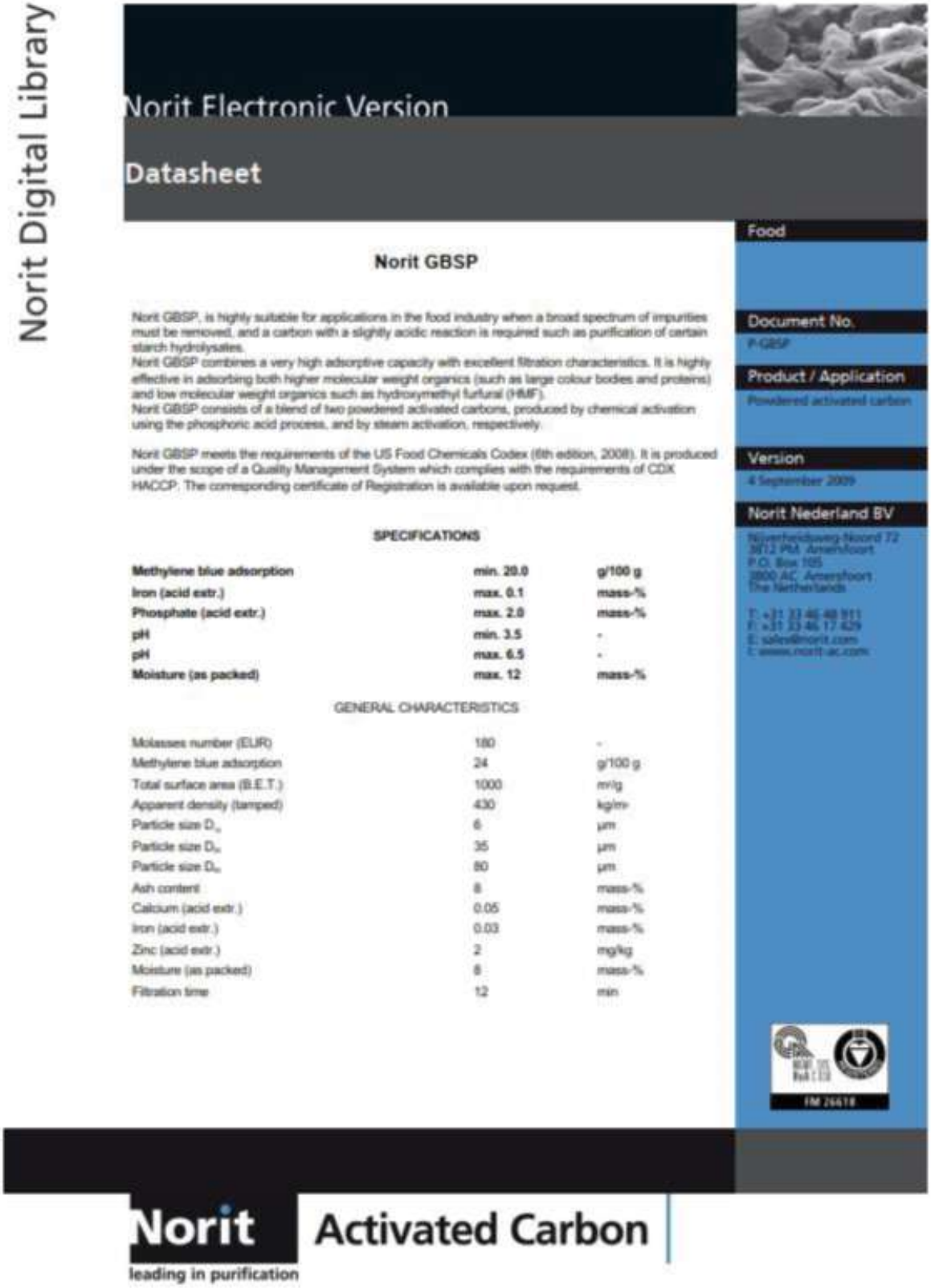

Norit Digital Library

Norit Electronic Version

Datasheet

Food

Norit GBSP

Norit GBSP, is highly suitable for applications in the food industry when a broad spectrum of impurities must be removed, and a carbon with a slightly acidic reaction is required such as purification of certain starch hydrolysates.
Norit GBSP combines a very high adsorptive capacity with excellent filtration characteristics. It is highly effective in adsorbing both higher molecular weight organics (such as large colour bodies and proteins) and low molecular weight organics such as hydroxymethyl furfural (HMF).
Norit GBSP consists of a blend of two powdered activated carbons, produced by chemical activation using the phosphoric acid process, and by steam activation, respectively.

Norit GBSP meets the requirements of the US Food Chemicals Codex (6th edition, 2008). It is produced under the scope of a Quality Management System which complies with the requirements of CDX HACCP. The corresponding certificate of Registration is available upon request.

Document No.

P-GBSP

Product / Application

Powdered activated carbon

Version

4 September 2009

Norit Nederland BV

Nijverheidsweg-Noord 72
3812 PM Amersfoort
P.O. Box 105
3800 AC Amersfoort
The Netherlands

T: +31 33 46 48 911
F: +31 33 46 17 429
E: sales@norit.com
I: www.norit-ac.com

FM 26618

SPECIFICATIONS

Methylene blue adsorption	**min. 20.0**	**g/100 g**
Iron (acid extr.)	**max. 0.1**	**mass-%**
Phosphate (acid extr.)	**max. 2.0**	**mass-%**
pH	**min. 3.5**	-
pH	**max. 6.5**	-
Moisture (as packed)	**max. 12**	**mass-%**

GENERAL CHARACTERISTICS

Molasses number (EUR)	180	-
Methylene blue adsorption	24	g/100 g
Total surface area (B.E.T.)	1000	m²/g
Apparent density (tamped)	430	kg/m³
Particle size D_{10}	6	µm
Particle size D_{50}	35	µm
Particle size D_{90}	80	µm
Ash content	8	mass-%
Calcium (acid extr.)	0.05	mass-%
Iron (acid extr.)	0.03	mass-%
Zinc (acid extr.)	2	mg/kg
Moisture (as packed)	8	mass-%
Filtration time	12	min

Norit Activated Carbon

leading in purification

Appendix B - Residuals

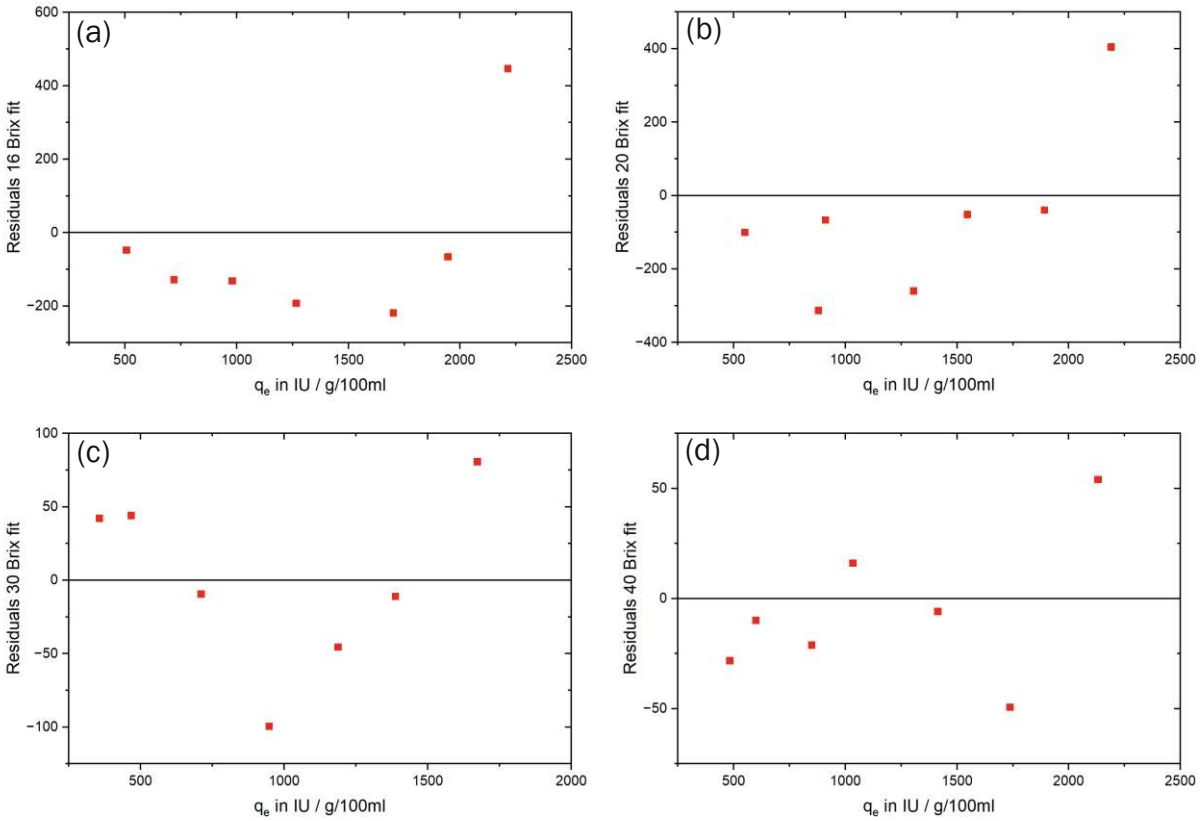

Figure B.1: Residuals of Henry isotherms for (a) 16 Brix, (b) 20 Brix, (c), 30 Brix, and (d) 40 Brix dilutions

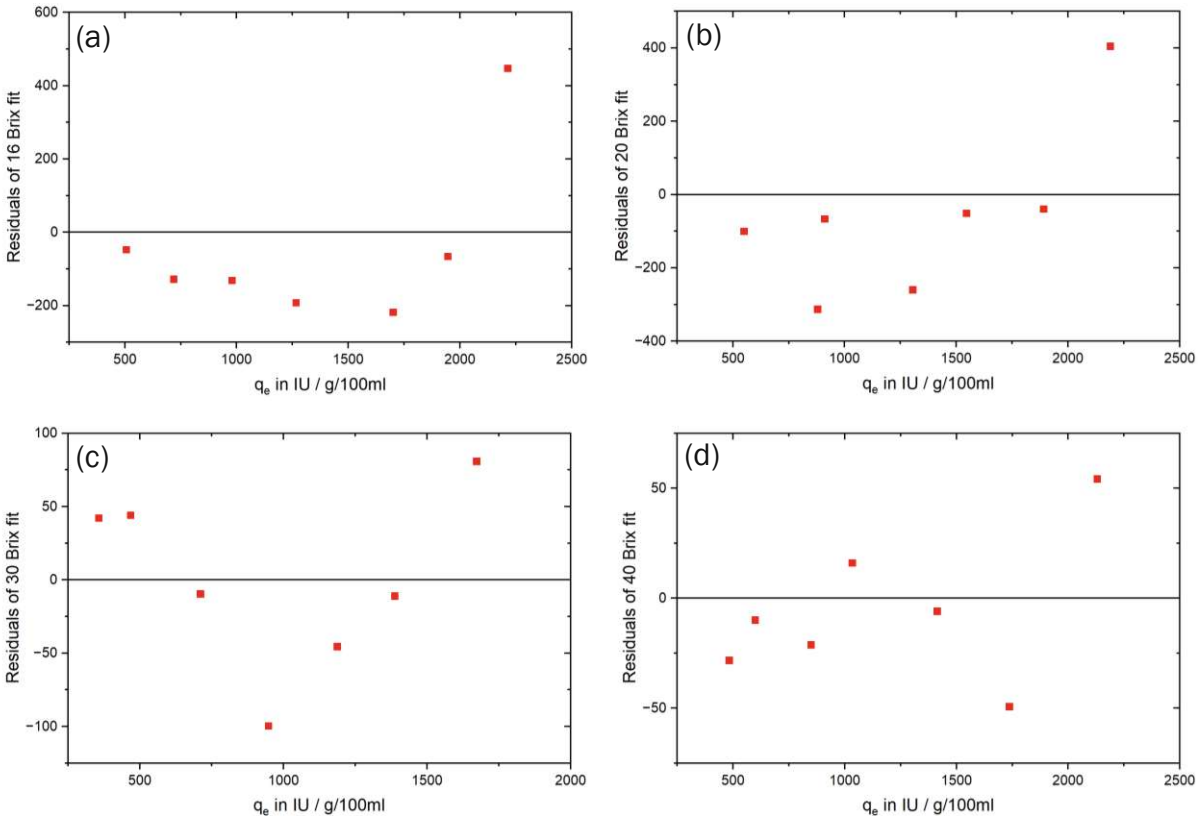

Figure B.2: Residuals of Langmuir isotherms for (a) 16 Brix, (b) 20 Brix, (c), 30 Brix, and (d) 40 Brix dilutions

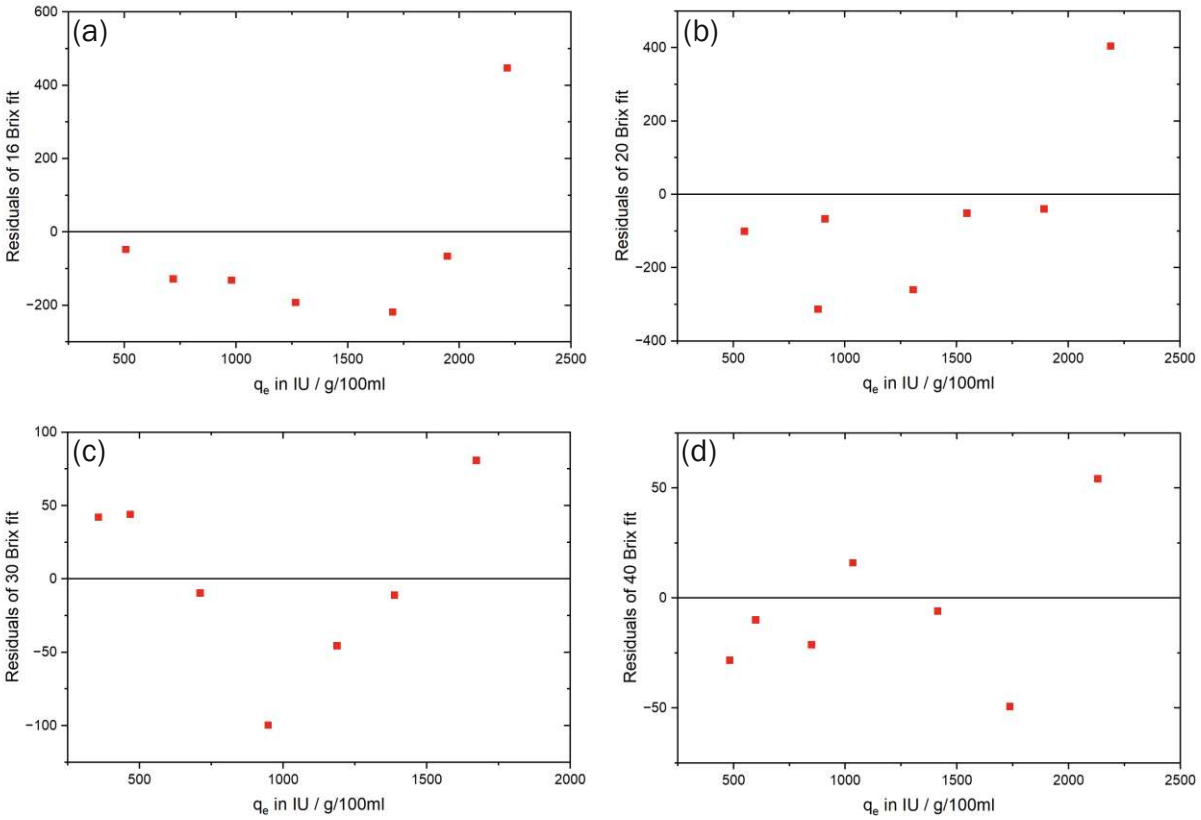

Figure B.3: Residuals of BET isotherms for (a) 16 Brix, (b) 20 Brix, (c), 30 Brix, and (d) 40 Brix dilutions

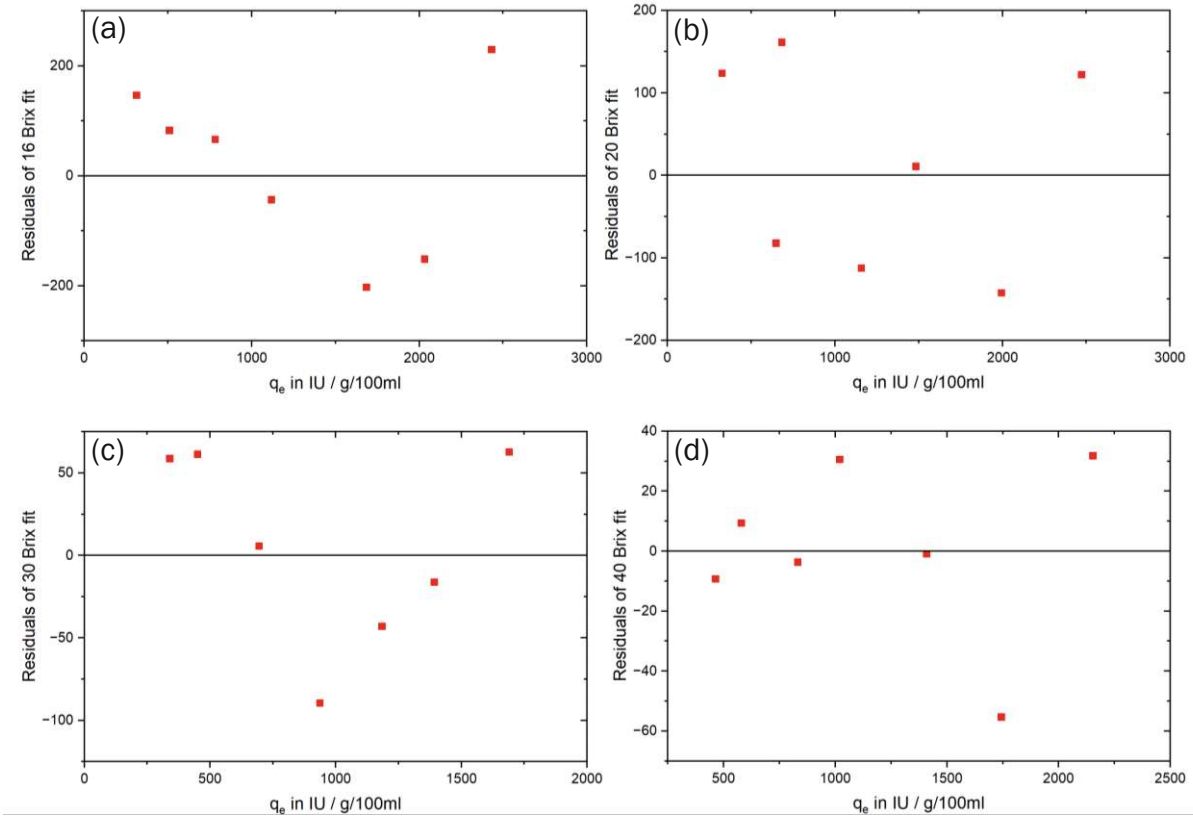

Figure B.4: Residuals of Freundlich isotherms for (a) 16 Brix, (b) 20 Brix, (c), 30 Brix, and (d) 40 Brix dilutions

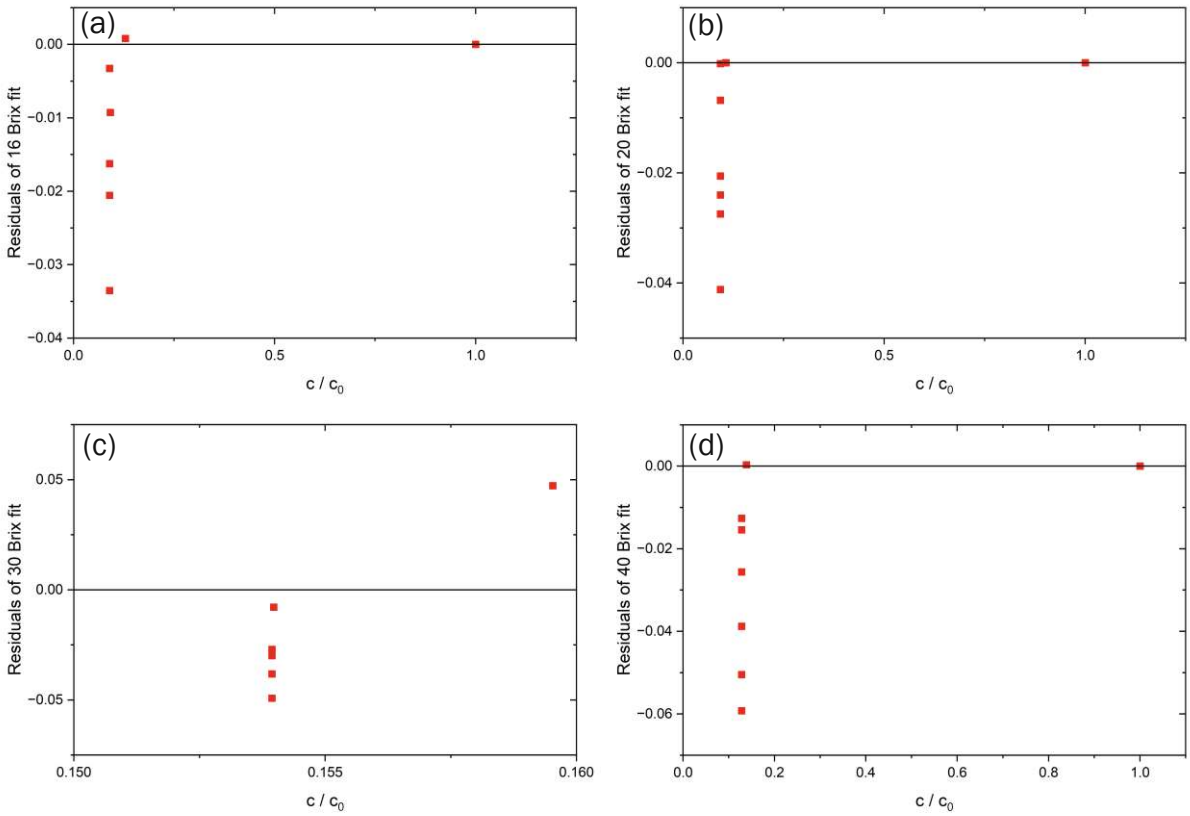

Figure B.5: Residuals of film diffusion model for (a) 16 Brix, (b) 20 Brix, (c), 30 Brix, and (d) 40 Brix dilutions

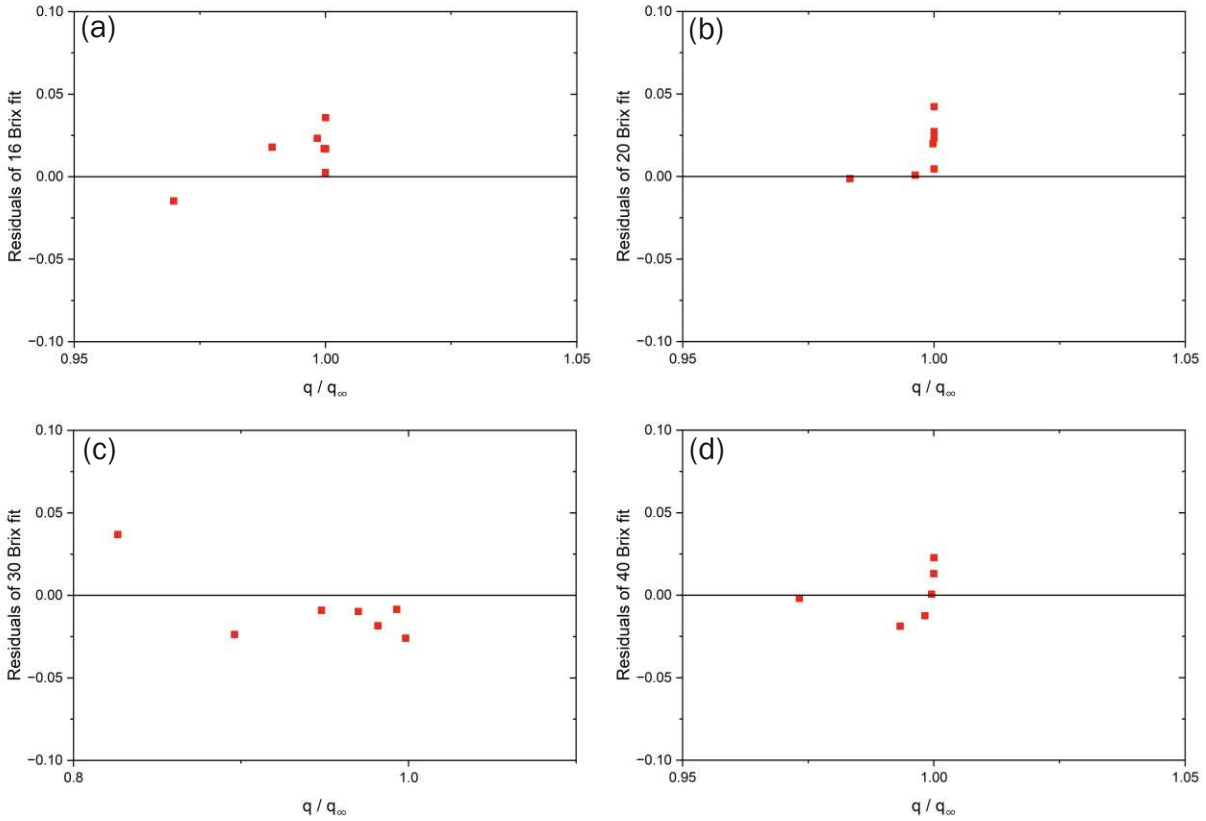

Figure B.6: Residuals of intraparticle diffusion model for (a) 16 Brix, (b) 20 Brix, (c), 30 Brix, and (d) 40 Brix dilutions

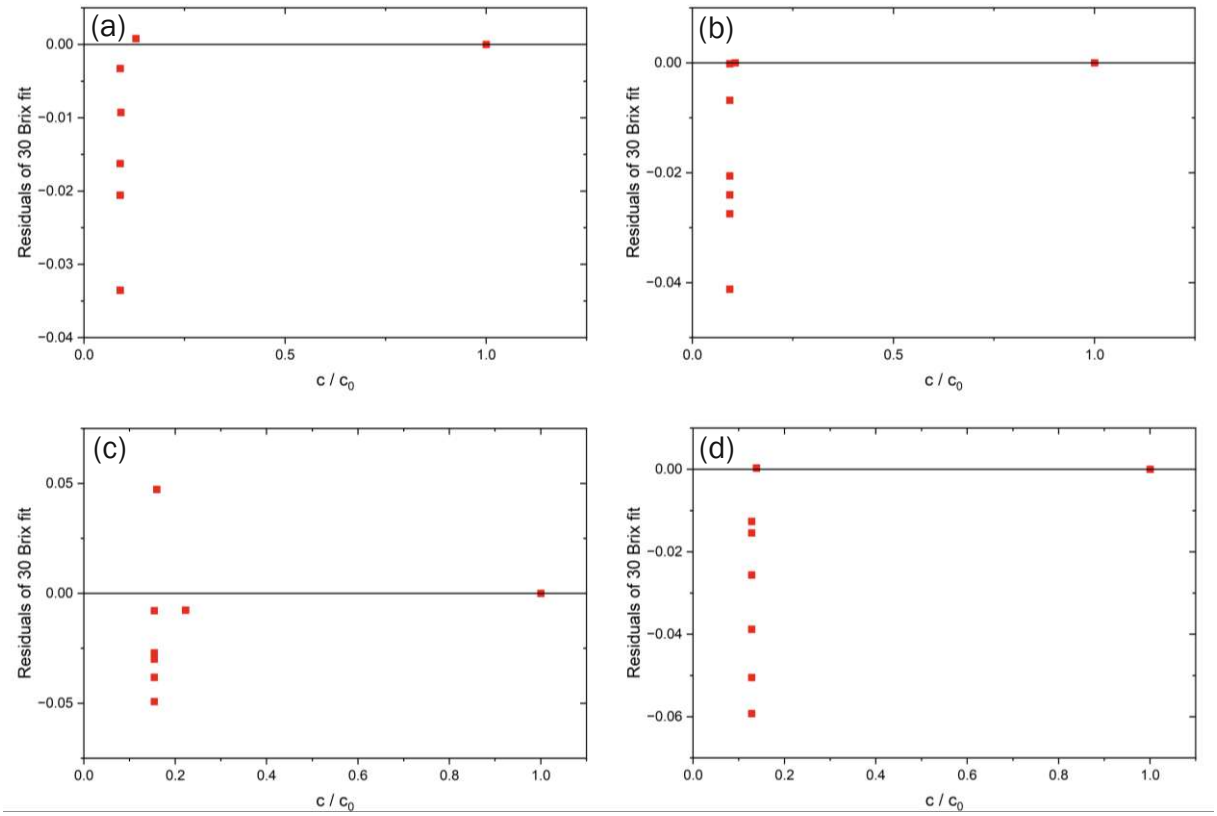

Figure B.7: Residuals of LDF model for (a) 16 Brix, (b) 20 Brix, (c), 30 Brix, and (d) 40 Brix dilutions

Appendix C - Solving Path of Film Diffusion

Mass transfer equation for film diffusion:

$$-\frac{\mathrm{d}c}{\mathrm{d}t} = k_F a_m \frac{m_A}{V_L}(c - c_s)$$

Initial conditions:

$$\bar{q} = 0, \quad c = c_0 \quad at \quad t = 0$$

Solving of the equation:

$$-\frac{\mathrm{d}c}{\mathrm{d}t} = k_F a_m \frac{m_A}{V_L}(c - c_s)$$

With the equilibrium condition

$$\bar{q} = q_s = K_H c_s \;\rightarrow c_s = \frac{\bar{q}}{K_H}$$

and the material balance equation

$$\bar{q} = \frac{V_L}{m_A}[c_0 - c(t)]$$

follows:

$$-\frac{\mathrm{d}c}{dt} = k_F a_m \frac{m_A}{V_L}(c - \frac{1}{K_H}\frac{V_L}{m_A}[c_0 - c(t)])$$

$$-\frac{\mathrm{d}c}{\mathrm{d}t} = k_F a_m \frac{m_A}{V_L}(c - \frac{1}{K_H}\frac{V_L}{m_A}c_0 + \frac{1}{K_H}\frac{V_L}{m_A}\mathrm{c})$$

$$-\frac{\mathrm{d}c}{\mathrm{d}t} = k_F a_m \frac{1}{K_H}\,(\frac{m_A}{V_L}K_H c - c_0 + \mathrm{c})$$

$$-\frac{\mathrm{d}c}{\left[\mathrm{c}\left(\frac{m_A}{V_L}K_H + 1\right) - c_0\right]} = k_F a_m \frac{1}{K}\,\mathrm{d}t$$

$$-\int_{c_0}^{c}\frac{\mathrm{d}c}{\left[\mathrm{c}\left(\frac{m_A}{V_L}K_H + 1\right) - c_0\right]} = k_F a_m \frac{1}{K}\int_0^t \mathrm{d}t$$

$$-\frac{\ln\left[\mathrm{c}\left(\frac{m_A}{V_L}K_H + 1\right) - c_0\right]}{\frac{m_A}{V_L}K_H + 1}\Bigg|_{c_0}^{c} = k_F a_m \frac{1}{K_H}\,t\Big|_0^t$$

$$-\frac{\ln\left[\mathrm{c}\left(\frac{m_A}{V_L}K_H + 1\right) - c_0\right]}{\frac{m_A}{V_L}K_H + 1} + \frac{\ln\left[c_0\left(\frac{m_A}{V_L}K_H + 1\right) - c_0\right]}{\frac{m_A}{V_L}K_H + 1} = k_F a_m \frac{1}{K_H}\,t$$

$$\ln\left[\frac{c_0\left(\frac{m_A}{V_L}K_H + 1\right) - c_0}{\mathrm{c}\left(\frac{m_A}{V_L}K_H + 1\right) - c_0}\right] = \left(\frac{m_A}{V_L}K_H + 1\right)k_F a_m \frac{1}{K_H}\,t$$

$$\frac{c_0\left(\frac{m_A}{V_L}K_H+1\right)-c_0}{\mathrm{c}\left(\frac{m_A}{V_L}K_H+1\right)-c_0}=\exp[\left(\frac{m_A}{V_L}K_H+1\right)k_F a_m\frac{1}{K_H}\ t]$$

$$\frac{c_0\frac{m_A}{V_L}K_H}{\mathrm{c}\left(\frac{m_A}{V_L}K_H+1\right)-c_0}=\exp[\left(\frac{m_A}{V_L}K_H+1\right)k_F a_m\frac{1}{K_H}\ t]$$

$$\mathrm{c}\left(\frac{m_A}{V_L}K_H+1\right)-c_0=c_0\frac{m_A}{V_L}K_H\exp[-\left(\frac{m_A}{V_L}K+1\right)k_F a_m\frac{1}{K_H}\ t]$$

$$c=c_0\frac{1}{\left(\frac{m_A}{V_L}K_H+1\right)}+c_0\frac{\frac{m_A}{V_L}K}{\left(\frac{m_A}{V_L}K_H+1\right)}\exp[-\left(\frac{m_A}{V_L}K_H+1\right)k_F a_m\frac{1}{K_H}\ t]$$

$$\frac{c}{c_0}=\frac{1}{\left(\frac{m_A}{V_L}K_H+1\right)}+\frac{\frac{m_A}{V_L}K}{\left(\frac{m_A}{V_L}K_H+1\right)}\exp[-\left(\frac{m_A}{V_L}K_H+1\right)k_F a_m\frac{1}{K_H}\ t]$$

Appendix D - Intraparticle Diffusion Model Data

Table D.1: Parameters for intraparticle diffusion model fitting

Dilution	16 Brix	20 Brix	30 Brix	40 Brix
α	0.09863	0.10195	0.18193	0.14672
γ_1	4.461	4.460	4.434	4.445
γ_2	7.693	7.691	7.665	7.677
γ_3	10.871	10.870	10.844	10.856
γ_4	14.033	14.032	14.006	14.018
γ_5	17.188	17.187	17.160	17.172
a_p / cm	0.0035	0.0035	0.0035	0.0035

Appendix E - Solving path of LDF

Mass transfer equation for

$$\frac{\mathrm{d}q}{\mathrm{d}t} = k_S^*(q_s - \bar{q})$$

Initial conditions

$$\bar{q} = 0, \;\; c = c_0 \quad at \quad t = 0$$

Boundary condition:

$$c = c_s$$

Solving of the equation:

$$\frac{\mathrm{d}q}{\mathrm{d}t} = k_S^*(q_s - \bar{q})$$

$$\mathrm{d}q = k_S^*(q_s - \bar{q})\mathrm{d}t$$

With the equilibrium condition

$$q_s = K_H c_s = K_H c$$

this leads to:

$$\mathrm{d}q = k_S^*(K_H c - \bar{q})\mathrm{d}t$$

$$\frac{\mathrm{d}q}{(Kc - \bar{q})} = k_S^*\mathrm{d}t$$

With the material balance equation

$$\bar{q} = \frac{V_L}{m_A}[c_0 - c] \rightarrow \mathrm{d}\bar{q} = \frac{V_L}{m_A}(-\mathrm{d}c)$$

follows:

$$\frac{\frac{V_L}{m_A}(-\mathrm{d}c)}{K_H c - \frac{V_L}{m_A}(c_0 - c)} = k_S^*\mathrm{d}t$$

$$\frac{-\mathrm{d}c}{\frac{m_A}{V_L}K_H c - (c_0 - c)} = k_S^*\mathrm{d}t$$

$$\frac{-\mathrm{d}c}{c\left(\frac{m_A}{V_L}K_H + 1\right) - c_0} = k_S^*\mathrm{d}t$$

$$-\int_{c_0}^{c} \frac{\mathrm{d}c}{\left(c\frac{m_A}{V_L}K_H c + 1\right) - c_0} = k_S^* \int_0^t \mathrm{d}t$$

$$\left.\frac{-\ln\left[c\left(\frac{m_A}{V_L}K_H + 1\right) - c_0\right]}{\frac{m_A}{V_L}K_H + 1}\right|_{c_0}^{c} = k_S^* t|_0^t$$

$$-\ln\left[c\left(\frac{m_A}{V_L}K_H+1\right)-c_0\right]\Big|_{c_0}^{c}=\left(\frac{m_A}{V_L}K_H+1\right)k_S^*t\Big|_0^t$$

$$-\ln\left[c\left(\frac{m_A}{V_L}K_H+1\right)-c_0\right]+\ln\left[c_0\left(\frac{m_A}{V_L}K_H+1\right)-c_0\right]=\left(\frac{m_A}{V_L}K_H+1\right)k_S^*t$$

$$-\ln\left[c\left(\frac{m_A}{V_L}K_H+1\right)-c_0\right]+\ln\left(c_0\frac{m_A}{V_L}K_H\right)=\left(\frac{m_A}{V_L}K_H+1\right)k_S^*t$$

$$\ln\left[\frac{c_0\frac{m_A}{V_L}K_H}{c\left(\frac{m_A}{V_L}K_H+1\right)-c_0}\right]=\left(\frac{m_A}{V_L}K_H+1\right)k_S^*t$$

$$\frac{c_0\frac{m_A}{V_L}K_H}{c\left(\frac{m_A}{V_L}K_H+1\right)-c_0}=\exp\left[\left(\frac{m_A}{V_L}K_H+1\right)k_S^*t\right]$$

$$\frac{c_0\frac{m_A}{V_L}K_H}{c\left(\frac{m_A}{V_L}K_H+1\right)-c_0}=\exp\left[\left(\frac{m_A}{V_L}K_H+1\right)k_S^*t\right]$$

$$c\left(\frac{m_A}{V_L}K_H+1\right)-c_0=c_0\frac{m_A}{V_L}K_H\exp\left[-\left(\frac{m_A}{V_L}K_H+1\right)k_S^*t\right]$$

$$c\left(\frac{m_A}{V_L}K_H+1\right)=c_0+c_0\frac{m_A}{V_L}K_H\exp\left[-\left(\frac{m_A}{V_L}K_H+1\right)k_S^*t\right]$$

$$c=c_0\frac{1}{\left(\frac{m_A}{V_L}K_H+1\right)}+c_0\frac{\frac{m_A}{V_L}K_H}{\left(\frac{m_A}{V_L}K_H+1\right)}\exp\left[-\left(\frac{m_A}{V_L}K_H+1\right)k_S^*t\right]$$

$$\frac{c}{c_0}=\frac{1}{\left(\frac{m_A}{V_L}K_H+1\right)}+\frac{\frac{m_A}{V_L}K_H}{\left(\frac{m_A}{V_L}K_H+1\right)}\exp\left[-\left(\frac{m_A}{V_L}K_H+1\right)k_S^*t\right]$$

Appendix F - Sugar Loss

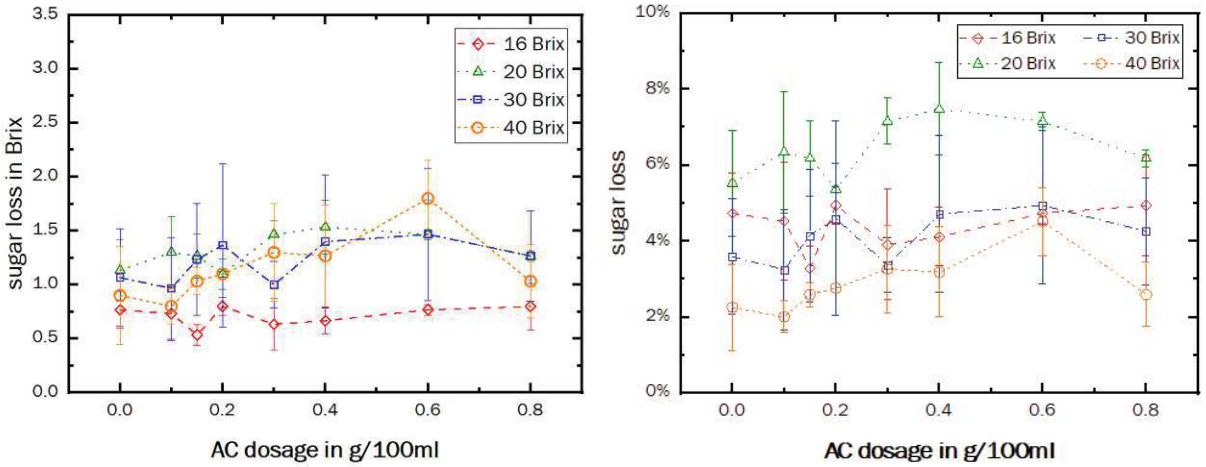

Figure F.1: Change of Sugar after achieving of equilibrium for different AC dosages in Brix

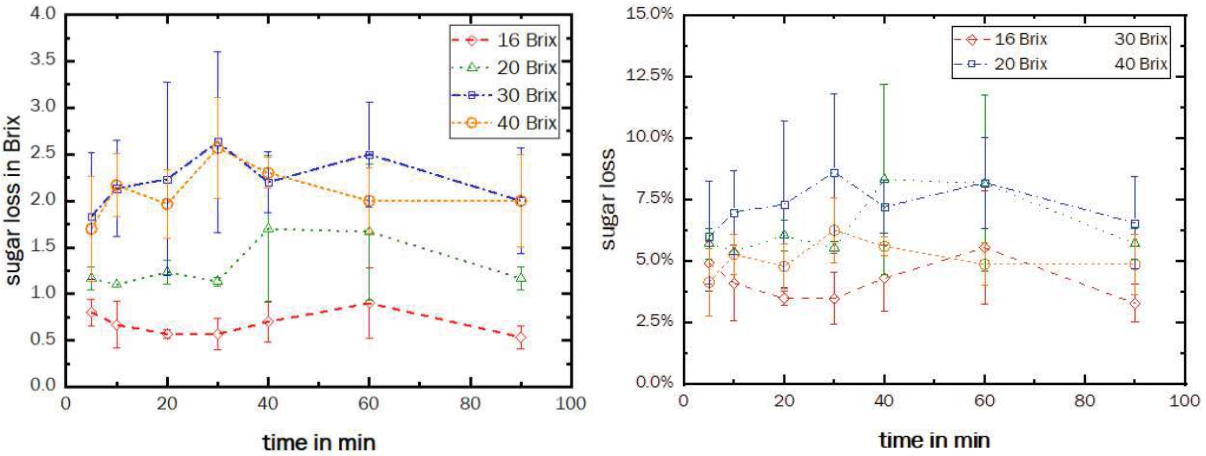

Figure F.2: Change of Sugar during the adsorption process for different dilutions

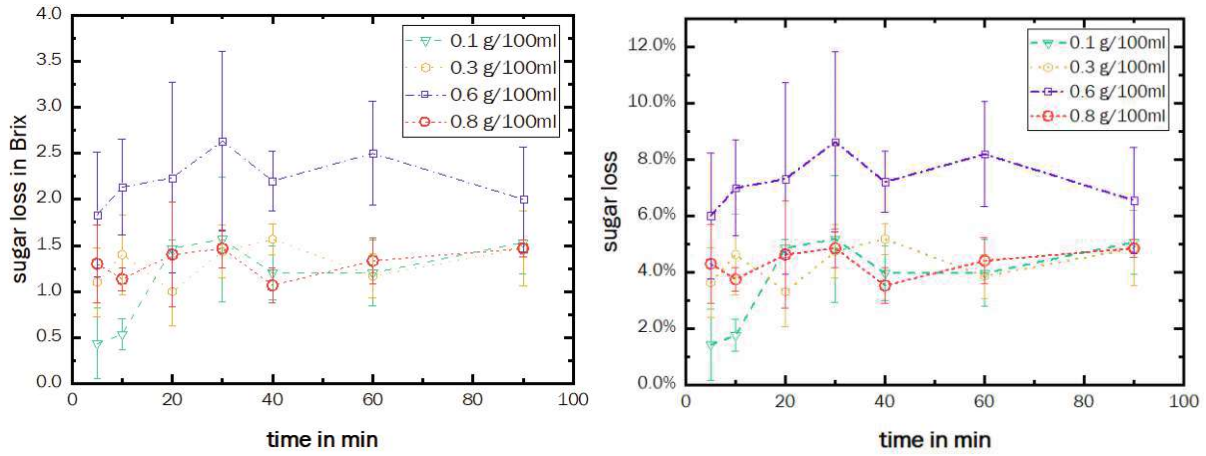

Figure F.3: Change of Sugar during the adsorption process for different AC dosages

Appendix G - UF Results

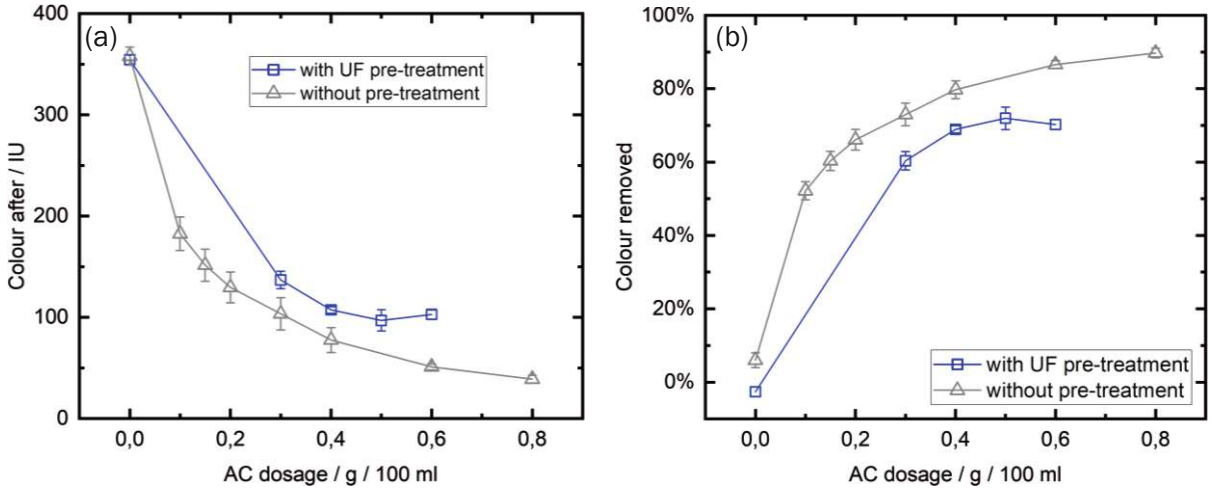

Figure G.1: (a) Colour after treatment with AC adsorption and loose UF (100 kDa) pre-treatment with an initial feed concentration of 30 Brix compared to a non-pre-treated syrup (b) colour percentage removed by the process

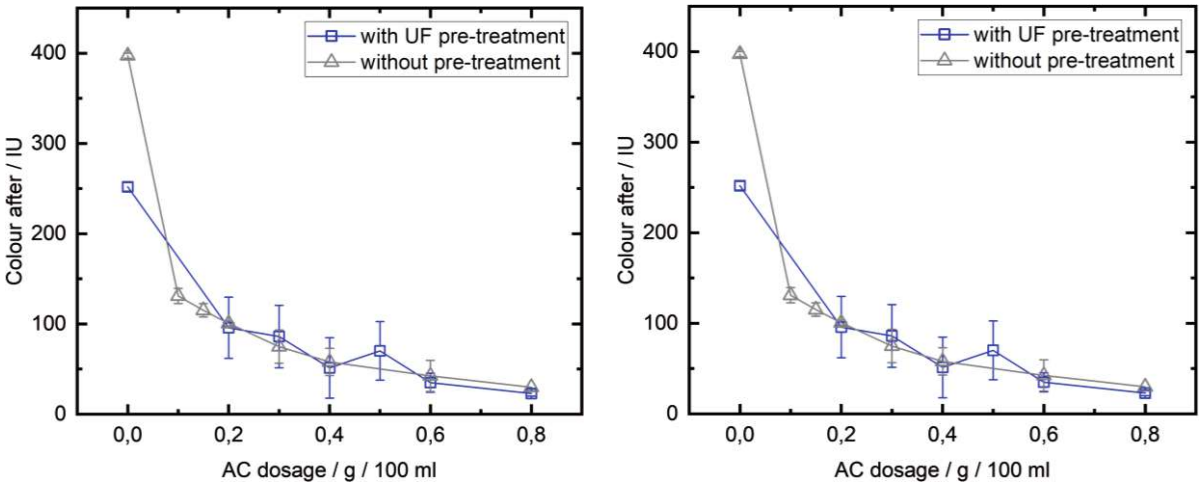

Figure G.2: (a) Colour after treatment with AC adsorption and tight UF (5 kDa) pre-treatment with an initial feed concentration of 20 Brix compared to a non-pre-treated syrup (b) colour percentage removed by the process